RICE UNIVERSITY

Light-Triggered Release of DNA from Plasmon-Resonant Nanoparticles

by

Ryan Huschka

A THESIS SUBMITTED
IN PARTIAL FULFILLMENT OF THE
REQUIREMENTS FOR THE DEGREE

Doctor of Philosophy

APPROVED, THESIS COMMITTEE:

Naomi J. Halas, Chair
Stanley C. Moore Professor in Electrical and Computer Engineering, Professor of Chemistry, Biomedical Engineering, Physics and Astronomy

Stephan Link
Assistant Professor of Chemistry and Assistant Professor of Electrical and Computer Engineering

Peter J. Nordlander
Professor of Physics and Astronomy and Electrical and Computer Engineering

Lin Ji
Associate Professor in Department of Thoracic and Cardiovascular Surgery, The University of Texas MD Anderson Cancer Center

Houston, TX
June 2012

ABSTRACT

Light-Triggered Release of DNA from Plasmon-Resonant Nanoparticles

by

Ryan Huschka

Plasmon-resonant nanoparticle complexes show promising potential for light-triggered, controllable delivery of deoxyribonucleic acids (DNA) for research and therapeutic purposes. For example, the approach of RNA interference (RNAi) – using antisense DNA or RNA oligonucleotides to silence activity of a specific pathogenic gene transcript and reduce expression of the encoded protein – is very useful in dissecting genetic function and holds promise as a molecular therapeutic. Herein, we investigate the mechanism and probe the *in vitro* therapeutic potential of DNA light-triggered release from plasmonic nanoparticles.

First, we investigate the mechanism of light-triggered release by dehybridizing double-stranded (dsDNA) via laser illumination from two types of nanoparticle substrates: gold (Au) nanoshells and Au nanorods. Both light-triggered and thermally induced releases are distinctly observable from nanoshell-based complexes. Surprisingly, no analogous measurable light-triggered release was observable from nanorod-based complexes below the DNA melting temperature. These results suggest that a nonthermal mechanism may play a role in light-triggered DNA release.

Second, we demonstrate the *in vitro* light-triggered release of molecules non-covalently attached within dsDNA bound to the Au nanoshell surface. DAPI (4',6-diamidino-2-phenylindole), a bright blue fluorescent molecule that binds reversibly to double-stranded DNA, was chosen to visualize this intracellular light-induced release process. Illumination through the cell membrane of the nanoshell-*ds*DNA-DAPI complexes

dehybridizes the DNA and releases the DAPI molecules within living cells. The DAPI molecules diffuse to the nucleus and associate with the cell's endogenous DNA. This work could have future applications towards drug delivery of molecules that associate with dsDNA.

Finally, we demonstrate an engineered Au nanoshell (AuNS)-based therapeutic oligonucleotide delivery vehicle, designed to release its cargo on demand upon illumination with a near-infrared (NIR) laser. A poly(L)lysine peptide (PLL) epilayer coated onto the AuNS surface (AuNS-PLL) is used to capture intact, single-stranded antisense DNA oligonucleotide, or alternatively, double-stranded short-interfering RNA (siRNA) molecules. A green fluorescent protein (GFP)-expressing human lung cancer H1299 cell line was used to determine cellular uptake and GFP gene silencing mediated by AuNS-PLL delivery vector. The light-triggered release of oligonucleotides could have broad applications in the study of cellular processes and in the development of intracellular targeted therapies.

Acknowledgments

The past five years, I have grown so much as a person and as a scientist in my career. I have had the pleasure to meet a great number of phenomenal people that have made getting a PhD such an enjoyable and memorable experience. I have many people to thank for my successes.

I would like to thank Dr. Naomi Halas, my research advisor, for giving me the environment to pursue cancer research, which has been a dream of mine for a long time. Under her guidance I have had the phenomenal opportunity to do research at Rice University, and the highly respected cancer institute, The University of Texas MD Anderson Cancer Center. Her guidance has made me a better critical thinker, communicator, writer, and presenter. Her enthusiasm for science, new discoveries, self-improvement, and solving relevant real-world problems, has made a big impact on me.

I would also like to thank Dr. Lin Ji, my collaborator at The University of Texas MD Anderson Cancer Center. He has graciously allowed me to work in his lab. Thank you for your help.

I owe a very big thank you to the Halas group members. Thank you to Aoune Barhoumi, for all of the research help. I enjoyed working on some very challenging projects with you. Thank you to Britt Lassiter and Mark Knight for the Halas journal club and helpful suggestions over the years, which have undoubtedly been a big part of my success in graduate school. Thank you to Surbhi Lal for all of the tedious work that you do to keep this group running smoothly. I will not miss writing the quarterly funding agency progress reports, but I will definitely miss your laughter and excellent daily attitude. Thank you to

Rizia Bardhan for all of the help in training me and giving me advice. Thank you to Ciceron Ayala-Orozco for help with growing silica, which sounds easy, but is not. Thanks Martha Alexander for all of the work you do to keep this group running. Thank you Lisa Brown. I don't know if I would have passed some of the physics courses if it were not for the late-night study sessions with you, Alvin, Sean, and Cyre. Jared Day, thanks for playing tennis and shooting some hoops (both good excuses to get out of the lab). Thank you Oara Neumann for always volunteering to help me take measurements. Thanks to the rest of the Halas group members for making this an excellent place to work: Shaunak Mukherjee, Nick King, Zheyu Fang, Felicia Tam, Alexander Urban, Amanda Jones, Michael McClain, Andie Schlather, Christyn A. Thibodeaux, Zhipeng Wang, Fangfang Wen, Yu Zhang, Sandra Bishnoi, Bruce Brinson, Joseph Cole, Tumasang Fofang, Nathaniel Grady, Janardan Kundu, Carly Levin, and Nikolay Mirin.

I owe a huge amount of my success to my parents, Martin and Kathy Huschka. Not only did they provide me with a great childhood, but they also made a number of sacrifices raising me, so that I could receive an excellent higher education. They have always supported my endeavor to purse a PhD in chemistry.

Finally, I would like to extend the greatest of gratitude to Amy, my wife, and Isaac my son. My success in graduate school could not have been possible without your support and the multitude of sacrifices you made. You both have loved me unconditionally through all of the late nights, successful days, and days when it seemed nothing would go right. For that, I thank you and I love you.

Table of Contents

List of Figures

List of Tables

Chapter 1

Introduction

Due to the unique optical properties of metallic nanoparticles, their use is becoming widespread in a variety of fields such as chemical and biological sensing,[1-4] localized surface plasmon resonance (LSPR) sensing[5-6], biomedical imaging[7-13], photothermal cancer therapy[7-8, 14-16], and solar energy collection.[17-19] Nanoparticles made of Au are particularly interesting for biomedical applications because Au is bioinert.[20] The Au surface can be easily functionalized typically via Au-thiol chemistry with therapeutics, MRI contrast agents, fluorescent markers, and targeting moieties. In this way, a nanoparticle can be designed to be a theranostic tool which is used to both diagnose and treat a particular disease. Upon excitation with light, Au nanoparticles support a plasmon resonance, a collective excitation of the conduction band electrons, which can be advantageously utilized for additional functionality. For example, the quantum yield of a fluorophore attached in the near vicinity of the nanoparticle is enhanced due to the plasmonic properties, which results in brighter fluorescence images and improved diagnostics.[10]

In this thesis, the plasmonic properties of silica-Au nanoshells, a spherical silica core surrounded by a thin layer of Au, are utilized to accomplish light-triggered release of molecules and deoxyribonucleic acids (DNA) noncovalently attached to the Au surface. The

advantage of this release strategy is spatial and temporal control over delivery of therapeutics for diseases such as cancer. The American Cancer Society predicts that one in two men and one in three women will be diagnosed with cancer in their lifetimes.[21] In addition to advances in traditional therapies such as surgery, radiation therapy, and chemotherapy, new therapy strategies need to be developed. Gene therapy shows great promise as a nontraditional therapy for cancer and other genetic diseases.[22-24] While traditional cancer therapies work by inducing cell death either by necrosis or apoptosis, gene therapy works by altering the cellular genome in order to modify or control the expression of proteins that are malfunctioning and causing cancer to grow. In this way gene therapy 'fixes' a mutated cell rather than destroying it.[25] The delivery of gene therapeutics is an extremely challenging problem and has been the focus of immense research.[26-34] Herein, the use of silica-Au nanoshells as a potential gene therapy delivery vector with light-triggered release functionality is investigated.

1.1. Scope of this thesis

Chapter 2 will give some general background on gene therapy as well as a description of both the nanoparticles and techniques used in this thesis. In Chapter 3, the observation of dehybridizing dsDNA bound to an Au nanoshell, in response to continuous wave (CW) laser excitation is reported. In Chapter 4, the mechanism of this dsDNA dehybridization is investigated by comparing the light-triggered dehybridization release behavior when dsDNA is attached to either nanoshells or nanorods. In Chapter 5, DAPI molecules, a common fluorescence small molecule used to stain the nucleus in fluorescence microscopy, non-covalently associate with the dsDNA attached to the Au nanoshell surface. After incubation

in an *in vitro* cancer cell line, the laser irradiation releases the DAPI molecules, which then diffuse to the genomic DNA and stain the cell nucleus. In Chapter 6, light-triggered release of gene therapeutics from Au nanoshells is performed to controllably deliver *in vitro* antisense ssDNA oligonucleotides and short-interfering RNA (siRNA) in order to regulate the biosynthesis of a target green fluorescent protein. Chapter 7 gives general conclusions from this thesis and provides future impact of this research.

Chapter 2

Background

2.1. Au Nanoshell Synthesis and Characterization

The nanoparticle predominately used within this thesis is the Au nanoshell, which consists of a spherical silicon dioxide (SiO_2) core surrounded by a thin layer of Au. The plasmon resonance of the nanoshell can be tuned from the visible to the infrared regions of the electromagnetic spectrum by changing the size of the core with respect to the thickness of the shell, Figure 2-1.[35] A thinner Au shell red-shifts the resonance and a thicker Au shell blue-shifts the resonance. Additionally, the plasmon resonance is dependent upon the dielectric of the core, shell and embedding medium.[36-38] This tunability is particularly advantageous for biomedical applications because the resonance can be tuned into the near-infrared (NIR) "water window" (~700-900 nm), where human tissue is maximally transparent allowing light to penetrate several inches.[39]

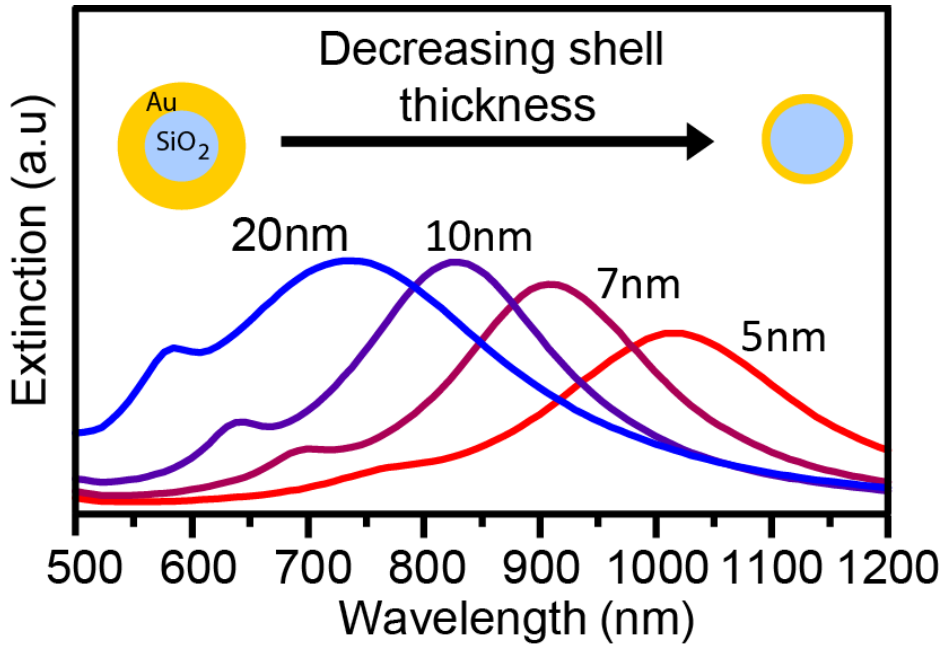

Figure 2-1. Theoretically calculated optical resonances of metal nanoshells with a 60nm radius silica core and varying Au shell thicknesses (20 nm, 10 nm, 7 nm, and 5 nm). Figure adapted from Ref. [35]

The SiO_2-Au nanoshell is fabricated following previously reported protocols.[40-41] First, monodisperse spherical silica nanoparticles are fabricated via the Stöber method, Figure 2-2A, which consist of a condensation reaction of tetraethyl orthosilicate (TEOS) at room temperature under alkaline conditions in an ethanol:water mixture. The silica cores are then functionalized with 3-aminopropyltriethoxysilane (APTES), Figure 2-2B. The triethoxy silane functional group of the APTES molecule attaches to the silica core, which leaves the primary amine functional facing outward. In a separate reaction, small Au nanoparticles ~2-3 nm in diameter are synthesized using tetrakis(hydroxymethyl)phosphonium chloride (THPC) as the reducing agent from the method reported by Duff, et al.[42]

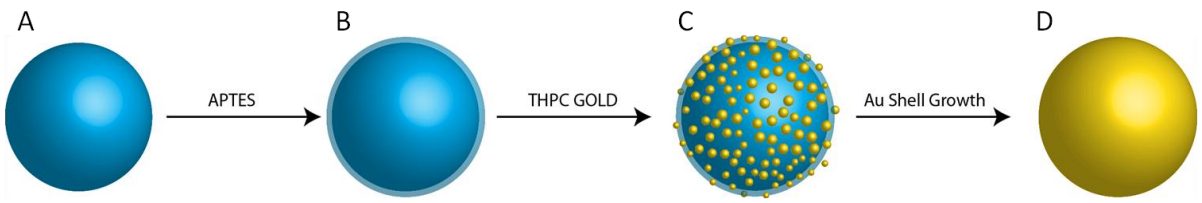

Figure 2-2. Schematic of nanoshell synthesis. (A) Silica core, (B)silica core functionalized with APTES, (C) 2-3 nm THPC Au "islands" attached, and (D) Au shell after electroless plating.

These 2-3 nm Au nanoparticles are then attached through the primary amine groups on the APTES-functionalized silica nanoparticles and serve as nucleation sites for future deposition and growth of the gold shell, Figure 2-2C. These silica cores decorated with THPC Au nanoparticles are added in the correct volume ratio to a potassium carbonate growth solution containing Au (III) chloride. A weak reducing agent (formaldehyde or carbon monoxide) is added, which reduces the Au (III) ions onto the Au islands, which then coalesce into a complete Au shell, Figure 2-2D. Starting with new reagents, Au nanoshells can be fabricated in approximately 4 weeks; however, if aged solutions are already prepared, nanoshells can be made in 2-4 days. For a detailed protocol, see appendix B.

The size of a nanoshell is denoted by the radius of the silica core (r_1) and the radius of the nanoshell (r_2), inset of Figure 2-3a. Figure 2-3 is characterization data for [r_1, r_2] = [59, 72] nm nanoshells, which consists of an UV-Vis-NIR spectrum (Figure 2-3a) and a scanning electron microscopy (SEM) image (Figure 2-3b).

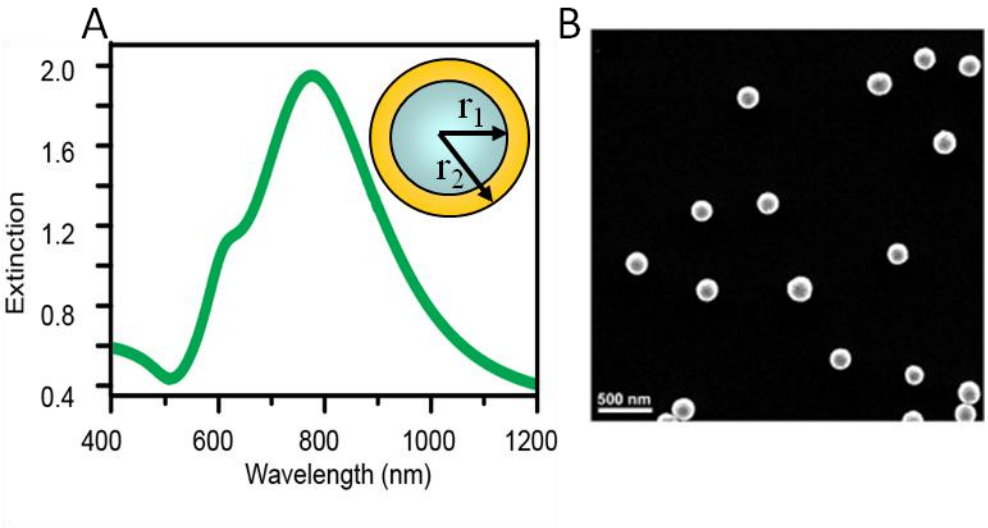

Figure 2-3. Characterization of silica-Au nanoshells. (a) Optical extinction spectra of $[r_1, r_2]$ = [59, 72] nm nanoshells ($\lambda_{max} \approx$ 800 nm). (b) SEM image of nanoshells corresponding to spectrum shown in (a).

2.2. Plasmon Hybridization

Plasmon hybridization is a very helpful intuitive model for describing the coupling observed in complex plasmonic systems. It is the electromagnetic analog of molecular orbital theory which is used to predict the interaction of atomic orbitals for the formation of molecular orbitals. For a silica core–Au shell nanoshell, plasmon hybridization explains the observed shifts in the plasmon resonance due to changes in the Au shell thickness, Figure 2-4. The model for a nanoshell is based upon the coupling of a spherical Au particle plasmon with an inner spherical cavity plasmon. The outside of the nanoshell acts as the spherical Au particle plasmon and the inside of the nanoshell acts at the inner spherical cavity plasmon. The coupling results in a lower energy symmetric mode and a higher energy antisymmetric mode. The symmetric mode is dipole active and can be excited by light; therefore it is often referred to as a bright mode. The antisymmetric mode is not dipole active and cannot be

excited by light; therefore it is often referred to as a dark mode. As the shell become thinner, the coupling between the outer spherical plasmon and the inner cavity plasmon become stronger which results in a larger energy splitting between the symmetric and antisymmetric modes. For the optically excited bright mode, this corresponds to a lowering in energy and a redshift in the UV/Vis extinction spectrum.

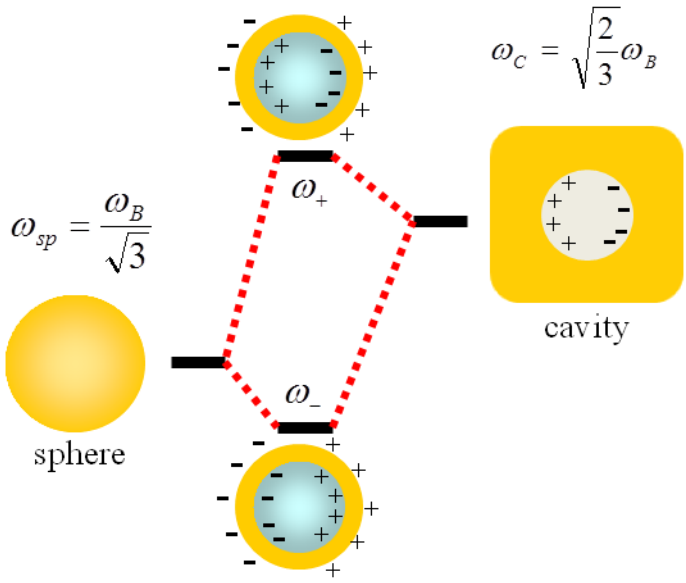

Figure 2-4. Intuitive plasmon hybridization model for a silica core, Au shell nanoshell. The coupling of a sphere plasmon and a cavity plasmon results in a lower energy symmetric mode (ω_-) and a higher energy antisymmetric mode (ω_+). Figure adapted from Ref. [43]

2.3. Au Nanorods Fabrication and Characterization

Au nanorods are another type of Au nanoparticle described in this thesis, and were synthesized using a previously published CTAB seed-mediated growth method.[44] Au

nanorods consist of strictly Au synthesized in an elongated rod-like structure. Nanorods have two primary plasmonic modes, whose excitation is sensitive to the polarization of incident light: the transverse mode, where the collective electronic oscillation of the plasmon occurs perpendicular to the long axis of the nanoparticle, and the longitudinal mode, where the plasmon oscillation occurs parallel to the long axis of the nanoparticle. While the resonance wavelength of the Au nanorod transverse plasmon is similar to that for Au colloid (~520 nm), the longitudinal resonance wavelength redshifts with increasing aspect ratio (AR),[45] which is defined as the nanorod length (l) divided by the nanorod width(w), AR= l/w, inset of Figure 2-5b.

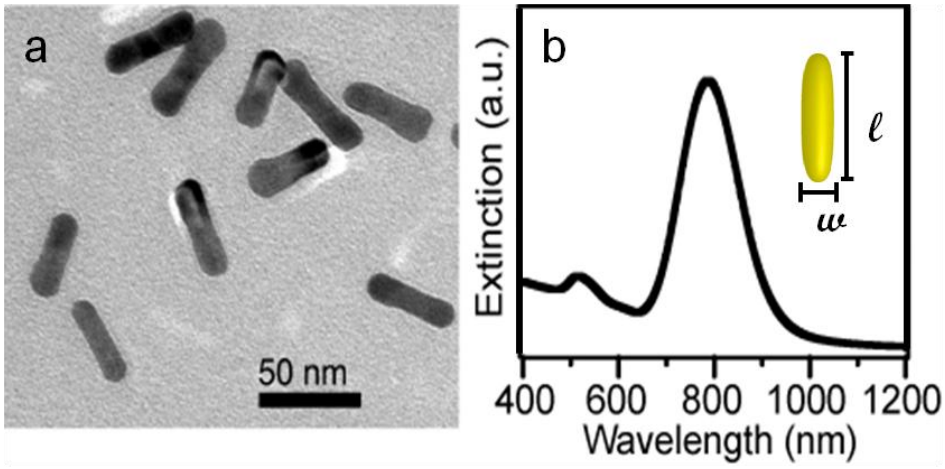

Figure 2-5. Characterization of Au nanorods. (a) Transmission electron microscope (TEM) image of [ω, ℓ] = [13, 47] nm) (B) Extinction spectra of solution of nanorods with ($\lambda_{max} \approx 788$ nm). Inset is schematic of nanorod.

The synthesis of Au nanorods consists of first making a seed solution of Au colloid stabilized by a bilayer of CTAB surfactant. To make the seed solution, Au (III) chloride ($HAuCl_4$) is mixed with a CTAB solution. Sodium borohydride ($NaBH_4$), a fast reducing agent, is quickly added which reduces the Au (III) ions into Au colloid. A CTAB bilayer

acts as a stabilizing layer around the Au colloid. Next, these seed particles are added to a growth solution consisting of $HAuCl_4$, silver (I) nitrate ($AgNO_3$), and Ascorbic acid, a slow reducing agent, dissolved in a CTAB solution. Once, the seed solution is added to the growth solution, the nanorods are placed in a 27°C water bath for 2 hours. The CTAB binds more strongly to the {110} facet compared to the {100} facet of Au. Therefore, the Au ions in the growth solution are preferentially reduced onto the {100} facet,[46] producing the rod-like shape. The reaction was stopped and the nanorods were concentrated by centrifugation and resuspended in Milli-Q water. If kept in the refrigerator, they were stable for months. For a detailed protocol of nanorod synthesis, refer to section 4.2.

Figure 2-5 shows the characterization data for [w, l] = [13, 47] nm nanorods, which consists of a transmission electron microscopy (TEM) image (Figure 2-5a) and an UV-Vis-NIR spectrum (Figure 2-5b).

2.4. Fluorescein-tagged DNA

Throughout this thesis, a common method to investigate light-triggered release of DNA from Au nanoparticles is to use fluorescently-tagged DNA oligonucleotides. Fluorescence is chosen because of its high sensitivity and is used to correlate fluorescence intensity with DNA concentration. Fluorescein is predominately used because fluorescein has a high quantum yield and does not absorb near the NIR 800nm laser, which reduces the rate of photobleaching. DNA oligonucleotides coupled with fluorescein are purchased from Integrated DNA technologies. The DNA concentration is determined by the absorption peak at 260 nm and the calculated extinction coefficient for the DNA oligonucleotide. For each known concentration, the fluorescence emission curve is measured using a fluorescence

spectrophotometer (Excitation λ: 495 nm, Emission Spectrum: 500-540 nm). Because the fluorescein emission peak wavelength is at 520 nm, a standard curve of fluorescence intensity at 520 nm versus DNA concentration was made, Figure 2-6A.

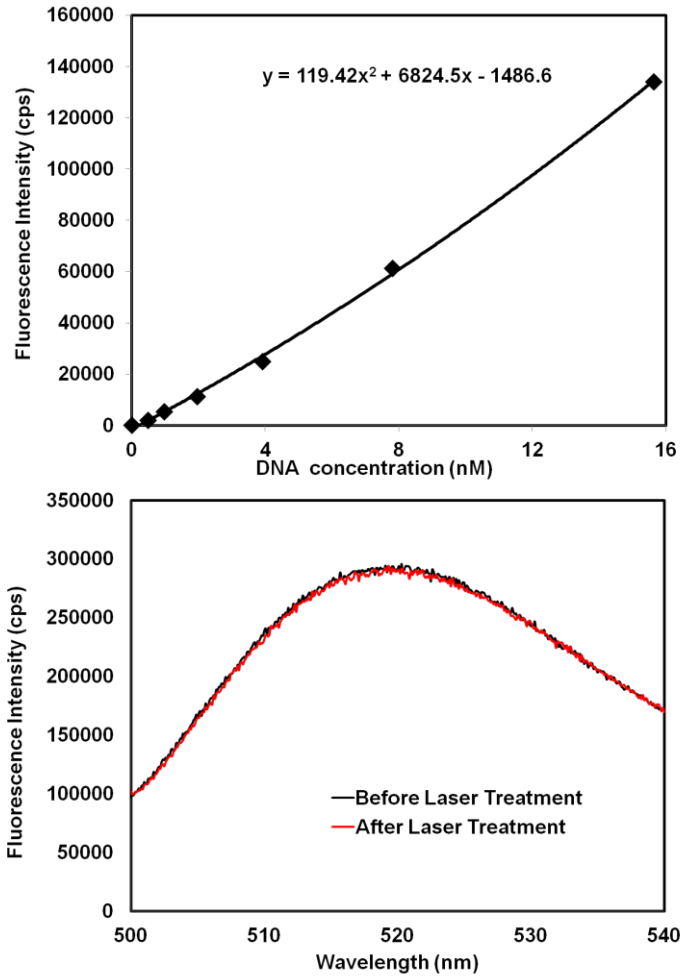

Figure 2-6. (A) Standard curve of DNA concentration (nM) versus fluorescence intensity at 520nm. (B) Emission spectra (Ex λ: 495nm) of fluorescein-tagged DNA before (black) and after (red) 800 nm laser irradiation at 1 W/cm2 for 5 minutes.

The fluorescence properties of fluorescein are pH dependent, so the fluorescein-tagged DNA is suspended in Tris-EDTA (TE) buffer (pH = 7.5) for all fluorescence measurements. Additionally, to reduce fluorescein photobleaching overtime solutions are

kept in the dark. In order to ensure that laser irradiation does not affect the fluorescence properties of fluorescein, the fluorescence intensity was checked before and after laser irradiation, which showed the fluorescence properties were unchanged, Figure 2-6B.

2.5. Flow cytometry

In this thesis, flow cytometry is used in Chapter 5 to measure the fluorescence of nuclei and in Chapter 6, when fluorescence activated cell sorting is used to separate living from necrotic cells. Flow cytometry is a common biological analysis technique used for a variety of applications including cell cycle analysis and viability, fluorescence activated cell sorting, DNA and RNA content, cell counting and cell complexity, as well as others.[47-48] Flow cytometry does multiparametric analysis of the physical and chemical makeup of each individual cell and can analyze thousands of cells per second. It works by the following process, Figure 2-7.

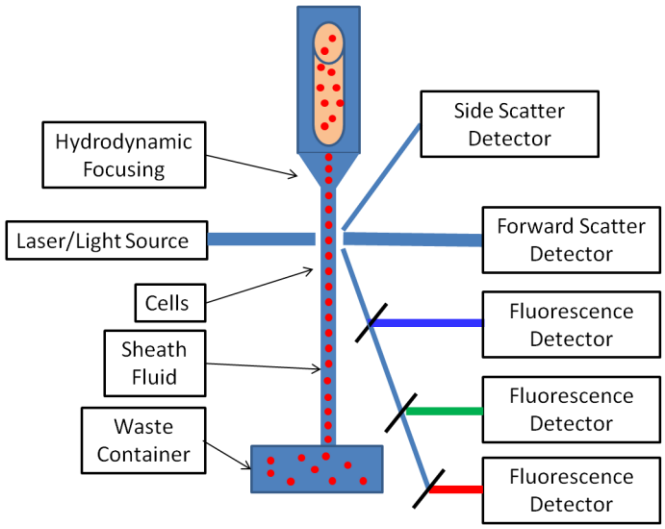

Figure 2-7. Schematic of a flow cytometry instrument.

First the cells are suspended in a stream of fluid and hydrodynamically focused into a "single-file" line in order to probe one cell at a time. A light source, either white light or a laser, is focused onto this thin stream of sheath fluid. As the cell passes through the light source it scatters light, which is picked up by forward-scattering and side-scattering detectors. The forward scattering detector gives information about the cell volume. The side-scattering detector gives information about cell complexity, such as the shape of the nucleus, cytoplasmic granules or membrane roughness. If the cell contains fluorescence signatures or fluorescence markers, then fluorescence detectors pick up these signals. Thousands of cells are analyzed within a short sampling time and the data is often plotted as a histogram for one parameter measurements or as a dot plot for two parameter measurements.

2.6. Gene therapy

The fundamental definition of gene therapy is to insert or alter genes—the DNA sequences containing all information needed to express specific proteins—in cells, resulting in therapeutic benefits for specific diseases. The goal is to control and modify the expression of certain specific proteins associated with the cause or occurrence of a disease. When a protein is undesirably expressed by unhealthy cells, inhibiting its functionality or arresting its expression is a process known as downregulation: conversely, enabling protein expression is referred to as upregulation. Following the completion of the sequencing of the human genome, gene therapy is the next logical step in the development of advanced medical treatments for human disease.

Recently, several approaches to gene delivery involving nucleic acids (DNA or RNA) have emerged as potential oligonucleotide-based therapeutic strategies for various diseases. There are four major classes of oligonucleotide therapy[25]: (i) Plasmid therapy, (ii) Antigene therapy, (iii) Antisense oligonucleotide and short interfering RNA (siRNA) therapy, and (iv) Aptamer therapy (Figure 2-8). Plasmid therapy targets DNA and introduces new genes that express proteins missing in cells. Plasmids are long, double-stranded DNA containing the foreign genetic code, delivered inside cells, to diffuse into the nucleus and become incorporated into the cell's genetic material.[49] Once integrated with the cell's DNA, plasmids become part of the genetic material, allowing continuous expression of a specific missing protein. Antigene therapy directly targets and binds to specific segments of DNA, preventing transcription to the mRNA and thus preventing protein expression. Antisense and siRNA therapies target messenger RNA (mRNA), the intermediary between DNA and functional protein, and can selectively inhibit the expression of a specific protein. Antisense is based on hybridizing a short ssDNA sequence (15–30 bases) to its complementary region on the mRNA; once bound, it blocks further translation of the specific mRNA, arresting protein synthesis.[50] siRNA is a double-stranded RNA sequence, nominally 20 base pairs long, containing the complement of the target mRNA. siRNA therapy involves a more complicated mechanism, wherein a combination of molecular complexes destroy the target mRNA and result in gene silencing.[51]. Aptamers are short single or double-stranded DNA that have been combinatorially selected to recognize and bind to specific target proteins, post-translationally, inhibiting their functionality for therapeutic benefit.[52] Here we focus on antisense oligonucleotide delivery.

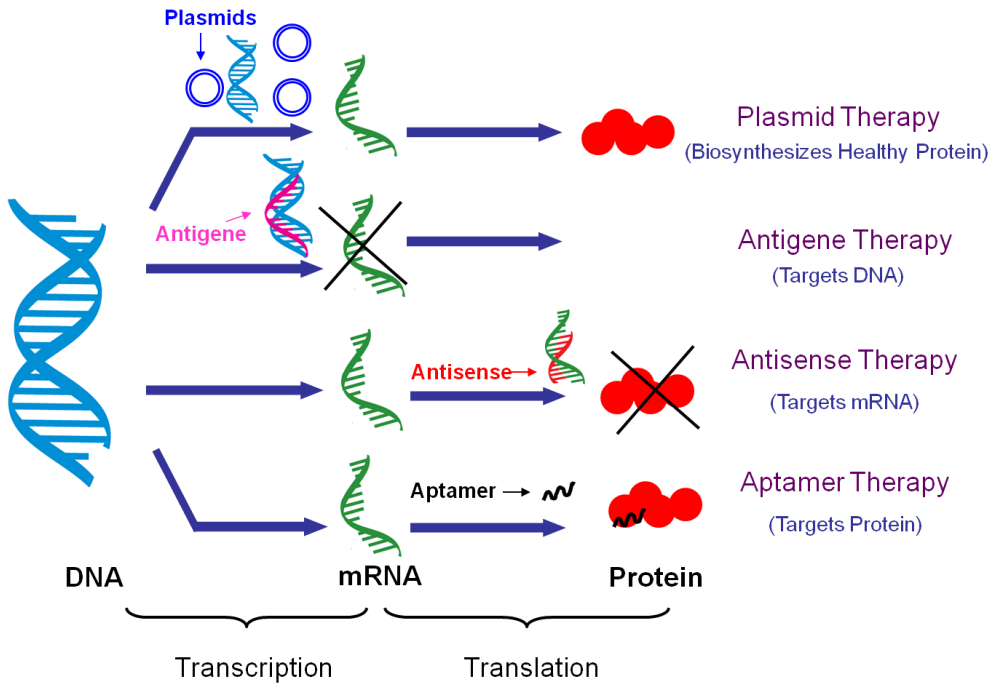

Figure 2-8.Schematic of the four major types of DNA-based therapies. Plasmid DNA enters the nucleus and biosynthesize new healthy protein. Antigene oligonucleotides enter the nucleus, form a triplex with the genomic DNA, and block transcription. Antisense oligonucleotides bind to mRNA, located in the cytoplasm, and block translation. Aptamers act as a conventional type of drug by targeting the malfunctioning protein directly.

2.7. Challenges of Antisense Oligonucleotide and siRNA Gene Therapy.

Antisense therapy was first suggested by Stephenson and Zamecnik 30 years ago.[53] The principle of antisense therapy is very simple: design a short single-stranded oligonucleotide to hybridize to a particular messenger RNA (mRNA) target, which then inhibits the translation of that specific mRNA sequence into its corresponding protein. Antisense therapy has been suggested as a therapeutic strategy for cancer, viral infections and inflammatory diseases.[28] However, there are several major inherent challenges to antisense

delivery that have impeded its translation into clinical practice.[54] Oligonucleotides by themselves cannot be injected directly into the bloodstream for systemic delivery, due to their rapid degradation (<20 min) by serum nucleases. A carrier that protects the oligonucleotides from enzymatic degradation is therefore essential to any practical delivery strategy. The DNA carrier must also be small enough and possess favorable chemical properties to extravasate (be removed from the bloodstream), be taken up by cells, deliver the oligonucleotide cargo into the cells of interest, and access the cell's genetic material so that it is available to perform its therapeutic mission. Intracellular uptake of foreign materials or structures, a process known as endocytosis, typically results in sequestration of the foreign object within an endosomal compartment inside the cell. Here again, the oligonucleotide may be subject to enzymatic degradation within the endosome. For the oligonucleotide to have its intended therapeutic effect, it must be released, or diffused from, the endosomal compartment into the cytosol and within an effective distance of the cell nucleus or ribosome, depending on its specific gene target. Originally, viruses were proposed as delivery vectors for gene therapy, because their own replication requires the injection of their genetic material into cellular hosts. Despite their inherent effectiveness in delivering oligonucleotides *in vivo*, viral vectors have induced unexpected and highly deleterious immune system responses in clinical subjects resulting in death, which is likely to prevent their ultimate approval for clinical use.[55]

To realize the promise of gene therapy as a new tool in advanced clinical medicine, safe and effective non-viral delivery vectors are critically needed.[56-57] An ideal non-viral gene therapy vector would have several important properties. It would (1) induce no immunogenic response,[26, 29, 58] (2)maintain high stability against nucleases in the circulatory

system,[27, 59] (3) target, and endocytosis into, specific cells of interest,[60] and (4) provide a means for the efficient release of oligonucleotide cargo from the endosomal compartment. These requirements have led to a strong and growing interest in Au nanoparticles of various shapes and sizes as non-viral vectors for gene therapy. The biocompatibility of Au nanoparticles and nanostructures is well established. Oligonucleotides can be bound to the surface of a Au nanoparticle in relatively dense monolayers, greatly increasing their stability against degradation by nucleases. The facile binding of various types of biomolecules to the surfaces of Au nanoparticles enables multiple functions to be imparted on the same nanoparticle 'platform': for example, combining oligonucleotide loading with antibody conjugation for targeting specific cells or tissues is realizable with this approach. Finally, remote-controlled release of DNA from a nanoparticle complex is made possible by the resonant optical properties of Au nanoparticles and nanostructures (Figure 2-3).[61-64] Resonant light absorption provides both spatial and temporal control for oligonucleotide release, which could be highly useful in research as well as in treatment scenarios. In addition, the energy input due to resonant light absorption and the accompanying local photothermal heating response may also assist diffusion of the oligonucleotides out of the endosomal compartment. In particular, nanoparticle-based complexes that respond to near infrared light, at wavelengths not significantly absorbed by cellular material, and release DNA upon resonant illumination would provide an ideal platform for light-controlled gene therapy.

2.8. Au nanoparticles and their photophysical properties

The combination of Au nanoparticles and biomolecules has enabled considerable advances in diagnostic and therapeutic nanomedicine.[65] In addition to biocompatibility and

ease of fabrication and functionalization, the optical properties of certain noble metal nanoparticles are ideal for biomedical applications. The interaction of light with noble metal nanoparticles results in collective oscillations of the free electrons in the metal known as localized surface plasmons. On resonance, a metallic nanoparticle interacts strongly with incident light, possessing an extinction cross section nominally five times its physical cross section. Resonant illumination can result in strong light scattering (useful in biological sensing and imaging) and strong absorption, with relative magnitudes depending upon absolute nanoparticle size. As absorbers, plasmon-resonant nanoparticles are unparalleled light-to-heat converters, dissipating energy via their lattice phonons.[66]

Due to their extraordinarily large absorption cross sections and their inability to re-emit light, the photothermal properties of metallic nanoparticles are arguably their dominant physical characteristic.[67-69] The physical process underlying the photothermal response of metal-based nanoparticles has been studied quite extensively using time-resolved, pulsed laser source measurement techniques.[70-72] Whether a nanoparticle absorbs or scatters light is a function of its size: small nanoparticles, essentially within the dipole, or quasistatic, limit (nominally <100 nm) are completely absorptive, while with increasing size the ratio of absorption to scattering cross section of a nanoparticle decreases in a complex manner. Ultimately, larger sized (micron-scale) particles are better scatterers than absorbers of light. Upon resonant illumination with an ultrashort laser pulse, absorptive metallic nanoparticles undergo a very rapid and dramatic increase in temperature (on the subpicosecond timescale). First, there is an initial transient regime where the electrons are at a much higher temperature than the atomic lattice of the nanoparticle. Following this initial rapid heating, the electron and lattice temperatures of the nanoparticle equilibrate on the timescale of a few picoseconds,

consistent with the inverse of the highest phonon frequency in the material. Both theoretical and experimental studies indicate that nanoparticle surface temperatures that result can easily exceed the boiling point of water, sometimes by several hundreds of degrees,[69] depending on the nanoparticle properties and illumination characteristics. In some cases, this can result in a melting/reshaping of the nanoparticle, changing its optical absorption characteristics irreversibly.[73-74] If the light-absorbing nanoparticle is immersed in a medium or fluid when illuminated, a non-equilibrium condition will exist between the hot nanoparticle and the cooler surrounding medium. At very low incident powers, this still can result in remarkably large temperature increases in the surrounding medium due to the presence of the hot nanoparticle.[75] At the lower illumination intensities of interest in biomedical applications, the photothermal response of the nanoparticle can result in heating of the local medium surrounding the nanostructure, which can be used for photothermal tumor ablation by inducing hyperthermia, with resultant cell death.[76] For the light-assisted delivery of nucleotides, sufficient incident intensities must be used to initiate the process of DNA melting on the nanoparticle surface, but must be significantly below the intensities where photothermal cell death may result.[76-79]

An additional property of the plasmon resonance of nanoparticles is the generation of nonequilibrium "hot" electron-hole pairs, a dominant mechanism for plasmon decay.[80] In addition to damping the plasmon resonance,[66] hot electrons can react with molecules at the surface of the metal nanoparticle, resulting in enhanced photoinduced charge transfer reactions.[81-83]

The plasmon-resonant frequencies of metallic nanoparticles depend strongly on particle geometry. The plasmon-resonant frequencies of metallic nanoparticles can be tuned

through the interaction, or hybridization, of plasmons supported by nanostructure geometry.[43, 84] This underlying principle, known as plasmon hybridization, has given rise to a large family of plasmonic nanoparticles whose resonances can be tuned to virtually any resonant frequency in the visible and infrared regions of the electromagnetic spectrum. For biomedical applications, a progression of Au nanostructures of various shapes and sizes has been developed with optical resonances in, or that can be tuned to, the near infrared (NIR) water window (690–900 nm).[35, 85-86] Blood and tissue are maximally transparent in this NIR spectral window, making it optimal for biomedical applications that utilize light.[39]

2.9. Thermal dehybridization of dsDNA

The temperature at which melting, or dehybridization, of double-stranded DNA in solution occurs is influenced by many factors, including composition and orientation of neighboring base pairs, sequence length, and salt concentration. For example, dsDNA with a higher percentage of Guanine–Cytosine (GC) pairs will have a higher melting temperature, because the GC pair compared to the Adenine–Thymine (AT) has greater stacking interactions and an additional third hydrogen bond. To predict the melting temperature of dsDNA in solution, the nearest neighbor (NN) model is used to determine nucleic acid stability based upon the composition and orientation of neighboring base pairs.[87-91] The NN model is based largely on experimental work over more than two decades that provided precise measurements of thermodynamic parameters.[92-98] These included specifically the binding free energy (ΔG), enthalpy (ΔH), and entropy (ΔS) for the 10 possible neighboring base pair combinations: AA/TT, AT/TA, TA/AT, CA/GT, GT/CA, CT/GA, GA/CT, CG/GC, GC/CG, GG/CC. So, by knowing the composition of dsDNA, the predicted ΔG can be

calculated by summing the ΔG_n values of each neighboring base pair plus a ΔG initiation value (ΔG_{int}).

$$\Delta G_{\text{Predicted}} = \Delta G_{\text{int}} + \sum \Delta G_{\text{n}} \qquad \textbf{(2-1)}$$

Similarly, ΔH and ΔS are calculated and used to predict the melting temperature (T_m) of complementary oligonucleotides. The total oligonucleotide strand molar concentration (C_T), and the theoretical ΔH and ΔS, are used:

$$T_m(1\text{M } Na^+) = \frac{\Delta H}{\left[\Delta S + R\ln\left(\frac{C_T}{4}\right)\right]} \qquad \textbf{(2-2)}$$

where R is the gas constant (1.987 cal K-1mol-1) [47]. The salt concentration also plays a critical role in dsDNA melting temperature. The T_m increases with increasing salt ion concentration due to the salt ions shielding the Coulombic repulsion between the negatively charged phosphate backbones of the oligonucleotides. If the salt ion concentration is low, the shielding decreases, so the dsDNA becomes less stable and the T_m decreases. There has been much debate whether the salt effect is sequence or length dependent; however, the most accurate empirical equation is a quadratic salt correction function that is sequence, composition, and length dependent.[99] Because of this extensive research effort, the Tm of dsDNA in solution is considered to be a relatively straightforward-to-predict value. However, binding dsDNA to nanoparticle surfaces for either thermal or light-induced release introduces

a new local environment for the DNA molecules which dramatically modifies solution-phase T_m values.

2.10. Au nanoparticle-based vectors for gene therapy

DNA can be bound to Au nanostructures by simple thiol chemistry or electrostatic attachment. DNA attached to Au nanostructures has an increased half-life from minutes to hours against attack by large nucleases due to the increased steric hindrance caused by attachment to the Au surface.[27] Additionally, polyvalent cations near the Au nanoparticle surface electrostatically repel dications located within the nucleases, also increasing oligonucleotide stability.[100]

Increasing the cellular uptake efficiency of therapeutic DNA is necessary for effective therapy. The attachment of either therapeutic oligonucleotides (DNA, siRNA) or existing transfection agents (cationic liposomes, cationic polymers, and dendrimers) to Au nanoparticles has been shown to universally increase cellular uptake and transfection efficiency. DNA/siRNA molecules condense when attached to the Au surface. Attaching other non-viral gene delivery vectors, such as lysine dendrimers, to Au nanoparticles has been shown to increase gene transfection 28-fold relative to the dendrimer alone.[57] Following cellular uptake, the oligonucleotides must be able to escape from the endosome, diffuse through the cell, and interact with the cell's genetic material. Currently, subsequent to cellular uptake, the DNA-bearing carriers are believed to be sequestered in the endosome. It is currently hypothesized that the use of light activated plasmonic nanostructures can effectively disrupt the endosome and release the DNA into the interior of the cell. Wu et al. have observed that light-induced endosomal disruption occurs with pulsed laser irradiation,

and suggested that transient cavitation of vapor microbubbles that form between the temperature gradient on the surface of the plasmonic Au nanoparticle and the surrounding medium are responsible for this disruption.[101]

A summary of different Au nanostructure-based gene therapies reported to date is shown in Table 2-1. Cellular delivery of DNA/RNA conjugated to Au nanoparticles can be effectively accomplished either with or without light activation. Without light activation, when the Au nanostructures are merely serving as carriers for transferring genetic material into cells, they do elicit a therapeutic response, either downregulation,[27, 102] or enhanced gene expression.[103] In general, however, the limited yield of non-light-activated therapy limits this therapeutic strategy. Light-responsive delivery vectors appear to overcome these challenges quite effectively and may be therapeutically more beneficial for controllable gene release than the non-light-activated approach.

Type of Au nanostructure	Wavelength of response (nm)	DNA/RNA binding chemistry	Type of gene therapy	Therapeutic target	Ref.
Nanorods	900	Nanorods capped with phosphatidylcholine interact with DNA electrostatically	Light activated	Plasmid DNA release	104
Nanorods	780–1100	Thiolated DNA covalently attach to Au surface	Light activated	DNA release, GFP gene expression, block mRNA translation of ERBB2	64, 105-106
Hollow nanoshells	800	Thiolated polyethylene glycol-RNA chemically bound to Au surface	Light activated	RNA interference	107
Nanospheres	520	Nanoparticles positively charged with dimethylethyl-ammonium interact electrostatically with DNA.	Light activated	T7 RNA polymerase	63
Hollow Nanoshell	800	Thiolated siRNA chemically bound to Au surface	Light activated	NF-κ***B*** p65 downregulation	108
Nanospheres	520	Ethylene glycol-alkylthiol modified RNA attach chemically to Au surface	Non-light activated	Firefly luciferase downregulation	102
Nanospheres	520–560	Plasmid DNA electrostatically attached to Au encapsulated in cationic liposomes	Non-light activated	Enhanced green fluorescent protein expression	109
Nanospheres	520	Positively charged aminated nanoparticles electrostatically attach to plasmid DNA	Non-light activated	Murine IL-2 mRNA expression	110
Nanospheres	520	Nanoparticles bearing primary ammonium groups bind with anionic DNA via ion-pairing	Non-light activated	β-Galactosidase reporter gene expression	103

Table 2-1. A summary of different Au nanostructures utilized for light activated and non-light activated gene therapy, their wavelength of response, DNA attachment chemistry, and therapeutic target.

As can be seen in Table 2-1, the combination of Au nanoparticles and light-activated DNA release has been recently identified by numerous groups as a potentially useful strategy for increased effectiveness in gene therapy. Several variations of this general approach have been demonstrated. DNA has been attached to functionalized Au nanoparticles via photoactive ester linkages, where near-UV irradiation has been used to cleave the ester moieties, releasing the DNA.[63] The potential practical biomedical applicability of this specific approach is limited, since for *in vivo* applications, NIR irradiation (690–900 nm) is highly preferable to near-UV light due to its far deeper penetration in tissue,[111] as well as its negligible mutagenicity relative to near-UV light. Therefore, plasmonic nanoparticles with resonances in the NIR region of the spectrum, such as nanoshells and nanorods, are preferentially being pursued. Nanorods either electrostatically attached to DNA[104] or covalently bound to thiolated DNA through the Au–S bond[105-106] were shown to release DNA when excited with a NIR pulsed laser at the plasmon resonance. However, ultrafast pulsed laser irradiation may reshape nanorods, which can modify their aspect ratio and their optical properties, including their resonant frequency.[106] Modifications in the nanorod geometry will reduce or eliminate the NIR absorption of these nanoparticles, and could effectively turn off NIR light-controlled release. Moreover, in biomedical applications, the reshaping of nanoparticles may also modify their pharmacokinetics and biodistribution, which may affect their safety and delay or eliminate their ultimate approval for human use. The melting and reshaping of nanorods can be circumvented by using a continuous wave laser.[64] Lee et al. conjugated thiol-modified dsDNA to nanorods, released the oligonucleotides upon NIR illumination, and successfully blocked the translation of ERBB2 mRNA in BT474 breast carcinoma cells. However, a very low percentage of cells showed protein downregulation:

further studies are warranted to quantify this response. Still, the overall strategy of near-IR triggered oligonucleotide release from Au nanoparticle-based vectors is highly promising. This collection of recently reported results is an excellent motivation for quantitative and mechanistic studies of the light-induced release process of DNA and siRNA from plasmon-resonant nanoparticle surfaces.

Chapter 3

Light-induced release of DNA from plasmon-resonant nanoparticles: Towards light-controlled gene therapy

This work was done in collaboration with Aoune Barhoumi, Rizia Bardhan, Mark Knight, and Naomi. J. Halas at Rice University

3.1. Introduction

Here we develop an Au-nanoparticle-based non-viral vector for antisense gene delivery consisting of double-stranded DNA (dsDNA) covalently attached to NIR-absorbing, plasmon-resonant Au nanoshells. Light-controlled release of ssDNA from Au nanoshells induced by resonant light absorption is demonstrated for oligonucleotide sequences of differing lengths and base compositions. The dehybridization temperatures of these sequences have been determined experimentally for both thermal and light-controlled dehybridization. Light controlled oligonucleotide release is found to occur with essentially no temperature increase of the ambient nanoparticle solution, in stark contrast to thermal release which occurs at significantly higher temperatures. Both dehybridization temperatures are found to be significantly below the solution-phase T_m for the same oligonucleotide. The

maximum dsDNA coverage, as well as the percentage of DNA released from the nanoparticle surface, are determined for both light-controlled and thermal DNA dehybridization, and are found to be quite different for these processes. This work is the first study quantifying the effects of light-controlled DNA release from plasmon-resonant nanoparticles relative to thermally driven DNA release: the characteristics observed here are likely to provide general insight and stimulus for further study of light-induced DNA release from other plasmonic nanoparticles.

Au nanoshells are spherical core–shell nanoparticles consisting of a silica core and Au shell with plasmon resonance frequencies controlled by the relative inner and outer radius of the metallic shell layer.[43, 84, 112] Au nanoshells can be designed to have their maximum absorbance in the NIR region of the spectrum.[113] This absorbance wavelength is particularly important for biomedical applications since it falls within the near infrared spectral water window where tissue is nearly transparent. When illuminated with NIR light of resonant wavelength Au nanoshells absorb a portion of the total electromagnetic energy incident on the nanoparticle complex and convert the light into heat, resulting in an increased temperature on the Au nanoshell surface. This nanoparticle-based light-to-heat conversion has been explored in other therapeutic applications, in particular for photothermal cancer therapy.[14] In this investigation, we study both purely thermal and light-controlled DNA dehybridization for DNA bound to nanoshell surfaces. The dsDNA has two strands: (1) a sense oligonucleotide with a thiol group on its 5′ end for covalent bonding to the Au nanoshell surface, and (2) a complementary antisense oligonucleotide, which is the therapeutic sequence. These two complementary oligonucleotides hybridize through Watson–Crick base pairing. In this study, the therapeutic payload is the antisense

oligonucleotide (ssDNA), and the principle is the same as antisense oligonucleotide therapy except Au nanoshells are the therapeutic carriers and light excitation controls the ssDNA release. Figure 3-1 shows a schematic of the Au nanoshell-based delivery system.

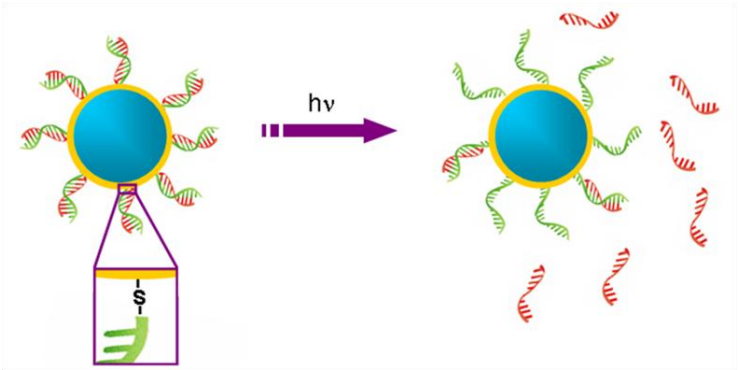

Figure 3-1. Schematic of light-controlled release of ssDNA from Au nanoshells. Green sequences are the thiolated sense sequences bound to the Au nanoshell surface, red sequences are the antisense sequences, released when nanoshells are illuminated with NIR light at their plasmon resonant frequency.

3.2. Experimental Methods

Au nanoshell synthesis. Au nanoshells were synthesized according to previously published procedures.[35, 114] The dimensions of the silica core (120 nm colloidal silica, Precision Colloids LLC, Cartersville GA) and the Au shell were chosen such that the peak plasmon resonance in aqueous suspension was 800 nm, corresponding to the excitation wavelength used in this experiment.

Thermal and light-driven DNA release To demonstrate thermal and light-controlled release of ssDNA, several DNA oligomers of varying lengths and compositions (purchased from Integrated DNA Technology Inc.) were utilized (Table 3-1). Prior to use, all thiolated DNA oligomers were reduced with 1,4-Dithio-DL-threitol (DTT, Fluka) and purified

with NAP5 purification columns (GE Healthcare). Non-thiolated DNA sequences were used as received, having been HPLC-purified by the vendor.

Oligonucleotide	Sequence (5′-3′)
$ST_{20}N1$ (70 bases)	CTGACGCTGGTTGCATCGGACGATACTACATGCCAGTTGGACT AACGGCGGGACAGCAGCTTTTTTTTT
SN2 (50 bases)	GCGGCAATCAGGTTGACCGTACATCATAGCAGGCTAGGTTGG TCGCAGTC
SN3 (30 bases)	TATGATCTGTCACAGCTTGATACTACTTCA
SN4 (20 bases)	TATGATCTGTCACAGCTTGA
SN3-comp (30 bases)	TGAAGTAGTATCAAGCTGTGACAGATCATA

Table 3-1. DNA sequences used in this study. The released sequences are shown: the capture sequences are complements of these sequences with a thiol on the 5′ end to ensure binding to the Au nanoshell surface. Labeled-sequences are the same released sequences with fluorescein on the 5′ end.

DNA hybridization was performed by mixing two complementary DNA sequences in a 1:1 M ratio in DNA hybridization buffer (TE/50 mM NaCl, pH = 7.5), heating the solution to 95 °C, then allowing it to cool slowly to room temperature in a large water bath. To ensure the maximum surface dsDNA coverage on the nanoshells, excess hybridized dsDNA was incubated with an aqueous suspension of Au nanoshells for at least 8 h. The dsDNA was first precipitated with ethanol to minimize salt concentration and avoid nanoshell aggregation.

Before the thermal or light-assisted dehybridization of dsDNA, the DNA/nanoshell mixture was centrifuged at least twice and resuspended in fresh buffer to remove excess free DNA in solution. Light-assisted release was performed as follows: 1 ml of nanoshells/DNA suspension was illuminated with a continuous wave laser (DioMed, λ = 800 nm, 1 W incident power). The temperature of the suspension (ambient temperature) was monitored with a thermocouple. For non-labeled DNA sequences, 1 mL aliquots were taken at different

temperatures and run in a 3% agarose gel. For fluorescein-labeled DNA samples, fluorescence measurements of the supernatant were performed. For thermal dehybridization, DNA/nanoshell suspension was heated in a water bath. Similarly, aliquots were obtained and run in gel electrophoresis or checked for fluorescence intensity.

DNA-nanoshell coverage and percentage release. To quantify the number of oligonucleotides on the nanoshell surface, a 12 mM mercaptoethanol solution (Sigma Aldrich) was used as a DNA-displacing solution. Mercaptoethanol rapidly displaces hybridized surface-bound oligonucleotide via a thiol exchange reaction.[115] This process is rapid and efficient because the oligonucleotide self-assembled monolayer (SAM) cannot block access of the mercaptoethanol to the Au surface. Additionally, mercaptoethanol forms a more tightly packed SAM due to its greater packing energy via Van der Waals forces than the DNA monolayer it displaces.

First, a standard curve of fluorescein-labeled DNA fluorescence intensity versus DNA concentration was experimentally determined. The amount of DNA bound to the nanoshell surface in a sample was determined by taking a fluorescence measurement of the supernatant before the mercaptoethanol displacing solution was added (background fluorescence) and after 24 h incubation with mercaptoethanol. Subtraction of the background fluorescence allowed us to obtain a value for the amount of DNA displaced. Nanoshell concentration was determined by using the Beer–Lambert law, the extinction coefficient was determined by Mie theory. Finally, the amount of DNA per nanoshell was calculated. Since the antisense strand was tagged with fluorescein, the amount of DNA released was easily quantified. After thermal or light-driven release of DNA, the difference in fluorescence

intensity was calculated and the percentage of DNA released was determined. In these experiments the displacing solution was not used.

3.3. Results and discussion

DNA dehybridization irreversibility. The purpose of this study was to compare the amount of ssDNA released by light-controlled and thermal dehybridization, and to obtain the effective DNA-ambient melting temperature for both processes. Dehybridization reversibility is a critical concern for these processes, since rehybridization of the released ssDNA back to the nanoparticle once the laser irradiation has ceased, if it occurs to a significant extent, would greatly limit the effectiveness of this strategy for gene delivery.

In the first experiment, a suspension of Au nanoshell/dsDNA (SN3 prehybridized with its thiolated complement) was prepared as described. The ssDNA antisense strand has a fluorescein label on its 5′ end. The prepared nanoparticles were divided into two samples. For both samples, DNA dehybridization was thermally induced. In one sample, an excess of the non-thiolated SN3-complement was added to solution. In the presence of the excess of the SN3-complement, the released SN3 DNA will preferentially hybridize to the excess SN3-complement in solution. For the other sample, no additional DNA was added to the solution. After thermal dehybridization of both samples under the same experimental conditions, the aliquots were centrifuged and the fluorescence intensity of the supernatant was measured. The released sequence was the only source of a fluorescence signal. If the released DNA rehybridizes with its complementary sequences left behind on the Au nanoshell surface, the amount of fluorescent DNA in solution will be significantly higher for the sample with the

excess DNA complement in solution and a measurably lower fluorescent signal when no SN3-complement is available in solution for competitive binding.

The results of this experiment are shown in Figure 3-2. Here it can be seen that the fluorescent signal due to the released DNA agrees for the two release conditions within experimental error, and that the DNA dehybridization on the Au nanoshell surface is an essentially irreversible process. This dehybridization irreversibility is critical for biological applications, and must be the case for the released DNA to be delivered to proceed to mRNA binding, in the case of antisense oligonucleotide therapy.

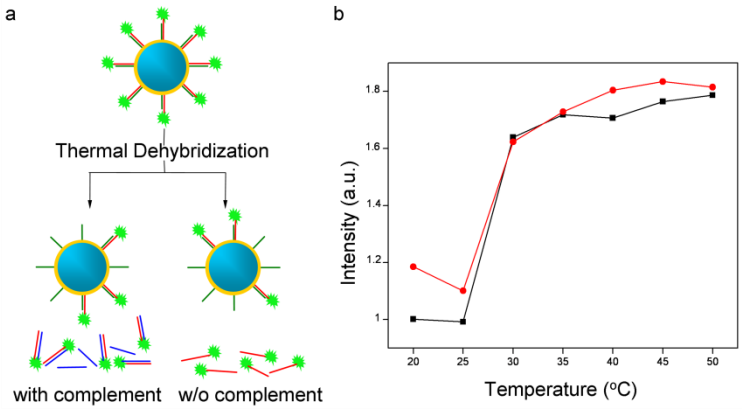

Figure 3-2. DNA dehybridization irreversibility. (a) Schematic depicting the released DNA behavior with and without complementary sequence. (b) Graph shows the amount of DNA released versus the temperature based on the released DNA fluorescence intensity with (red) and without (black) complementary sequence.

Two main factors contribute to the dehybrization irreversibility. First, rehybridization of the released ssDNA would require it to hybridize to the complementary sequences on the Au surface, a process well documented to be of low efficiency.[115] In addition, after dehybridization, the sense sequence on the nanoparticle surface may loop and bind non-specifically directly onto the Au surface, preventing rehybridization. This effect would be likely for all metal surfaces with high affinity to DNA. It is worth noting that the presence of

the SN3-complement in solution did not appreciably affect either the DNA melting temperature (around 35 °C) or the amount of DNA released. At low temperatures, however, the amount of DNA released in the presence of the excess SN3-complement sequence is slightly higher due to non-thermal DNA release, either due to non-thermal dehybridization or the presence of some non-specifically bound ssDNA on the nanoparticle surface.

Thermal release of ssDNA. dsDNA dehybridization is an essential process in all biological systems as well as many DNA-based nanotechnology applications. The mechanism of dsDNA thermal dehybridization has been thoroughly studied.[116] It has been shown that dsDNA attached to surfaces, in particular Au surfaces, behaves differently than free dsDNA in terms of melting temperature and phase transition.[117]

We first studied the thermal dehybridization of dsDNA attached to Au nanoshell surfaces. Gel electrophoresis has been used to determine the amount of ssDNA released, a process requiring no fluorescent labeling of the DNA. In the 3% agarose gel used in this work, the pore size is much smaller than the nanoshell diameter. Consequently, the nanoshells in the DNA/nanoshell suspension are trapped in the gel electrophoresis wells. Only free DNA will migrate through the gel matrix. Comparing the bands intensities of the released ssDNA from aliquots taken at different temperatures reveals the progression of the DNA release in the DNA/nanoshell sample, since the band intensity is proportional to the concentration of DNA.

DNA melting curves, obtained by monitoring the UV fluorescence (from the DNA-associated dye Syber green) in the gel column as a function of solution-ambient temperature, are shown for thermal DNA dehybridization (Figure 3-3a) and for light-induced DNA dehybridization (Figure 3-3b). The UV absorption intensity is directly proportional to the

amount of DNA released. The maximum of the first derivative of these curves, corresponding to the temperature of maximum DNA release, is defined as the DNA melting temperature, T_m. For both thermal and light-induced DNA release, the derivative plots are shown as insets. The melting temperature of the 20 base dsDNA (SN4 with its thiolated complement] attached to Au nanoshells was experimentally determined to be 37 °C (Figure 3-3a). The melting temperature of the same dsDNA sequence in solution, not confined to Au surface, is expected to be nominally 50 °C at 50 mM salt concentration (IDT DNA). Although the salt concentration on the nanoshell/DNA solution is likely to be somewhat lower than 50 mM due to ethanol precipitation of the DNA prior to binding to the nanoshell surfaces, there is still clearly a significant decrease in the DNA melting temperature when DNA is bound to the Au surface relative to the anticipated solution-phase T_m. The same trend was consistent for all DNA sequences investigated in this study. It is interesting to note that DNA melting temperature depression for DNA bound to an Au surface is still a matter of debate: both increasing and decreasing T_m for DNA on Au nanoparticles relative to the corresponding solution phase value have been reported.[117-118]

Under the experimental conditions described above, the T_m of the dsDNA sequence attached to Au nanoshell surfaces has shown a significant decrease.[117] Most likely, the high affinity of DNA to the Au surface is playing an essential role in the T_m reduction. In solution, the T_m depends solely on DNA strand length and base composition. However, when one strand of the duplex is attached to a surface, the T_m may be affected by the influence of the surface on the duplex stability. Because of the high affinity of ssDNA to the Au surface, the single-stranded DNA form is more favorable than when in solution, which would result in a decrease in DNA melting temperature.

Light-induced release of ssDNA. The DNA melting curve for light-induced DNA dehybridization is shown in Figure 3-3b, with the first derivative of the melting curve shown in the inset. Here the T_m of the 20 base DNA sequence, the same sequence used in thermal dehybridization, is 27 °C. This corresponds closely to the ambient temperature of the DNA-nanoshell suspension. This lack of temperature increase corresponds to two possible mechanisms for DNA release. These are: (1) a non-equilibrium thermal mechanism, where the irradiated nanoparticle undergoes a strong and rapid temperature increase at its surface sufficient to melt the DNA but not sufficient to raise the ambient solution temperature, or (2) a non-thermal mechanism, such as charge transfer to the DNA adsorbate, resulting in DNA dehybridization driven by Coulomb repulsion. Further experimentation would be needed to specifically identify which mechanism or mechanisms may be responsible for the DNA release.

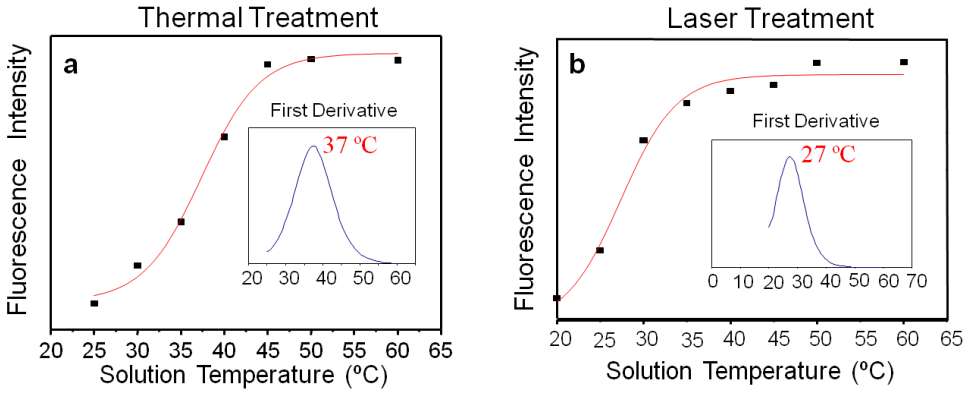

Figure 3-3. Thermal (a) and light-induced (b) release of ssDNA from dsDNA-coated nanoshells in solution. The melting curves for 20 base dsDNA attached to Au nanoshell surface are shown. Insets show the first derivatives of the melting curves, depicting the melting temperatures Tm of each process.

To examine this ambient-temperature light-induced dehybridization further, both thermal and light-assisted dehybridization experiments were performed on three other

sequences (30, 50, and 70 bases). Correspondingly, similar distinct decreases in the T_m due to thermal dehybridization and to light-assisted dehybridization of dsDNA attached to nanoshells were observed (Figure 3-4). For all sequences studied, light-assisted DNA dehybridization is observed to occur at essentially ambient temperature. While further studies are warranted to determine the specific light-induced release mechanism, the fact that release occurs at ambient temperature over a range of oligonucleotide lengths and compositions is extremely encouraging for gene therapy applications. The fact that laser-induced gene release can occur in a regime where the laser irradiation does not increase the ambient temperature indicates that this process may be useful for the safe release of oligonucleotides in cells without inadvertently compromising cell viability.

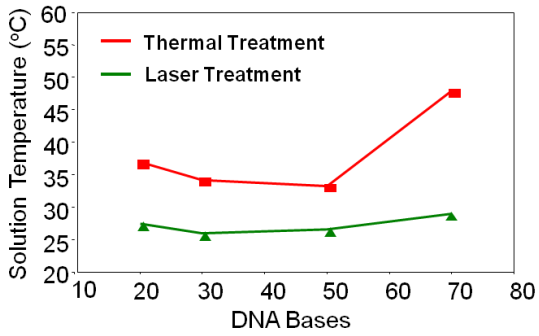

Figure 3-4. Comparison of the light-induced (green) versus thermal (red) dehybridization of dsDNA sequences of different lengths tethered to Au nanoshells. For all DNA sequences studied, the light-assisted melting temperatures are lower than 30 °C which makes this system suitable for releasing ssDNA as long as 70 bases in biological applications.

Surface coverage and percentage release. DNA surface coverage on nanoshells was determined using a previously reported protocol with minor modifications.[115] In this procedure, (i) the concentration of nanoshells is determined from the extinction spectra and Mie theory, (ii) the emission intensity of fluorescence-labeled DNA displaced from the

nanoshell surface is measured, and (iii) the fluorescence intensity is correlated to the DNA concentration through a standard, previously determined curve. The number of molecules and the percentage of ssDNA released from the nanoshell surface can be determined by comparing the fluorescence intensity before and after thermal or light illuminated DNA release.

The coverage of dsDNA molecules on Au nanoshells was determined to be 6400 dsDNA molecules/nanoshell which corresponds to 14.6 pmol/cm^2. This coverage is consistent with previous results of oligonucleotide surface coverage on Au films (18.1 ± 3 pmol/cm^2).[115] Due to the 150 nm diameter size of the NS particle, its surface is more analogous to a Au film compared to a small Au nanoparticle. This observation is consistent with published results indicating that the packing density of oligonucleotides on the surface becomes analogous to packing densities on a Au film when a spherical Au nanoparticle substrate approaches 150 nm in diameter.[119-120] The decrease in packing density determined for DNA on nanoshells relative to that reported for planar Au surfaces may be due to (1): the use of dsDNA in our studies instead of ssDNA, and (2) a decreased salt concentration needed to prevent nanoshell aggregation, which reduces electrostatic repulsion between DNA chains and decreases overall packing density.[115]

The percentage of DNA released was determined for the cases of both thermal and light-induced DNA dehybridization. While ~90% of the ssDNA is released for thermal dehybridization, only ~50% of the total available ssDNA is released for the light-induced process. The fact that these release percentages are so remarkably different provides strong support for a fundamental difference between the thermal and light-induced DNA dehybridization process. While it is not surprising that the thermal release process, conducted

under equilibrium conditions, results in the greatest percentage of ssDNA released from the nanoshell surface, it raises significant further questions regarding the actual release mechanism or mechanisms involved in light-driven DNA release. It is also important to note that the number of ssDNA molecules released per nanoshell in the case of light-induced release (3169 ssDNA/nanoshell) is considerably larger than the number of molecules released by the same process on nanorods (250 molecules/nanorod).[64] This possible dependence of yield on the aspect ratio of the nanoparticle also suggests that this process occurs under highly non-equilibrium conditions on the nanorods surface, or that a charge-transfer mechanism may be important in the release process.

3.4. Conclusions

Both thermal and light-triggered dehybridization of dsDNA, wherein one complementary strand was covalently bound to Au nanoshells, was investigated. In contrast to dehybridized ssDNA in solution, dehybridization of dsDNA bound to an Au nanoparticle surface is shown to be essentially irreversible. The melting temperatures of dsDNA bound to nanoshell surfaces was assessed for both thermally-induced and resonant light-induced dehybridization. A large difference in T_m was observed for each process, and each process occurs at a T_m substantially lower than the corresponding melting temperature of the same oligonucleotide in solution.

The light-induced dehybridization of dsDNA bound to Au nanoshells appears to occur at the solution-ambient temperature for all dsDNA sequences and lengths studied. The coverage of dsDNA on Au nanoshell surfaces was quantified and shown to correspond closely to packing densities obtainable on planar Au films. By quantifying surface coverage

of dsDNA, we were also able to determine the percentage of ssDNA released for both the thermal (~90%) and the light-induced (~50%) release process. These studies point to some very interesting and dramatic differences between thermal and light-induced processes on plasmon-resonant nanoparticle surfaces. Not only does this system provide a promising potential for light-controlled gene release for gene therapy, it also provides a new and exciting context where the rich chemical physics of substrate–adsorbate interactions may prove relevant to our understanding of light-actuating nanoparticle complexes.

Chapter 4

Light-Induced Release of DNA from Au Nanoparticles: Nanoshells and Nanorods

This work was done in collaboration with Jorge Zuloaga, Mark W. Knight, Lisa V. Brown, Peter Nordlander, and Naomi J. Halas at Rice University.

4.1. Introduction

For many reasons, Au nanoparticle-based complexes show great promise for a wide variety of biomedical applications. Their small size relative to eukaryotic cell dimensions facilitates intracellular uptake (endocytosis), providing an effective method for the transfection of adsorbate "cargo" molecules into the intracellular environment. Au nanoparticle surfaces can be readily functionalized with thiolated molecules, taking advantage of the strong Au-S bond, enabling the formation of functional nanocomplexes. This "Au nanoparticle + molecular layer" platform provides a general functional strategy for designing nanocomplexes with specific, and often multiple, functionalities. Examples of functional or multifunctional nanocomplexes constructed in this manner include enhanced

fluorescence and MRI contrast agents for bioimaging, delivery vectors for molecular chemotherapeutics or oligonucleotides for gene therapy. [10, 57, 121-122]

Au-based nanoparticles of various morphologies offer additional functionality because of their optical properties, derived from the characteristics of their localized surface plasmon. Examples of Au-based nanoparticles of interest for biomedical applications include nanoshells, nanorods, nanocages, and other geometries,[86, 123-129] that allow the plasmon resonance to be shifted from the visible into the physiological "water window" in the near infrared region of the spectrum.[39] Illumination at their plasmon resonant frequency results in light absorption, where the absorbed energy is efficiently converted to heat and can be exploited for hyperthermal cancer therapy[130-131] or photothermal drug delivery.[31, 101, 105, 122] Plasmonic nanoparticles larger than the dipole (i.e., quasistatic) limit are also highly effective light scatterers, a property advantageous for bioimaging.[132] Additionally, plasmonic nanoparticles can modify the optical density of states of nearly adjacent fluorophores, decreasing their radiative lifetime and increasing their quantum yield, enhancing their fluorescence.[12, 133-136] This property is particularly advantageous for bioimaging, since it can be used to improve the quantum yield of fluorophores already in widespread use, enhancing popular imaging modalities such as optical tomography.[137-138] An additional property of the plasmon resonance of nanoparticles, frequently overlooked, is the generation of nonequilibrium "hot" electron-hole pairs, a dominant mechanism for plasmon decay.[80] In addition to damping the plasmon resonance,[66] hot electrons can react with molecules at the surface of the metal nanoparticle, resulting in enhanced photoinduced charge transfer reactions.[81-83]

The light-triggered, remotely controlled release of oligonucleotides from plasmonic nanoparticle-based complexes is an important application that has recently begun to be investigated. Thus far, light-induced release has been demonstrated using two general strategies. One approach consists of attaching the cargo molecules to be delivered directly to the nanoparticle surface, typically through a Au-thiol bond, then using femtosecond laser pulses to reshape the nanoparticles and break the Au-S bond.[31, 104-106] This approach presents significant risk for *in vivo* applications: the incident energy sufficient to reshape plasmonic nanoparticles may very well be sufficient to induce cell death, and the smaller sized nanoparticles resulting from this process have been shown to have toxic effects. [139-140] In the second method, a "host" molecule is first attached to the nanoparticle surface, typically via a Au-thiol bond, then the cargo molecule is complexed, not to the nanoparticle surface, but to the host molecule via weaker, noncovalent interactions. When this type of nanocomplex is illuminated with light at a wavelength corresponding to the plasmon resonance of the dressed nanoparticle,[64, 122, 141-142] the attraction between host and cargo species is reduced and the therapeutic molecules are released. This release strategy shows excellent promise for light-controlled delivery due to the relatively low laser power densities and short irradiation times required to achieve release of molecular cargo.

Recently we demonstrated light-induced release of single-stranded deoxyribonucleic acid (ssDNA) from plasmonically tunable Au nanoshells, nanoparticles consisting of a spherical silica (SiO_2) core surrounded by a Au shell.[143] Nanoshells with their plasmon resonance wavelength at 800 nm were coated with double-stranded DNA (dsDNA), where one strand of the DNA possessed a terminal thiol moiety on its 5' end for attachment to the nanoshell surface. In this configuration, one strand of the DNA serves as the host molecule.

The complementary DNA cargo sequence hybridized to the host molecule was nonthiolated, and therefore, when hybridized, was bound only to its DNA complement host and not the nanoparticle surface. Upon 800 nm laser illumination, the dsDNA was dehybridized, releasing the nonthiolated ssDNA sequence. The properties of light-induced DNA release performed in this manner were compared to that of thermally induced DNA release, where the nanocomplex solution was immersed in a thermal bath and the amount of DNA released as a function of solution ambient temperature was observed.[143] Several striking differences between light-induced release and thermally induced release of ssDNA from this nanocomplex can be observed. For the light-induced case, DNA release occurs with minimal increase in solution ambient temperature, and appears largely independent of oligonucleotide length in the 20-70 base pair range. Thermally-induced release occurs at the DNA melting temperature, which is dependent upon oligonucleotide and composition, attachment to the nanoparticle surface, and properties of the solution, such as ion and nanoparticle concentration. Another marked difference between light-induced and thermally-induced release is the efficiency of DNA release. In the light-induced case, only a fraction of the ssDNA loaded onto the nanocomplexes is released, whereas for thermal release, virtually all the ssDNA cargo is released when the solution ambient temperature is increased above the DNA melting temperature. These contrasting properties prompt questions regarding the light-induced ssDNA release process, and motivate the current study.

Here we directly compare the light-induced and thermally-induced release of ssDNA from two different types of plasmonic nanoparticles: Au nanoshells and Au nanorods. Both types of nanoparticles were designed and synthesized with spectrally overlapping plasmon resonances. The release of ssDNA from both types of nanocomplexes

was quantified for both light-triggered and thermally induced ssDNA release. For light-induced ssDNA release from nanoshells, both light-induced and thermally induced contributions to ssDNA release are distinctly observable as the solution ambient temperature increases due to laser heating. This release profile allows us to discriminate clearly between the light-induced and thermally induced contributions to ssDNA release in the light-induced case. For nanorod-based complexes, both light-induced and thermally induced ssDNA release show virtually the same thermal profile, with a clear threshold for DNA release occurring at the DNA melting temperature in all cases. This contrast between nanoshell-based and nanorod-based light-induced ssDNA release can be interpreted in terms of an additional, nonthermal contribution that assists ssDNA dehybridization in the light-induced case. In our experiments, this contribution appears to be more efficient for nanoshell-based complexes than for the nanorod-based complexes investigated.

4.2. Experimental

Au Nanoshell Fabrication. Au nanoshells were synthesized according to previously published procedures.[35, 129] The dimensions of the silica core (120 nm colloidal silica, Precision Colloids LLC, Cartersville GA) and the Au shell were chosen such that the peak plasmon resonance in aqueous suspension was 800 nm, corresponding to the laser excitation wavelength used in this experiment.

Au Nanorod Fabrication. Au Nanorods were synthesized using a previous published CTAB seed-mediated growth method.[44] To make seed solution, 0.25 mL of 0.01M $HAuCl_4$ was mixed with 7.5 mL of 0.1M CTAB solution. Under vigorous stirring, 0.6 mL of ice-cold 0.01M $NaBH_4$ was quickly added. The solution turns from an amber yellow color to

a pale brown color. It is essential that the temperature of $NaBH_4$ is maintained at ~0 °C prior to mixing with CTAB and $HAuCl_4$ for proper growth of nanorods. This solution was stored in a water bath at 27°C until further use. To make growth solution, 475 mL of 0.1M CTAB was combined with following solutions under slow stirring in the following order: 20 mL of 0.01M $HAuCl_4$, 3mL of 0.01M AgNO3, 3.20 mL of 0.1M Ascorbic acid. Addition of the Ascorbic acid changes the solution from yellow to colorless. Finally, 3.60 mL of the seed solution was added to the growth solution, then it was removed from the stirring plate and placed in a 27°C water bath for 2 hours. The reaction was both stopped and the nanorods were concentrated by centrifugation (6600 rcf, 20 min) and finally resuspended to 16 mL in Milli-Q water.

Ligand Exchange of Nanorods. The CTAB on the nanorod surface was replaced with mercaptohexanoic acid (MHA) using a previously reported roundtrip phase transfer ligand exchange method.[106, 144] First the CTAB is replaced with dodecanethiol (DDT): 4 mL of the nanorod solution is placed in a glass vial and pure DDT is added on top. Upon the addition of acetone, the nanrods are extracted into the DDT organic phase by swirling for a few seconds. The aqueous phase becomes clear indicating ligand exchange. Next, the DDT organic phase is diluted with toluene and centrifuged to remove the excess DDT. Methanol may be needed to precipitate the nanorods prior to centrifugation. The supernatant was pipetted off and the DDT coated nanorods were resuspended in 2-3 mL of toluene by bath sonication for ~1 min. These DDT coated nanorods were then added to 9 mL of 0.01M MHA in toluene at ~80°C and vigorously stirred. Reflux and stirring continued until visible aggregation of the nanorods occurred (~10-12 min), which indicates that MHA has replaced the DDT, because MHA is insoluble in toluene. The solution was then allowed to cool to

room temperature, washed twice with toluene and once with isopropanol via decantation. The isopropanol deprotonates the carboxylic acid. The aggregates resuspended in 1x Tris-Borate-EDTA (TBE) buffer.

DNA Functionalization of Nanoshells and Nanorods. DNA was hybridized by combining a thiolated sequence (5'- HS - $(CH_2)_6$ - TCAAGCTGTGACAGATCATA 3') with its complementary sequence that was tagged with a fluorophore on the 5' end (5'-FLUOROSCEIN-TATGATCTGTCACAGCTTGA-3') in a 1:1 M ratio. DNA hybridization was performed in DNA hybridization buffer (TE/50 mM NaCl, pH = 7.5). The solution was heated to 95°C then allowed to cool slowly to room temperature in a large water bath. The dsDNA was then precipitated with ethanol to minimize salt concentration and avoid nanoshell aggregation. For attaching dsDNA to nanoshells and to ensure the maximum surface dsDNA coverage on the nanoshells, excess hybridized dsDNA was incubated with an aqueous suspension of Au nanoshells for at least 8 h. The excess DNA was removed by centrifugation and the dsDNA-NSs were resuspended in 1x TE buffer (IDT, pH 7.5) For attaching dsDNA to nanorods charge screening is necessary to shield the negative charge of the phosphate backbone on the dsDNA with the negative charge on the ligand exchanged nanorods, which have mercaptohexanoic acid on them. This charge screening was performed using previously published methods.[106, 144] The excess DNA was removed by centrifugation, and then the nanorods-dsDNA were resuspended in 1x TE buffer (IDT, pH = 7.5).

Thermal Treatment. A 3mL solution of the NS-dsDNA sample was placed in a centrifuge tube, then the centrifuge tube was placed in a water bath and the water bath was heated slowly (~1°C/minute) while stirring. The slow heating and stirring ensures that the NS-dsDNA sample is in thermal equilibrium. The solution temperature is monitored by a

thermocouple. The dehybridization and release of the fluorescein-tagged ssDNA is monitored by taking aliquots out of the solution as the solution temperature rises. Each aliquot is allowed to cool and then centrifuged, which separates the released DNA from the NSs. For each aliquot, the fluorescence intensity of the supernatant is measured, then by using a standard curve of fluorescence intensity versus DNA concentration, the concentration of DNA is quantified. Finally, dividing the DNA concentration by the nanoshell concentration, which is obtained from a UV-Vis extinction measurement, results in a quantitative DNA release curve.

Red Laser Treatment. Setup was the same as the thermal treatment, except the centrifuge tube was not placed in a water bath. The volume in all experiments was kept constant because the release of DNA was monitored as a function of solution temperature. Keeping the volume the same insures that any changes in the rate of heating are a result of the photothermal properties of the nanoparticle and not the volume of solution. For the 800 nm laser a DioMed 15 Plus Laser was fiber coupled. The end of the fiber couple was placed above the sample (Power 1 W, Spot size Diameter = 1 cm, Optical Intensity = Power/Beam Cross section = 1.3 W/cm^2).

Green Laser Treatment. Setup was the same as the Red laser treatment. A Coherent Verdi 532 nm laser was used (Power = 1W, Spot size Diameter = 2.25 mm, Optical Intensity= 25 W/cm^2).

Near-field Calculations. Near-field optical properties were calculated using a commercially available Finite-Element Method (FEM) package (COMSOL Multiphysics 3.5). The total electric field was calculated in the frequency domain using the RF module. The particles are defined to have a Au dielectric function as determined by Johnson and

Christy.[145] The particles were embedded in a surrounding spherical volume of water (eps=1.77). The surrounding medium is in turn embedded in a spherical perfectly matched layer (PML). The particles were excited with a plane wave. The simulation space is discretized into tetrahedral finite elements. The mesh size, simulation space volume, and PML thickness are chosen so that further changes in them do not affect the simulation results.

Instrumentation. Scanning electron microscope (SEM) images were obtained using a FEI Quanta 400 environmental SEM at an accelerating voltage of 25 k. Transmission electron microscope (TEM) images were taken using a using a JEOL JEM-2010 TEM. Extinction spectra were obtained using a Cary 5000 UV/Vis/NIR spectrophotometer. Fluorescence emission were obtained using Jobin Yvon Fluoromax 3.

Total Extinction Cross Section. Total Extinction Cross Section = Particle concentration (Particles/mL) x Volume (cm^3) x theoretical extinction cross section/nanoparticle (cm^2). Theoretical Extinction cross section for nanoshell = $1.277x10^{-13}$ m^2 and for nanorods = $3.75x10^{-14}m^2$.[146] For all experiments the total extinction cross section was normalized and checked experimentally by taking a UV-Vis of the solutions to confirm that both Nanoshell and nanorod solutions had the same extinction value.

4.3. Results and Discussion

Synthesis and Characterization of Au Nanoshells and Au Nanorods. Both Au nanorods and Au nanoshells are prime examples of nanoparticles whose properties are geometrically tunable across a range of wavelengths in the visible and near-infrared regions of the spectrum. Nanorods have two primary plasmonic modes, whose excitation is sensitive to the polarization of incident light: the transverse mode, where the collective electronic

oscillation of the plasmon occurs perpendicular to the major axis of the nanoparticle, and the longitudinal mode, where the plasmon oscillation occurs parallel to the major axis of the nanoparticle. While the resonance wavelength of the Au nanorod transverse plasmon is similar to that for Au colloid (~520 nm), the longitudinal resonance wavelength increases with increasing aspect ratio.[45] Similarly, for nanoshells, the wavelength of the plasmon resonance can be tuned from the visible into the near-infrared by varying the thickness of the Au shell relative to the size of the silica (SiO_2) core. [43]

The nanoparticles used in this series of experiments are shown schematically in Figure 4-1A. Silica core/Au shell nanoshells were synthesized using previously published methods.[35] A scanning electron microscope (SEM) image of [r_1, r_2] = [60, 76] nm nanoshells is shown in Figure 4-1B. The core and shell radii were obtained from particle size statistics obtained from SEM images of over 100 silica core particles and 100 Au-coated nanoshells. Au nanorods were synthesized according to the seed-mediated growth method using Cetyltrimethylammonium Bromide (CTAB) as a surfactant.[44] This method results in nanorods with high yields and a low polydispersity, to ensure uniform nanoparticle-to-nanoparticle plasmon resonance wavelengths. A representative transmission electron microscopy (TEM) image of [w, l] = [13, 47] nm nanorods is shown in Figure 4-1C. These length and width measurements are from particle size statistics of over 100 nanorods from TEM images. The extinction spectra of the nanoshells and nanorods synthesized for these experiments are shown in Figure 4-1D. The extinction maximum of nanoshells was observed at 797nm, and that of nanorods was observed at 788 nm, well within the broader spectral envelope of the nanoshell plasmon resonance. For all experiments, the optical density of the samples were adjusted to be equivalent at the laser wavelength of 800 nm For the

nanoparticles used, the extinction cross section of a nanorod is nearly an order of magnitude smaller than that of a nanoshell, therefore maintaining a constant optical density required a higher nanorod concentration relative to nanoshells. To adjust the optical density of the two solutions to be roughly equivalent for both samples, we used a concentration of 30 pM for nanoshells and 1 nM for nanorods. Keeping the optical density equivalent for both samples allows quantitative comparisons of light-triggered release for both nanoparticle morphologies.

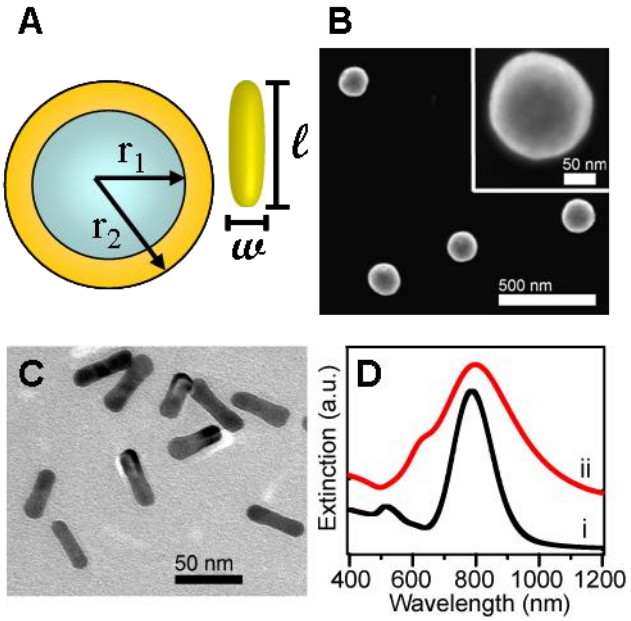

Figure 4-1. . (A) schematic of nanoshells ([r_1, r_2] = [60, 76] nm) and nanorods ([w, l] = [13, 47] nm) used in this series of experiments. (B) SEM image of nanoshells and (C) TEM image of nanorods. (D) Extinction spectra of solution of (i) nanorods with ($\lambda_{max} \approx$ 788 nm) and (ii) nanoshells with ($\lambda_{max} \approx$ 797 nm). Spectra are slightly vertically offset for clarity.

Attachment of DNA to Au nanoshells and Au nanorods. Both types of nanoparticles were functionalized with DNA oligonucleotides. In both cases, the cargo sequence is tagged with a fluorescein molecule in order to quantify nanoparticle surface coverages and ssDNA

release. The host and cargo DNA were hybridized, then bound to the nanoparticle surfaces via the thiol modification on the host DNA. The nanoshells were incubated with hybridized dsDNA as previously reported.[143] Hybridized dsDNA was attached to the nanorods by using a roundtrip phase transfer ligand exchange method[144] (See Methods section). Nanorods require a different functionalization protocol because of the need to displace residual CTAB molecules remaining on the as-synthesized nanorods following growth. This method allows dsDNA functionalization of nanorods without any harsh sonication or heating steps that other functionalization methods require. For both nanoshells and nanorods, the same 20-base dsDNA sequence is used (see Methods section).

To confirm dsDNA attachment to both the nanoshells and nanorods, mercaptoethanol was used to displace the dsDNA.[115] After displacement, the sample was centrifuged to separate the displaced DNA from the nanoparticles, a necessary step to isolate the fluorescently-tagged DNA from the Au nanoparticles, since fluorescence quenching or enhancement may occur. The fluorescence of the supernatant was measured, and the amount of DNA displaced was quantified. Dividing by the nanoparticle concentration, obtained from UV-Vis extinction measurements, yields the number of DNA molecules released per nanoparticle. For nanorods, the surface coverage is ~40 dsDNA per nanorod (normalized by surface area is ~ 4.4 pmol/cm^2); for nanoshells the coverage is approximately ~5000 dsDNA per nanoshell (~11.5 pmol/cm^2). The lower surface coverage observed for nanorods is a result of a much smaller surface area per nanoparticle (the nanorod surface area is nominally 33 times smaller than the nanoshell surface area), and is also due to the difficulty of functionalizing nanorods caused by the bilayer of CTAB surfactant surrounding the Au nanorod in solution, which limits coverage for dsDNA functionalization. Although CTAB-

free synthesis methods exist, they typically have a significantly higher degree of polydispersity and therefore significant inhomogeneous broadening of the spectral lineshape, and were therefore not pursued for this series of experiments.

Light-induced and thermal release of cargo DNA from Au Nanoshells. Thermal treatment consists of placing a 3 mL solution of the nanoshell-dsDNA sample in a centrifuge tube, placing the centrifuge tube in a water bath and heating the water bath slowly (~1°C/minute) while stirring. The slow heating and stirring ensures that the nanoshell-dsDNA sample is in thermal equilibrium during the entire course of the measurement. Laser treatment consists of placing a 3mL solution of the nanoshell-dsDNA sample in a centrifuge tube, then irradiating the sample with a continuous wave NIR laser (λ_{LASER} = 800 nm, 1.3 W/cm^2) at the peak plasmon resonance of the nanoshell while stirring the sample. Due to the photothermal properties of nanoshells, this laser excitation also results in bulk heating of the solution. In both thermal and laser treatments, the solution temperature is monitored by a thermocouple. The dehybridization and release of the fluorescein-tagged ssDNA is monitored by removing aliquots from the solution as the solution temperature rises. Each aliquot is centrifuged to separate the released DNA from the nanoparticles, and the fluorescence intensity of the supernatant is monitored to determine the number of ssDNA molecules released per nanoparticle.

A schematic of the release of DNA from Au nanoshells is shown in Figure 4-2A, where the host DNA sequence is shown in red, and the cargo DNA sequence is depicted in blue. A comparison of light-induced and thermally induced DNA release from nanoshells is shown in Figure 4-2B. The thermally induced release (Figure 4-2B, black squares) is characteristic of DNA melting, with a sharp onset at the effective DNA melting temperature.

The melting temperature of DNA is determined as half the increase in released DNA, which, for the nanocomplexes shown here, occurs at 60^{o} C. By comparison, light-induced DNA release (Figure 4-2B, red circles) results in a quite different DNA release curve. A significant fraction of the DNA is released at solution temperatures well below the DNA melting temperature. Approximately 20% of the DNA was observed to be released below the melting temperature threshold. The inset shows an expanded view of the temperature range below that of the DNA melting temperature range. For ambient solution temperatures above 50°C, DNA release is extremely similar for both heating mechanisms.

The percentage of DNA released under illumination appears highly reproducible within each prepared batch, yet varies at the batch-to-batch level in the nominal range of 20-50% over a range of experimental factors, depending upon nanoshell concentration, illumination geometry, and adsorbate concentration and structure.[117, 143] We also observe that the thermally induced release, which results in nearly 100% DNA release, shows batch-to-batch variations in the DNA melting temperature that vary based on nanoparticle and adsorbate concentration. To ensure that the Au-thiol bond was not broken in these experiments, a control experiment was performed in which a fluorescently tagged thiolated single-stranded DNA sequence was attached to Au nanoshells. Under identical thermal and laser treatment conditions, the release of this thiolated ssDNA was not observed, which demonstrated the Au-thiol bond is not broken as a result of either the thermal or laser treatments (Appendix A, Figure A-1).

The amount of time required for the entire heating process in the laser treatment is approximately 12 minutes (top axis, Figure 4-2B), however, the light-induced release begins immediately, making this method suitable for controlled delivery of therapeutic molecules.

The time scale is not linear: at higher temperatures, more time is required to heat the solution, due continuous heat loss by the experimental container to the surroundings during the course of the experiment.

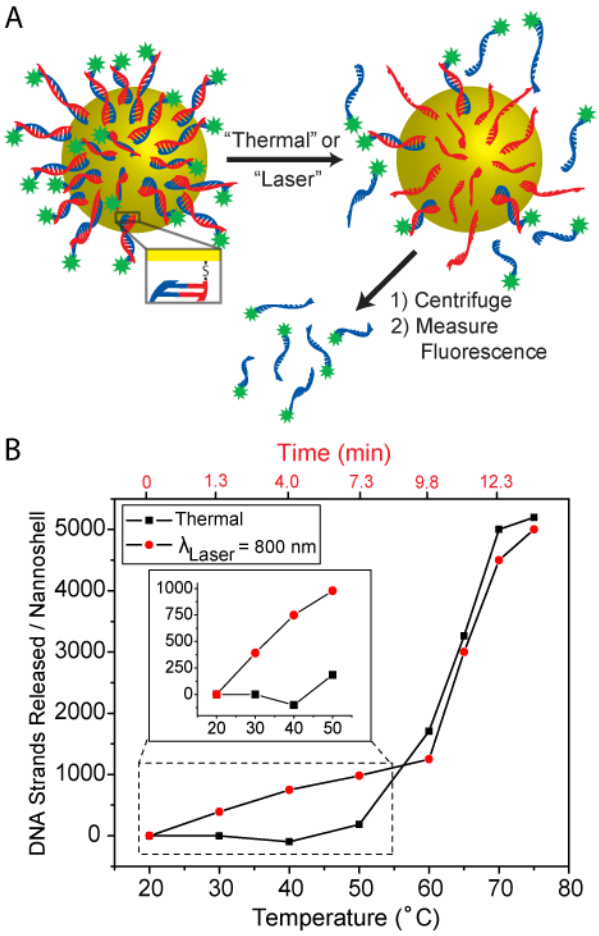

Figure 4-2. Thermal and Light-Triggered release of ssDNA from nanoshells .(A) Schematic of ssDNA release from Au nanoshells. The thiolated host sequence (red) attaches to the Au surface. The cargo complementary sequence (blue) is tagged with a fluorescein molecule (green). Upon heating (thermal treatment) or illumination with laser light (laser treatment) the fluorescein-tagged sequence is released and subsequently separated from the nanoshells by centrifugation. The fluorescence is then measured and normalized by nanoshell concentration. (B) Number of DNA strands released per nanoshell as a function of solution temperature for thermal treatment (black squares) and laser treatment (red dots). The inset shows the expanded view of the temperature range prior to thermal melting where light-triggered release is observed.

Light-induced and thermal release of cargo DNA from Au Nanorods. The light-induced release of DNA from nanorods (Figure 4-3A) was investigated with an identical protocol to that used for nanoshells. For each nanorod-dsDNA sample we compared the thermal treatment DNA release curve to the laser treatment DNA release curve with all of the experimental conditions for the nanorod-dsDNA samples identical to the nanoshell-dsDNA experiments (see methods section). Additionally, we investigated the light-induced release of DNA from nanorods by exciting the transverse plasmon resonance of the nanorod with a 532 nm CW laser. For nanorods, we fully expected to see a similar trend in the light-induced process with respect to our observations for nanoshells, but to our surprise, the nanorods did not exhibit light-induced release of DNA.

The thermal treatment of the nanorod-dsDNA sample results in a ssDNA release curve with a melting temperature of ~ 45°C (Figure 4-3B, black squares). NIR laser irradiation (λ_{LASER} = 800 nm, 1.3 W/cm^2), which drives the longitudinal plasmon resonance of the nanorod results in a ssDNA release curve (Figure 4-3B, red dots) that looks extremely similar to the thermal ssDNA release curve, with no measureable increase in DNA release at temperatures significantly below the thermal temperature. The inset highlights the temperature range, 40°C and below, prior to thermal melting where light-induced release would be clearly distinguishable if it were observed. The entire heating process for the longitudinal laser treatment on the nanorod-DNA sample takes about 6 minutes (Figure 4-3B, top axis) which is approximately half the time of the nanoshell sample. This faster heating in the nanorod solution occurs because the nanorods absorb a higher percentage of light than they scatter due to their smaller size. The optical density (total extinction cross section) of both the nanoshell-DNA and nanorod-DNA samples were kept constant, so the nanorod

solution absorbs a higher percentage of the light resulting in faster heating of the sample. The lack of light-induced release below the DNA melting temperature is therefore surprising if the process is driven by a nonequilibrium thermal mechanism: however, the thermal response observed here is consistent with another recent study of this system.[147]

Next, we investigated light-induced release of DNA from nanorods when the transverse plasmon resonance is excited. The thermal treatment for this nanorod-DNA sample (Figure 4-3C, black squares) results in a dsDNA melting temperature of ~ 50°C. The laser treatment (λ_{LASER} = 532nm, 25 W/cm^2) exciting the transverse plasmon results in a DNA release curve that again looks similar to the thermal treatment (Figure 4-3C, green dots). The inset highlights the temperature range, 45°C and below, prior to thermal DNA release where light-induced release would be distinguishable, if it were observed. The heating with the 532 nm laser for the transverse excitation of nanorods occurs the fastest (3.5 minutes), but light-induced release was still not observed. The faster heating occurs for several reasons. At this excitation wavelength, direct absorption of light by water is significantly greater than at 800 nm; additionally, the intensity of the incident laser was increased from 1.3 to 25 W/cm^2 to compensate for the smaller absorption cross section of the transverse plasmon resonance. Also, for randomly oriented nanorods in solution under polarized light excitation, twice as many will be excited with transverse polarization relative to longitudinal polarization since there are twice as many orientations where the transverse plasmon would be excited.[146] If we compare the nanoshell and the nanorod heating experiments during the time window prior to DNA melting: for nanoshells there was significant DNA release, while for nanorods there was virtually no DNA release.

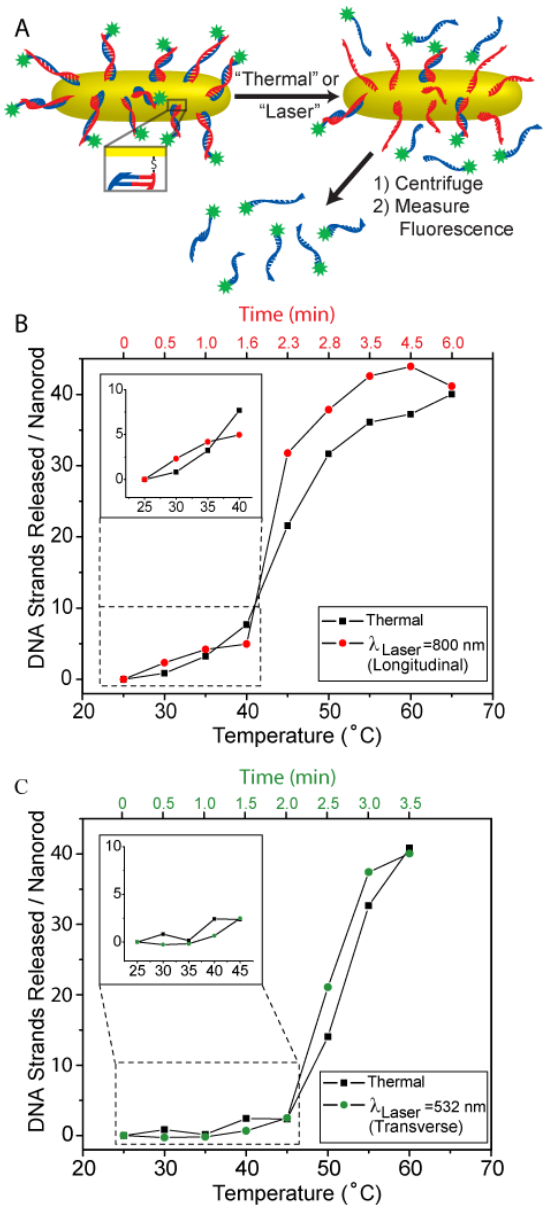

Figure 4-3. Thermal and Light-Triggered Release of ssDNA from Au nanorods. (A) Schematic of ssDNA release. The thiolated sequence (red) attaches to the Au surface. The complementary sequence (blue) is tagged with a fluorescein molecule (green). Upon heating (thermal treatment) or illumination with laser light (laser treatment) the blue sequence is released and separated from the nanorods by centrifugation. The fluorescence is then measured and normalized by nanorod concentration. (B-C) Number of DNA strands released per nanorod as a function of solution temperature for thermal treatment (black squares) and laser treatment with either (B) a near-infrared laser (λ_{laser}=800 nm) at the longitudinal resonance of the nanorod (red dots) or (C) a visible green laser (λ_{laser}=532 nm) at the transverse resonance of the nanorod (green dots). The inset shows the expanded view of the temperature range prior to thermal melting where light-triggered release is not observed.

As is clearly observed, the laser-induced DNA release that is observed on nanoshell substrates occurs at a significantly lower solution temperature than DNA melting on the same nanoparticle substrate, indicating that dehybridization of DNA occurs faster than macroscopic heating of the solution. There are two plausible mechanisms that may account for this behavior: a nonequilibrium thermal mechanism, or a nonthermal mechanism. In a nonequilibrium thermal process, the irradiated nanoparticle would undergo a very rapid local temperature increase at its surface, providing enough local heating to melt the DNA molecules prior to increasing the ambient solution temperature. A nonthermal mechanism would involve a process related to the excitation of the nanoparticle surface plasmon, such as the transfer of hot electrons from the metal to the adsorbate DNA,[80, 148] which would increase the electrostatic repulsion between DNA strands resulting in DNA dehybridization.

Following excitation, the nanoparticle plasmon can decay either by radiative damping (scattering) or energetic relaxation (absorption via Landau damping), which creates nonequilibrium electron-hole pairs.[149] These "hot" excited electrons undergo rapid electron-electron scattering and within a few femtoseconds establish a nonequilibrium hot electron distribution that can be characterized by an elevated temperature. This hot electron distribution then thermalizes with the lattice via electron-phonon coupling on a picosecond timescale. This energy is then dissipated to the surrounding medium via phonon-phonon coupling within hundreds of picoseconds, which results in heating of the ambient solution.[66] When molecules are adsorbed on the metallic nanoparticle surface, excited "hot" electrons can transfer to the adsorbate prior to thermalization.[82-83, 149] Numerous groups have observed photoinduced charge transfer under low intensity CW laser illumination conditions at the peak plasmon resonance of metal nanoparticles.[82, 148, 150]

Nonequilibrium Thermal Mechanism. To understand our observations of DNA release relative to the energy dissipation and heating occurring in our nanoparticle solutions we need to understand these processes in greater detail. In all experiments reported, the interparticle distances are sufficient to eliminate interparticle coupling between the plasmon-enhanced electric fields, which can affect the local heat generated around a nanoparticle. For the nanoshell-dsDNA and nanorod-dsDNA solutions, the particle density is 1.8×10^{10} nanoshells/mL and 6.14×10^{11} nanorods/mL, which gives an interparticle spacing of 3.8 μm and 1.2 μm, respectively. Each individual nanoparticle can be considered as an independent heat source, and plasmon coupling can be neglected. The localized increase in temperature around a single nanoparticle depends upon the absorption cross section, laser intensity, size of the nanoparticle, and thermal conductivities of both the metal and surrounding medium. [67-69, 151-152] The temperature increase on the surface of an individual nanoparticle in aqueous solution is:[151]

$$\Delta T_{NP} = \frac{\sigma_{abs} I}{4\pi R_{eq} \beta \kappa_{water}} \qquad \textbf{(4-1)}$$

where σ_{abs} = absorption cross section (m^2), I = intensity of the incident light (W/m^2), R_{eq} = radius of a sphere with the same volume as the particle $\left(R_{eq} = \left(3V_{NP}/4\pi\right)^{1/3} m\right)$ $\left(R_{eq} = \left({}^{(3V_{NP})}/_{4\pi}\right)^{1/3} m\right)$, β = Thermal capacitance coefficient dependent on nanoparticle aspect ratio (AR) $\left(\beta = 1 + 0.9658\left(\ln^2(AR)\right)\right)$ $\left(\beta_{NP} = 1 + 0.96587 \ln^2(AR)\right)$ and κ_{water} = thermal conductivity of water. For the thermal capacitance coefficient, the aspect ratio of the nanoshell and nanorod is 1 and 3.6, respectively. For our series of experiments, the

absorption cross sections for nanoshells and nanorods used were $\sigma_{abs,NS} = 1x10^{-14} m^2$, $\sigma_{abs,NR} = 2.75x10^{-15} m^2$,[146] $I = 1.3\,W/cm^2$, $R_{eq,NS} = 75nm$, $R_{eq,NR} = 11.6nm$, $\beta_{NS} = 1$, $\beta_{NR} = 2.65173$, and $\kappa_{water} = 0.6\,W/mK$. Based on these parameters, we calculate theoretical temperature increases of $\Delta T_{NS} = 2.3x10^{-4}\,K$ and $\Delta T_{NR} = 1.5x10^{-4}\,K$ at the nanoshell and nanorod surfaces, respectively. These small increases in temperature on the surface of the nanoparticles are primarily a result of the low CW optical intensities used in these experiments (1.3 W/cm^2). To obtain a significant temperature increase on the nanoparticle surface, optical intensities would be required to be ~10^4-10^5 W/cm^2, requiring pulsed laser sources.[152] The observed ambient solution heating must therefore be a result of accumulative heating, in agreement with similar analyses by Govorov and coworkers.[67-69]

Nonthermal Mechanism. The very small increases in nanoparticle surface temperature estimated for our experimental conditions suggest that a nonthermal mechanism may be responsible for light-triggered release. Since the creation of nonequilibrium hot electrons is a direct result of plasmon excitation of the nanoparticle, the greatest number of hot electrons will be generated by illumination at the plasmon resonance of the nanoparticle, where absorption is the highest. The probability of charge transfer increases with an increasing number of hot electrons. Because hot electron generation is dependent upon absorption, the magnitude of the nanoparticle absorption cross section will affect hot electron generation. For the $[r_1, r_2]$ = [60, 76] nm nanoshells and [w, l] = [13, 47] nm nanorods used in these studies, the nanoshell to nanorod absorption cross section ratio is approximately four $(\sigma_{abs,NS}/\sigma_{abs,NR} \approx 4)$, making it significantly more likely for hot electron-induced charge transfer to occur at the surface of a nanoshell.

Brus and coworkers have previously demonstrated that enhanced photochemistry can occur in areas of intense local fields at metal surfaces. [149, 153-154] To evaluate the properties of plasmon-resonant local fields on nanoshells and nanorods specific to these studies, the near-field optical properties of nanoparticles of the dimensions used in our experiments were calculated using the Finite-Element Method (FEM), Figure 4-4. The dielectric function for Au determined by Johnson and Christy was used[145] and the nanoparticles were assumed to be embedded in H_2O (see methods for simulation details). For 800 nm laser excitation the maximum enhancements calculated for nanoshells ([r_1, r_2] = [60, 76] nm) and nanorods ([w, l] = [13, 47] nm) were 7 V/m, (Figure 4-4A, i) and 38 V/m (Figure 4-4A, ii), respectively. While the maximum electromagnetic field enhancement is largest for nanorod longitudinal excitation, this large local field is confined only to the tips of the rods and decays rapidly with increasing distance from the nanorod surface (Figure 4-4B, Nanorod). By comparison, the weaker local field on the nanoshell surface is distributed over a larger surface area and decays more slowly with increasing distance (Figure 4-4B, NS). Although the field enhancement maxima are larger on the nanorod surface, the surface area providing these large field enhancements is much smaller on the nanorod (Figure 4-4A, inset). If charge transfer correlates with regions of large local field on the nanoparticle surface, fewer DNA molecules would be susceptible to charge transfer-induced processes in a nanorod-based than in a nanoshell-based complex. For a single nanorod, assuming a uniform coverage of dsDNA on the nanorod surface, approximately 12 dsDNA strands (6 on each end) on average, would be located on the ends of the nanorod where the enhancements are the highest. Therefore, although a nonthermal mechanism for DNA release is in principle possible on any plasmonic nanoparticle surface, in the complexes fabricated for this series of

experiments, the number of DNA molecules released by this mechanism, per nanoparticle, should be far greater from the nanoshell-based complex than from the nanorod-based complex.

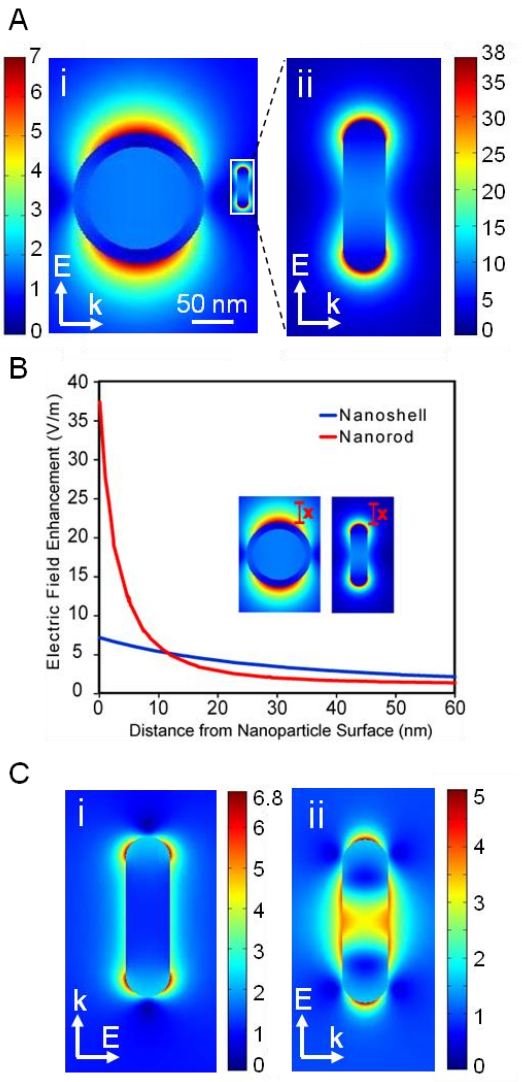

Figure 4-4. Near-field intensity enhancements of nanoshells ([*r*1, *r*2] = [60, 76] nm) and nanorods ([w, l] = [13, 47] nm) calculated using the Finite-Element Method (FEM). (A) Enhancements for a (i) nanoshell and (ii) nanorod (longitudinal polarization) when driven at λ = 800 nm. Inset of nanorod depicts the size difference between nanoshells and nanorods. (B) Electric field enhancement as a function of distance from the nanoparticle surface in the polarization direction for nanoshells (blue) and nanorods (red). (C) Nanorod enhancements when driven at λ = 532 nm for: (i) transverse polarization and (ii) longitudinal polarization.

If the transverse resonance is excited, then the local field will affect a greater number of dsDNA molecules, because the transverse plasmon would excite a greater area of the rod. However, the release of ssDNA upon transverse excitation with a 532 nm laser was not observed experimentally (Figure 4-3C). This result can most easily be explained because the transverse resonance is highly damped due to interband transitions, attenuating the near field for the transverse nanorod plasmon.

Additionally, in order to attach dsDNA to Au nanorods, an alkanethiol is required during the roundtrip phase transfer ligand exchange method. Although direct attachment of dsDNA to nanorods was attempted, it was determined that the roundtrip phase transfer ligand exchange method used for these set of experiments gave the most reliable and highest dsDNA surface coverage. The residual alkanethiol molecules on the surface of the nanorod could be playing a role in regards to the charge transfer process. This effect would only be noticed in areas of high electric field, where hot electrons are generated; and for nanorods, this area of enhanced electric field is much smaller compared to nanoshells. Further study may be needed to investigate the effect the alkanethiol has on light-triggered release.

Finally, the dsDNA packing density for these nanorod-dsDNA samples (~4.4 pmol/cm^2) presented in this article is approximately half that of nanoshells (~11.5 pmol/cm^2), which could potentially affect the light-triggered release process. However nanorod-dsDNA samples with packing densities comparable those on nanoshells (~120 DNA/nanorod, ~13.2 pmol/cm^2), still did not exhibit light-triggered release with the 800 nm laser excitation (Appendix A, Figure A-2). Additionally, the fluorescence intensity of the fluorescein-tagged DNA was unaffected by laser irradiation (Appendix A, Figure A-3)

4.4. Conclusion

We have examined the process of light-induced DNA release, relative to thermally induced DNA melting, on specially functionalized Au nanorod and nanoshell complexes. A clear distinction between light-induced DNA release, occurring at temperatures well below thermal release, and thermally-induced DNA release was observed on nanoshell-based complexes. For nanorod-based complexes treated under the same irradiation conditions only thermally-induced release of DNA was observed. In our experimental regime, where irradiation of the nanocomplexes is performed using low-intensity CW laser sources, the nanoparticle surface temperature increases appear minimal, and a nonequilibrium thermal mechanism involving high local temperatures at the nanoparticle surface appears unlikely for light-induced release. Instead, it appears quite feasible that the observed light-induced release may be explained by a nonthermal model, where hot electrons produced by plasmon decay are transferred to the adsorbate host-cargo system, facilitating dehybridization well below the DNA melting temperature. While both complexes should be responsive to such a release mechanism, differences in absorption cross sections and DNA densities on the nanoparticle surfaces render this effect observable only on nanoshell based complexes, for the present set of experimental conditions. Further examinations of this process should enable the development of light-induced release based vectors for a wide range of nanoparticle morphologies, and the design of more efficient plasmonic nanoparticle-based delivery vectors.

Chapter 5

Visualizing light-triggered release of molecules inside living cells

This work was done in collaboration with Oara Neumann (equal contributor), Aoune Barhoumi, and Naomi. J Halas at Rice University. Lin Ji from The University of Texas MD Anderson Cancer Center allowed me to use the cell culture facility in his lab.

5.1. Introduction

Strategies for the directed release of controlled quantities of molecules inside living cells are in high demand for drug delivery,[155] gene therapy,[156-157] and tissue engineering.[158-159] The release mechanisms of most delivery vectors depend on processes such as diffusion, dissolution, chemical and enzymatic reactions, or changes in various environmental factors such as temperature, pH, solvent, and ionic concentrations.[156, 160-163] For example, transfection reagents such as polyethylenimine act as a proton sponges following endocytosis, absorbing protons in the low-pH environment of the endosome, causing it to swell and eventually rupture, facilitating gene delivery.[164] This type of environmental control of molecular release varies with cellular location and cell type, and can result in

unpredictable release. A physical release mechanism that does not rely on the specific chemical properties of the cellular environment would be highly useful and more easily generalizable to various cell types.[165] Light-induced release is a particularly attractive option: the high spatial and temporal control that lasers provide would be highly useful for initiating and following intracellular processes dynamically, at the single cell level.[31, 106, 166-170]

Plasmonic nanoparticles, metal-based nanostructures supporting collective electronic oscillations, are highly promising potential candidates for facilitating controlled light-triggered release, due to their large optical cross sections, their geometrically-tunable optical resonances[171-172] and their strong photothermal response.[173-174] Because of their large cross sections and extremely low quantum yield, metallic nanoparticles convert optical energy to thermal energy with high efficiency upon resonant optical illumination.[69, 175] Resonant optical illumination of the nanoparticle triggers the controlled dehybridization and release of DNA molecules adsorbed onto the nanoparticle surface.[168, 170] Au nanoparticles are also biocompatible, easy to fabricate, and can be functionalized with a wide variety of host-carrier molecules capable of noncovalent accommodation of guest molecules.[160, 170]

Au nanoshells, metallodielectric nanoparticles comprised of a spherical dielectric core covered by a thin Au shell, have been successfully employed in a range of biomedical applications[176-178] including photothermal cancer therapy.[174, 179-180] The plasmon resonance wavelength of a nanoshell can be varied by changing the core size and shell thickness.[172, 181] This tunability is particularly important for biomedical applications because the nanoshell can easily be designed to have a large absorption efficiency in the near infrared (NIR) water

window (690-900 nm), where blood and tissue are maximally transparent and light can penetrate tissue to depths of several inches.[182]

Recently we demonstrated light-induced dehybridization of double-stranded DNA (*ds*DNA) attached to Au nanoshells.[170] Nanoshells of dimensions $[r_1, r_2] = [63, 78]$ nm with the plasmon resonance wavelength at 800 nm were coated with *ds*DNA, where one strand of the DNA had a thiol moiety on its 5' end, facilitating covalent attachment to the nanoshell surface by a Au-thiol bond. The complement DNA sequence was nonthiolated, and therefore bound only to its complementary DNA sequence and not to the nanoparticle surface. Upon illumination with NIR light at the nanoshell plasmon resonance wavelength, the *ds*DNA was dehybridized, releasing the antisense sequence. This process is highly efficient, resulting in the dehybridization and release of nominally 50% of the DNA from the complexes upon illumination, with no apparent temperature increase in the solution ambient. DNA antisense therapy has been explored extensively as a class of gene therapy and has highly promising potential to provide safe and effective treatments for a multitude of diseases and genetic disorders.[183]

Here we show that, in addition to light-controlled release of DNA, the nanoshell-*ds*DNA complex serves as an effective host and light-triggered release vector for other types of molecules. Many types of guest molecules can associate with *ds*DNA, either by intercalating between adjacent base pairs or by binding in either the major or minor groove of the DNA double helix.[184] The driving forces for association can include π-stacking, hydrogen bonding, van der Waals forces, hydrophobic and polar interactions, and electrostatic attractions; therefore, *ds*DNA can host a large variety of guest molecules via noncovalent bonds.[184-185] DAPI (4',6-diamidino-2-phenylindole), a water soluble blue

fluorescent dye that binds reversibly with *ds*DNA (Figure 5-1) is the molecule we chose to deliver, to demonstrate and clearly visualize the light-induced intracellular release. DAPI was chosen because of its bright fluorescent properties, stability and negligible toxicity.[186] DAPI binds preferentially to the minor grooves of *ds*DNA: its association with DNA causes a large increase in its quantum yield.[186-190] The selectivity of DAPI to *ds*DNA makes it a frequently used, standard stain for cell nuclei in fluorescence microscopy.[189-190]

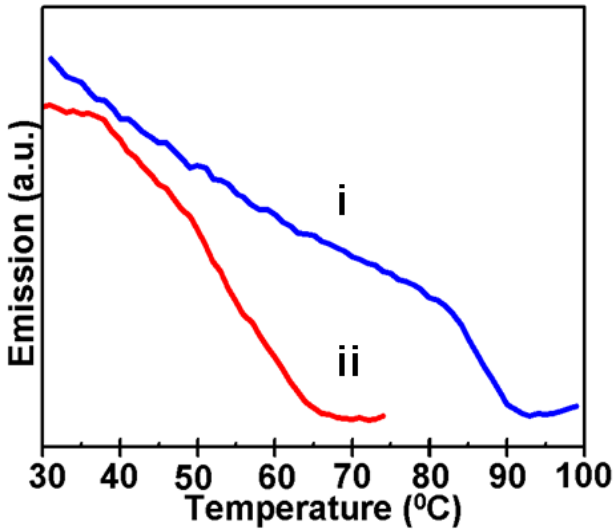

Figure 5-1. Fluorescence emission of DAPI as a function of temperature (heat rate is of 10C/min) showing reversible binding of DAPI (i) from dsDNA in solution and (ii) from nanoshell-dsDNA-DAPI complexes. As the DAPI is released, the fluorescence emission intensity decreases.

5.2. Experimental Methods

Reduction of thiolated ssDNA. The oligonucleotides used in this study are: 26-bp DNA oligo: 5'-GAT ATC CTA TAC GGA ATT CGA ATT CG-3', 50bp DNA oligo: 5'-GAC TGC GAC CAA CCT AGC CTG CTA TGA TGT ACG GTC AAC CTG ATT GCC GC-3', and the complementary 26bp and 50bp ssDNA sequences for both strands. DNA was

purchased from Integrated DNA Technologies (IDT) Inc. The thiolated ssDNA [26 or 50 bp] was incubated with 100 mM of DTT (reducing agent) in 100 mM sodium mono-phosphate buffer at pH=7.5. The mixture was incubated at room temperature for 1 hour to allow for complete reduction of the disulfide bonds. The solution was then filtered through a NAP-5 column to remove the excess DTT. Elution of the column with water was performed to collect the purified ssDNA in H2O. The concentration of the ssDNA stock solution was determined by measuring its absorbance at 260 nm, using a UV-Vis-NIR spectrophotometer (Cary 5000, Varian Inc.).

Nanoshells preparation and DNA Functionalization. Silica core-Au nanoshells were fabricated using a method previously described.[191-192] Au-silica nanoshells were fabricated with core and shell dimensions of $[r_1, r_2]$ = [63, 78] nm, corresponding to a nanoshell plasmon resonance at 800 nm in aqueous solution, which is the wavelength of the excitation laser used in the photothermal experiments. *ds*DNA was hybridized by mixing two complementary *ss*DNA sequences at a 1:1 molar ratio in DNA hybridization buffer (Tris EDTA (TE)/50mM NaCl, pH=7.5), heating the solution to 95^0C for 10 min in a large water bath and then cooling slowly to room temperature. *ds*DNA was attached to nanoshells via overnight incubation and continuous shaking. To remove the excess *ds*DNA the solution was washed three times by centrifugation and resuspension in TE buffer.

DAPI stained DNA-functionalized nanoshells. DAPI (Sigma) was used without further purification. The concentration of the DAPI stock solution was determined spectrophotometrically using the molar absorption coefficient (ε_{342}nm=23,000 $M^{-1}cm^{-1}$ for DAPI in water). The stock DAPI solution was kept stored at -20^0C. After purification the

NS-*ds*DNA complexes were incubated overnight with DAPI solution and then washed three times by centrifugation and resuspension in TE buffer to remove the excess DAPI.

Cell Preparation and Nanocomplex incubation. The H1299 lung cancer cells are cultured in media (Gibco) supplemented with 5% heat-inactivated fetal bovine serum, 1% antibiotics and maintained in a 37°C incubator with 5% CO_2 air. Cells were initially seeded in 6-well plates at a density of 400,000 cells/well 24 hours prior to incubation with nanoshell-*ds*DNA-DAPI complexes. The nanoshells were added to the serum containing media in a NS:Cell ratio of 10,000:1. After 1 hours of incubation with nanoshell-*ds*DNA-DAPI complexes, the media was aspirated off. Cells were washed two times with PBS. Cells were detached from the plate with trypsin and the cells were finally suspended in additional media.

Laser Treatment. Half of this cell/media suspension underwent laser treatment (5 minute illumination at 80o nm with continuous wave laser, 1W/cm2). The other half did not receive a laser treatment. This laser power and time is chosen from previous DNA dehybridization studies. After laser treatment, both samples (laser and no laser) were allowed to incubate for 1 hour to allow released DAPI molecules to diffuse to the nucleus.

Isolation of Nuclei and Flow Cytometry. Nuclei were isolated using Nuclei Isolation Kit: Nuclei EZ Prep (Sigma Aldrich, NUC101-1KT). Briefly, the cells were collected via centrifugation (500xg/4°C/5min). Washed once with PBS. Resuspended and centrifuged twice in Nuclei EZ Prep lysis buffer. Final suspension was in 250 uL of PBS. Flow cytometry was performed on BD influx. The excitation laser was a 355nm solid state UV laser. Emission was collected at 460nm. Data was analyzed by FlowJo and the histograms were normalized by % of max.

Statistical Analysis. For statistical analysis, the SEM (standard error of the mean) was calculated by dividing the standard deviation by the sample size. Sample size for Figure 5-6a: 19,100. Sample size for Figure 5-6b: 47,800. Because of the large sample sizes, the data was treated as being normally distributed, which is preferred over using a nonparametric statistic test. An unpaired t-test was performed to determine the significance at a 95% confidence interval. The p-value reported is a two-tailed p-value. A p-value less than 0.05 is determined to be statistically significant.

Cytoviva Microscope. The Cytoviva microscope is a dark-field/epifluorescence microscope. Excitation and emission filters on the dual mode fluorescence microscope are used to choose the right wavelengths of light for fluorophore excitation and emission collection. All images are taken with a 40x objective. The white light source is an Expo Cytoviva X-cite series 120 light source, mounted on an Olympus BX41 microscope. The camera is a Dage Technologies Exponent CCD camera.

Cytoviva Sample Preparation. After laser treatment, cells were plated and grown on chamber slides as previously described. Chamber slides are used so that the walls of the slide can be removed and imaging can be done on the slide. After 12 hours of incubation, cells were washed three times with 1x PBS. A fixing solution (4% paraformaldehyde) was added to the chamber slide and allowed to incubate for 15 minutes at room temperature. The fixing solution was aspirated off and the cells were washed three times in 1x PBS. A staining solution of Alexa Fluor 488 (5.0 μg/mL in PBS) was added to the chamber slide and allowed to incubate for 10 minutes at room temperature. Staining solution was aspirated off and the cells were washed twice with 1x PBS. The cells were then mounted with anti-fade fluorescence mounting medium and glass coverslip.

5.3. Results and Discussion

A schematic of the light-triggered molecular release is shown in Figure 5-2. Initially, nanoshell-*ds*DNA complexes were loaded with DAPI by incubation of DAPI with the nanoshell-*ds*DNA complexes. Next, the nanoshell-*ds*DNA-DAPI complexes were incubated with H1299 lung cancer cells, where intracellular uptake was verified using both dark-field and bright-field microscopy. Upon illumination with an 800 nm CW laser, corresponding to the peak resonant wavelength of the nanoshell complexes (Figure 5-3), the DAPI molecules were released from the nanoshell complexes. Subsequent to release, the DAPI diffused through the cytoplasm and into the cell nucleus, where it preferentially bound and stained the nuclear DNA. To the best of our knowledge, this is the first light-controlled delivery system that can be tailored to release quantifiable amounts of nonbiological molecules, within living cells by remote means, on demand.

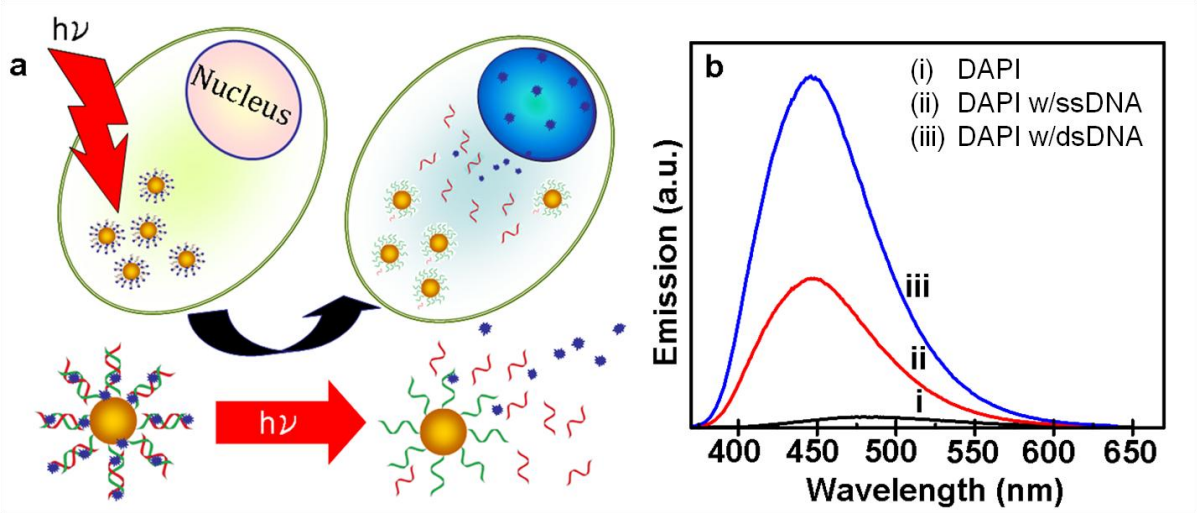

Figure 5-2 Light-induced DAPI release. (a) Schematic diagram of the light-induced DAPI release and diffusion inside the cell. (b) Fluorescence emission of (i) DAPI only, (ii) DAPI with ssDNA, and (iii) DAPI with dsDNA.

The DAPI fluorescence emission intensity drastically increases as a result of DAPI molecules binding to DNA (Figure 5-2b). As an isolated molecule, DAPI has a low quantum yield (Figure 5-2b, i), [187] however, when DAPI is attached to single stranded DNA (*ss*DNA) (Figure 5-2b, ii), a weak electrostatic attraction binds the cationic DAPI molecules to the negatively charged phosphate backbone of the DNA, resulting in a slight increase in its fluorescence intensity. [187] When the DAPI molecules bind to the minor grooves of the *ds*DNA (Figure 5-2b, iii),[187, 190] the increased rigidity and stabilization significantly increases its quantum yield.[186] DAPI binding to the *ds*DNA also displaces H_2O molecules initially solvating the DNA oligomers, significantly reducing intermolecular proton transfer between H_2O and DAPI, resulting in an additional increase of DAPI fluorescence intensity.[187-188, 193]

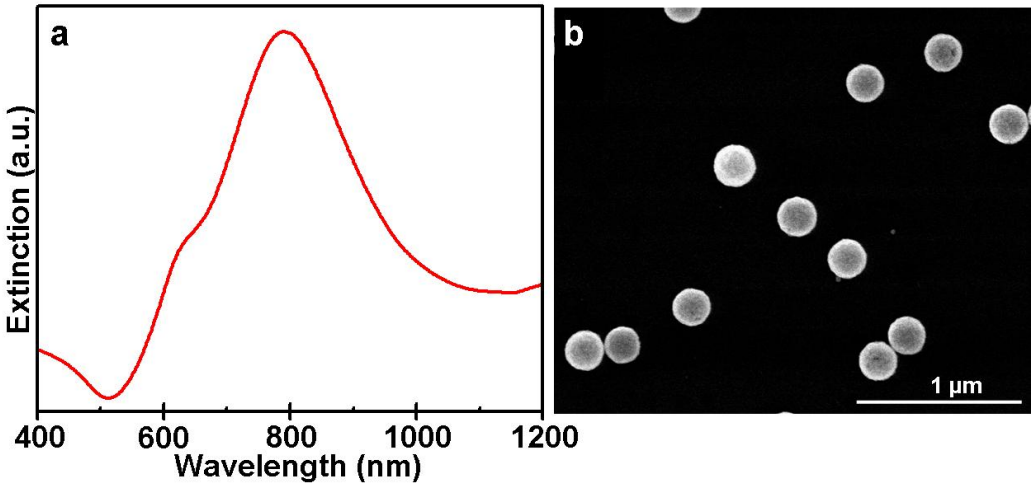

Figure 5-3. (a) Extinction spectra of [r_1, r_2] = [63, 78] nm NSs in water. (b) SEM image of NSs on silicon substrate.

The specific base-pair composition of the *ds*DNA plays an important role in determining the number of DAPI molecules that will bind to the *ds*DNA.[194] Previous studies have shown that DAPI preferentially binds to regions rich with adenine (A) and thymine (T) nucleotide bases because DAPI forms hydrogen bonds with A-T bases pairs.[190] The DAPI molecule is 14-15 Å long, corresponding to an overlap of three base pairs.[187-189, 194] In our experiments, since it is desirable to bind as many DAPI molecules as possible to improve the staining of the nucleus after light-induced release, we designed a 26-base pair sequence with multiple A-T-rich regions with segments of three or more consecutive A-T base pairs to specifically enhance DAPI loading (Figure 5-4).

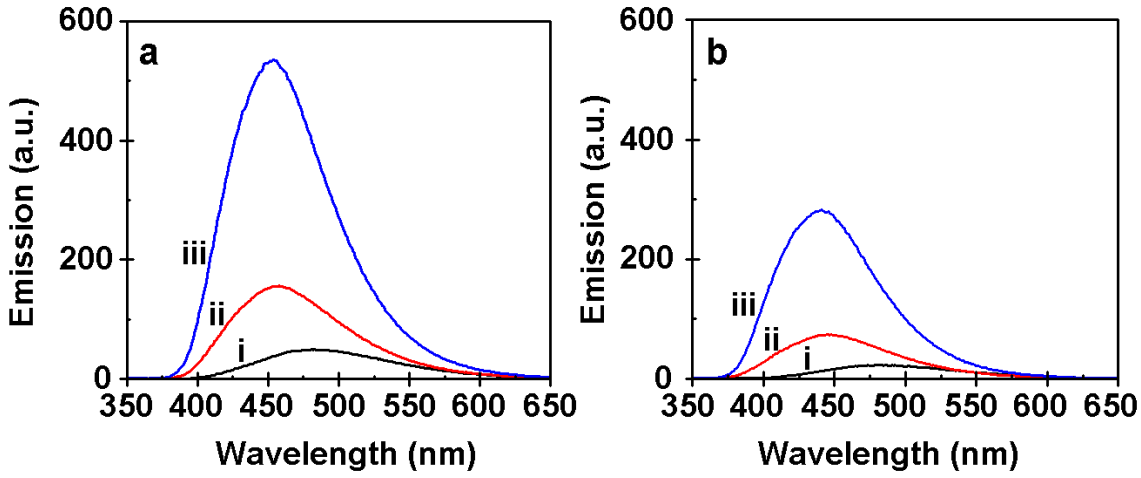

Figure 5-4. Fluorescence spectra of (i) DAPI alone, (ii) DAPI with *ss*DNA, and (iii) DAPI with *ds*DNA solutions; (A) 26 bp DNA and (B) 50 bp DNA oligonucleotide, demonstrating the affinity for AT-rich binding sites. The DNA oligonucleotides used in this study are: 26-bp DNA oligo: 5'-GAT ATC CTA TAC GGA ATT CGA ATT CG-3' and 50bp DNA oligo: 5'-GAC TGC GAC CAA CCT AGC CTG CTA TGA TGT ACG GTC AAC CTG ATT GCC GC-3'

To use this light-triggerable complex for molecular release in live cells, the complex must first be effectively taken up by the cells of interest. To facilitate cell uptake, the nanoshell-*ds*DNA-DAPI complexes were incubated with H1299 lung cancer cells in serum containing cell culture medium for 1 hour. After incubation, the cells were fixed and internalization of the nanoshell-*ds*DNA-DAPI complexes was imaged using both dark field (Figure 5-5a-b) and bright field (Figure 5-5c) microscopy. Nanoshells in this size range both absorb and scatter light: their strong scattering cross section enables them to be easily visualized by optical microscopy. In Figure 5-5a, a H1299 cell with its cell membrane marked by the green fluorescence dye Alexa Fluor 488 WGA (wheat germ agglutinin) is shown. Internalized nanoshells are easily seen as diffraction-limited bright spots in this image. As a control, cells not incubated with the nanoshell-*ds*DNA-DAPI complexes showed no observable bright spots when imaged in the same manner (Figure 5-5B).

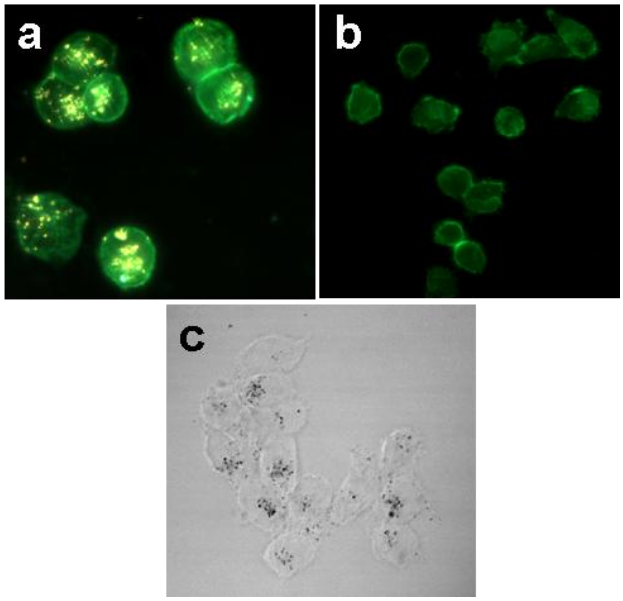

Figure 5-5. Nanoshell-dsDNA-DAPI Cell uptake. Dark field/epifluorescence images of (a) H1299 lung cancer cells incubated with nanoshell-dsDNA-DAPI complexes, (b) nonincubated cells (control). (c) Bright field image of middle slice of H1299 lung cancer cells incubated with nanoshell-dsDNA-DAPI complex.

Because the dark-field images are two-dimensional, these images alone do not give clear evidence whether the nanoshell complexes have been endocytosed, or are merely adsorbed onto the outer membrane of the cell. Bright-field imaging was used to further investigate cellular uptake. Obtaining images at varying depths of field within an individual cell allows us to clearly visualize in three dimensions the nanoshell distribution within the cell. Figure 5-5c is a slice from the middle of the cell showing clear diffraction-limited dark spots corresponding to nanoshell complexes, verifying that the nanoparticles are internalized within the cell. Internalization of nanoshells is in agreement with observations by Ochsenkühn *et al*, who used TEM sections of NIH-3T3 fibroblast cells to confirm nanoshell uptake.[195]

At first thought, it is surprising that the nanoshell-*ds*DNA-DAPI complex is internalized into cells because the negatively-charged phosphate backbone on the DNA should experience electrostatic repulsions with the negatively-charged cell membrane.[196] However, previous studies by Chithrani *et al* and Giljohann *et al* suggest that Au nanoparticles functionalized both with and without DNA adsorb extracellular serum proteins from the cell culture media.[196-197] The adsorbed extracellular proteins then interact with the cell membrane and facilitate cellular uptake in an adsorptive endocytosis pathway. Conversely, recent studies by Ochsenkühn *et al* show that nanoshell uptake increases in the absence of extracellular proteins, suggesting the possibility of a passive, nonendocytotic uptake mechanism.[195] While in our studies nanoshell complex uptake is clearly visualizable in H1299 cells, the precise uptake mechanism is not clearly identifiable, and is likely to depend on a variety of factors including cell type, functionalization of the nanoparticle, and incubation conditions.

To investigate intracellular light-induced molecular release, the H1299 cells incubated with nanoshell-*ds*DNA-DAPI complexes were illuminated with a NIR CW laser (1 W/cm^2, 800 nm) for 5 minutes. This irradiation time and laser power level were determined from previous experiments,[170] which demonstrated after 5 minutes of laser irradiation no additional dehybridization of the DNA occurred. This laser power and time allow the DAPI to be released while minimizing laser exposure to the H1299 cells. After laser irradiation, samples were placed in an incubator for one hour to allow time for released DAPI molecules to diffuse to the nucleus. Next, the nuclei of the cells were isolated by lysing the cell membrane and the DAPI fluorescence intensity was quantified by flow cytometry. Nuclei isolation is necessary to ensure that flow cytometry only measures fluorescence from DAPI

molecules bound to genomic DNA in the nucleus and does not measure fluorescence from DAPI molecules in the cytoplasm.

Evidence of DAPI release is shown by the normalized flow cytometry histograms of DAPI fluorescence intensity versus number of nuclei from H1299 cells incubated with nanoshell-*ds*DNA-DAPI before and after laser treatment (Figure 5-6). After laser treatment, the fluorescence intensity of the nuclei increased, demonstrating that DAPI molecules were released from the nanoshells, diffused through the cytoplasm and into the cell nuclei, binding with the genomic DNA. Prior to laser irradiation, some DAPI fluorescence is observed within the cells (Figure 5-6c, left) and measured by flow cytometry (Figure 5-6a-b, before laser). This DAPI fluorescence signal originates from both excess DAPI molecules present in the sample and DAPI molecules which were non-controllably released from the complexes during the incubation and prior to laser irradiation.

The bar graph depicts the mean DAPI fluorescence intensity ± SEM (standard error of the mean) increase from before laser (59.7±0.21) to after laser (79.8±0.33) (Figure 5-6a). A ~33% increase in fluorescence intensity. An unpaired t-test of the two means was performed at a 95% confidence level, which resulted in a two-tailed p value of $p < 0.0001$, which is statistically significant. This observed increase in DAPI fluorescence after laser treatment (~33%) demonstrates that the nanoshell-*ds*DNA complex effectively released its guest molecules from the *ds*DNA host carriers inside the cells. Epifluorescence images of H1299 cells incubated with nanoshell-*ds*DNA-DAPI before (Figure 5-6c, left) and after (Figure 5-6c, right) laser treatment visually show the increase in DAPI fluorescence intensity. The cell membrane is marked by the green dye, Alexa-Fluor 488 wheat germ agglutinin.

The plasmon resonant illumination of the nanoshells is crucial for DAPI release into the cells. To test this hypothesis, a control experiment consisting of H1299 cells incubated with DAPI only (no nanoshells) was conducted (Figure 5-6b). The cells were irradiated with the NIR laser under conditions identical to the previous experiment. The mean DAPI fluorescence intensity ± SEM did not significantly increase after laser irradiation (237±0.86 to 239 ± 0.95, $p = 0.1188$), indicating that DAPI release does not occur without the presence of the nanoshell-*ds*DNA complex. It is important to note that the mean fluorescence intensity is higher for the control (Figure 5-6b) compared to the nanoshell-*ds*DNA-DAPI sample (Figure 5-6a) due to multiple washings of the nanoshell-*ds*DNA-DAPI sample.

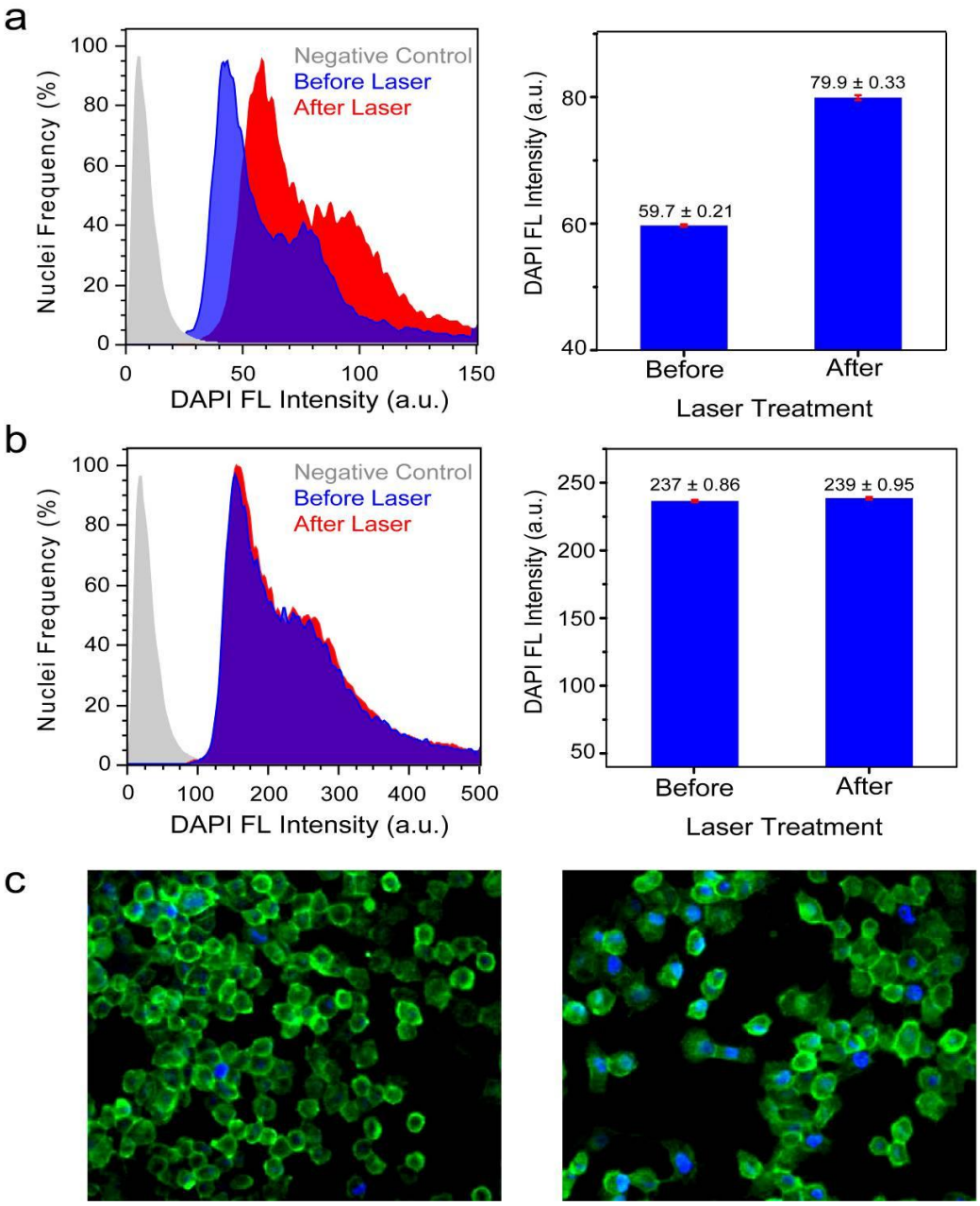

Figure 5-6 Light-induced DAPI release. (a-b) Flow cytometry histograms of DAPI Fluorescence (Ex: 355nm/Em: 460 nm) versus number of isolated nuclei from H1299 cells incubated with a) nanoshell-dsDNA-DAPI and b) DAPI (control). Negative control (gray), treated cells without laser irradiation (blue) and treated cells with laser irradiation (red). Bar graphs display the mean DAPI fluorescence intensity ± SEM before and after laser irradiation. (c) Epifluorescence images of H1299 cells incubated with nanoshell-dsDNA-DAPI (left) before and (right) after laser treatment. The cell membrane is marked by the green dye, Alexa-Fluor 488.

The shape of the flow cytometry histograms for both before laser and after laser are consistent with nuclei stained with DAPI.[198-199] DAPI is routinely used to study the cell cycle because it binds to DNA stoichiometrically. Looking at the before laser histogram in Figure 5-6a as an example, the tallest peak (~40) originates from nuclei with two sets of chromosomes. This peak is the tallest because in a typical cell cycle, a cell spends the longest portion of time with two sets of chromosomes; therefore, the probability of a cell having two sets of chromosomes is the highest. The second, smaller peak (~80), double the fluorescence intensity of the tallest peak, indicates nuclei which have exactly double the amount of DNA, four sets of chromosomes, and are ready to enter mitosis and divide. The nuclei with fluorescence intensities in between these two peaks indicate cells which are currently synthesizing DNA prior to mitosis. The negative control histogram (gray) has a single peak because in the absence of DAPI every nuclei essentially fluoresces identically resulting in a signal which is attributed to autofluorescence (background).

To ensure that this method for light-triggered intracellular molecular release would be useful for biomedical applications, such as drug delivery, a cytotoxicity assay was performed to investigate both the effects of nanoshells and laser irradiation on cell viability. Propidium iodide (PI) was chosen as a marker to distinguish viable from non-viable cells, because it is a membrane-impermeable dye which is excluded from viable healthy cells.[200] When a cell membrane is damaged, PI enters the cell, stains the *ds*DNA in the nuclei and emits red fluorescence; however, undamaged cells will not fluoresce. Flow cytometry was used to observe changes in PI fluorescence intensity for a large sample size of 30,000 cells. The negative control (Figure 5-7a) consisted of cells which were not incubated with nanoshell-*ds*DNA-DAPI and did not undergo laser treatment. The fluorescence observed in Figure

5-7a is attributed to autofluorescence and PI staining caused by apoptotic and necrotic cells already present in the experiment, with damaged membranes. The nanoshell-*ds*DNA-DAPI complexes were then incubated with H1299 cells for 12 hours. Following incubation, the cells were divided into two samples: cells not treated with the laser (Figure 5-7b) and cells treated with the laser for 10 minutes (Figure 5-7c). Figure 5-7b shows no significant increase in PI fluorescence intensity, demonstrating that nanoshell-*ds*DNA-DAPI complexes are not cytotoxic under the experimental conditions of the study.

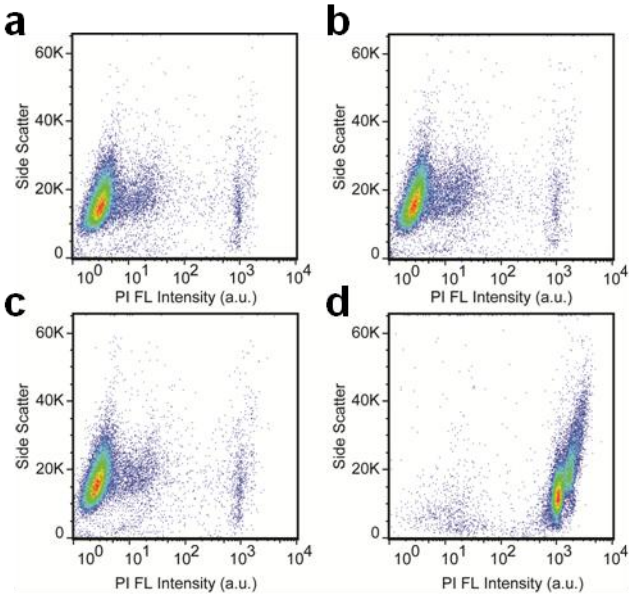

Figure 5-7 Flow cytometry cytotoxicity assay. All plots are side-scattered light (SS) versus Propidium Iodide (PI) intensity. (a) Negative control: H1299 cells not incubated with nanoshell-dsDNA-DAPI and no laser treatment. Cells incubated with nanoshell-dsDNA-DAPI for 12 hours: (b) without laser treatment and (c) with laser treatment. (d) Positive Control: Cells were treated with 0.1%Citrate/0.1%Triton, which permeates the cell membrane, allowing PI to stain the dsDNA in the nucleus.

More interestingly, cells incubated with nanoshell-*ds*DNA-DAPI complexes and irradiated with the laser for 10 minutes, Figure 5-7c, also show no significant increase in PI fluorescence intensity. This demonstrates that the light-triggered release procedure did not

adversely affect the cells. Considering nanoshells are well-known for their use in photothermal therapy, this result may be surprising; however, the illumination conditions for this experiment (1W/cm2, 5 minutes) were significantly below those used for photothermal induction of cell death in cell culture (4W/cm2, 4-6 minutes).[174] Figure 5-7d represents a positive control sample of cells treated with 0.1% Citrate/0.1% Triton solution, which permeates the cell membrane, allowing PI to enter the cell and stain the nucleus, resulting in a large increase in PI fluorescence intensity.

5.4. Conclusion

In conclusion, nanoshells functionalized with *ds*DNA were successfully used to transport DAPI molecules into living cells. Successful uptake of nanoshells into H1299 cells was achieved. DAPI molecules, initially bound to the *ds*DNA on the NS surface, are released due to the illumination of the nanoshell-*ds*DNA-DAPI complex with the appropriate NIR light. DAPI molecules initially released in the cell cytoplasm diffuse into the cell nucleus and bind to the genomic DNA of the cell. The staining of the cell nucleus with the released DAPI was quantified using flow cytometry. A cytotoxicity assay demonstrated that nanoshell uptake is nontoxic and that laser irradiation of nanoshell-laden cells under the conditions where DAPI release occurs does not induce cell death.

This nanoshell-*ds*DNA system could be extended to a multitude of other guest molecules that associate with the host *ds*DNA carrier including small organic fluorophores,[185] steroid hormones,[201] and therapeutic molecules.[184-185, 201] For example, the quest to find *ds*DNA intercalators that inhibit the uncontrollable replication of tumor cells comprises an entire field of cancer research. Currently, there are more than 130 FDA

approved anti-cancer drugs that specifically target DNA.[202] For *in vivo* clinical applications, however, before the DNA intercalator can reach the genomic DNA, it must overcome several hurdles, such as metabolic pathways and cytoplasmic and nuclear membranes. As a result, the failure of DNA therapies to offer successful clinical treatments is primarily due a lack of viable delivery methods rather than effectiveness of the DNA intercalator to treat cancer.[184] This nanoshell-*ds*DNA delivery vector preserves the guest molecule by minimizing non-desired interactions with other molecules and it provides light-triggered release with controllable delivery.

Chapter 6

Gene silencing by Au-nanoshell-mediated delivery and laser-triggered release of antisense oligonucleotide and siRNA

This work was done in collaboration with Aoune Barhoumi and Naomi J. Halas from Rice University and Qing Liu, Jack A. Roth, and Lin Ji from The University of Texas MD Anderson Cancer Center.

6.1. Introduction

RNAi- the use of short-interfering RNA (siRNA) or antisense DNA oligonucleotides to silence or interrupt the activity of specific genes and downregulate expression of their encoded proteins- has been proved very useful in dissecting genetic function.[22] This approach holds considerable promise for the development of a new class of molecular therapeutic drugs that interferes with disease-causing or -promoting genes, particularly those that encode so-called 'non-druggable' targets not amenable to conventional therapeutics.[203] However, the main obstacle to achieving gene silencing *in vivo* by RNAi technologies is delivery of therapeutic siRNAs or antisense oligonucleotides, currently becoming a major

topic in cancer therapy. This goal faces many challenges, such as the direction of specific gene targets to the appropriate tissue and cell types at safe and effective dosages, and maintenance of oligonucleotide stability in circulation. Strategies for enhancement of cellular uptake and methods for monitoring distribution and therapeutic efficacy are also needed.[23-24, 34, 203] Overcoming these obstacles requires new delivery vehicles and targeting approaches. Lipid and polymer-based vehicles for administration of siRNAs have been developed and tested for delivery to lung, liver and other local tumors in animal models, including non-human primate.[24, 203-204] These RNA or DNA oligonucleotide delivery carriers present a variety of potential problems to the patient - toxicity, immune and inflammatory responses, and gene control and targeting issues.[23-24, 34, 203-205] Realizing the full potential of RNAi-based molecular therapeutics requires new strategies[32, 106, 108, 206-213] to substantially improve delivery efficiency, toxicity profiles, monitoring techniques, and pharmacological and therapeutic efficacy.

Gold nanoparticles show potential to offer 'on-demand' release in response to optical laser excitation due to their plasmon resonance, the collective oscillation of the electrons. [57, 105, 143] Recently, two strategies for light-triggered release have been investigated. One strategy consists of covalently attaching the gene therapeutic to the gold surface. Upon femtosecond laser pulses, the nanoparticles either break apart or reshape into small gold nanoparticles, which breaks the covalent bond and releases the gene therapeutic.[31, 104-106, 108] The second strategy consists of covalently attaching a 'carrier' molecule to the gold surface and then loading the 'cargo' gene therapeutic molecule onto the 'carrier' molecule, typically by weaker non-covalent bonds. Upon laser illumination, the nanoparticle absorbs energy, which weakens the attraction between the carrier and cargo molecules and releases the

therapeutic entity.[64, 122, 141-142] While both strategies show promise, the second strategy may be advantageous due to the relatively low laser power densities and short irradiation times required to release the therapeutic cargo.

Gold (Au) nanoshells (NSs) composed of a spherical silica core coated with a thin Au shell, show potential to offer 'on-demand' release in response to optical excitation. The plasmon resonance of Au nanoshells can be tuned from the visible region into the near infrared (NIR) by changing the core size and the thickness of the gold shell.[35] The NIR resonance of NSs enables biomedical applications because the nanoshell can be easily fabricated to maximally absorb in the NIR "water window", where bodily tissue is maximally transparent.[39] Au nanoshells have been used extensively in biomedical applications including photothermal cancer therapy.[14-15, 78, 214-215] Additionally, Au possesses a very well-established Au-thiol bond chemistry that allows easy functionalization of the nanoshell surface with a wide variety of ligands and targeting moieties.[212, 216]

Recently we demonstrated resonant light-induced release of single-stranded DNA (ssDNA) from Au nanoshells.[143, 217-218] A monolayer of double-stranded DNA (dsDNA) was attached to the nanoshell surface via a thiol modification on the 5' end of a complementary, carrier sequence, while a therapeutically antisense sequence to be released was hybridized to its carrier complement via Watson-Crick base-pairing. Continuous wave laser radiation at 800 nm released the non-thiolated DNA strand from the nanoshell surface. In this previous work, the thiolated DNA sequence is the 'carrier' molecule that holds the therapeutic ssDNA 'cargo'. This rudimentary light-triggered delivery system is limited to the release of single stranded oligonucleotides. However, its demonstration suggests that noncovalent binding

may be used to create a more general 'carrier' platform capable of delivering a range of different types of oligonucleotide therapies upon NIR irradiation.

Cationic poly(L)lysine peptides are a promising oligonucleotide carrier. Poly(L)lysine has been used extensively as a transfection reagent for gene therapeutics.[219-221] Due to the fact that it is positively charged at physiological pH, poly(L)lysine associates electrostatically with the negatively charged phosphate backbone of antisense DNA or siRNA oligonucleotides. In addition, the poly(L)lysine can protect the synthetic oligonucleotide-based molecular therapeutics from enzymatic degradation by nucleases during transport and can increase cellular uptake.[220, 222]

In this study we developed an NS-based antisense RNAi oligonucleotide delivery system. This nanotherapeutic delivery vector consists of an Au nanoshell functionalized with a cationic poly(L)lysine (PLL) peptide (Cysteine(C)-Tyrosine(Y)-Serine(S)-Lysine$(K)_{50,}$) carrier arm for electrostatic capture of intact, negatively-charged therapeutic RNAi oligonucleotides. The thiol side chain on the cysteine amino acid attaches to the gold surface, the tyrosine and the serine amino acid serve as spacer and the fifty lysine amino acids result in a net positive charge. To demonstrate the general utility of this delivery system, two types of RNAi 'cargoes', single-stranded antisense DNA oligonucleotides (ssDNA) and double-stranded siRNA are alternatively loaded onto the nanoshell-poly(L)lysine (NS-PLL) vector. Laser irradiation of the NS-PLL delivery vector controllably releases the therapeutic oligonucleotides at a controlled time point (Figure 6-1). We investigated the release profile of the ssDNA and quantified the number of ssDNA molecules released by both thermal and laser-induced treatment in solution and in living cells *in vitro*. Fluorescently-tagged ssDNA was used to investigate intracellular light-triggered release and

endosome rupture. The NS-PLL vector was also used to deliver either the GFP gene-specific antisense DNA oligonucleotide (AON-GFP), or siRNA (siGFP), to evaluate cellular uptake and gene silencing potential of this approach in GFP-expressing H1299 lung cancer cells *in vitro*.

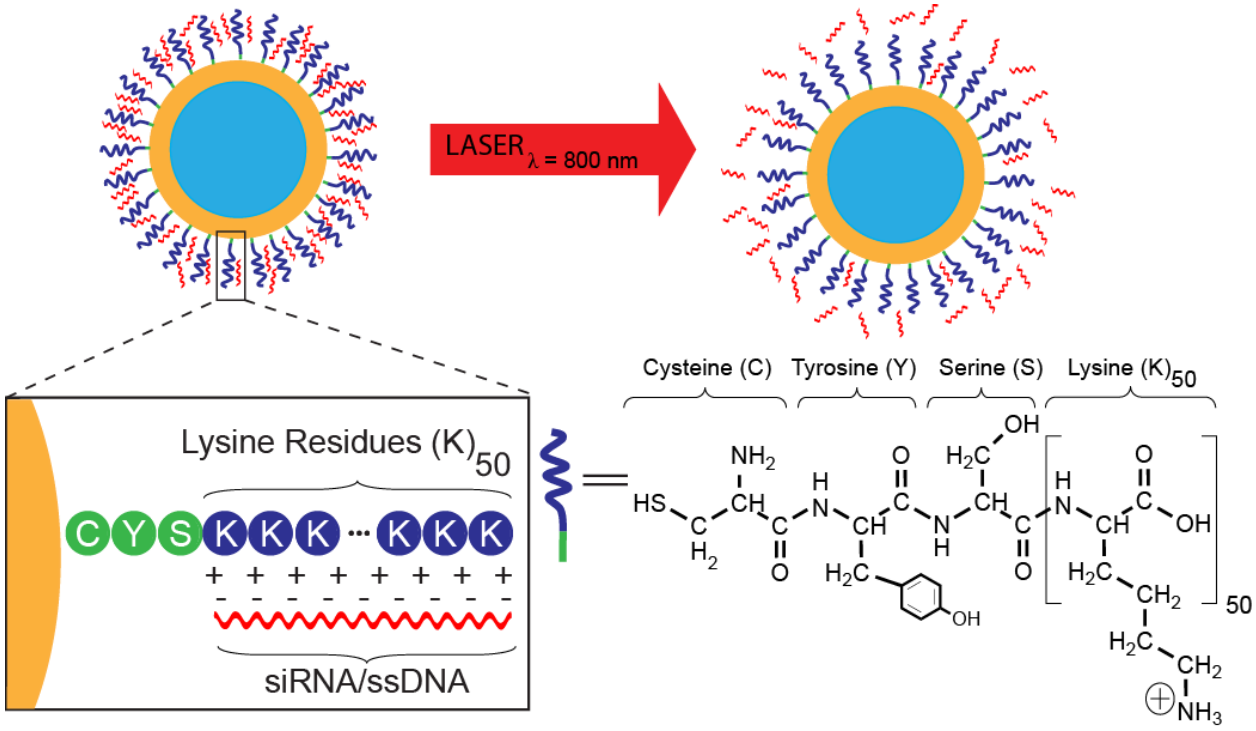

Figure 6-1. Au-Nanoshell Polylysine (NS-PLL)-based therapeutic RNAi oligonucleotide delivery system. The negatively charged phosphate backbone of the siRNA/ssDNA (red) is electrostatically attached to the cationic peptide (blue), which consists of one cysteine, one tyroosine, one serine, and fifty lysines amino acids. Upon laser irradiation, the siRNA/ssDNA is released.

6.2. Results and Discussion:

Nanoshell synthesis and polylysine functionalization.

Au nanoshells were synthesized according to a previously published method.[35] The dimensions of the silica core and the Au shell ($[r_1, r_2]$ = [60, 82] nm) were designed so that the peak plasmon resonance in an aqueous suspension occurred at 800 nm, corresponding to the laser excitation wavelength used in this experiment. The PLL peptide (Cysteine (C)-Tyrosine(Y)-Serine(S)-Lysine$(K)_{50}$) was custom synthesized (Biomatik USA, LLC) The peptide was received as a lyophilized powder and resuspended in Milli-Q water. An excess of the PLL peptide (see methods section) was added to a solution of nanoshells. This solution was allowed to incubate for 24 hours on a rocker at room temperature. The excess PLL was removed by centrifugation and resuspended in Milli-Q water. ζ-potential measurements confirmed PLL attachment (Table 6-3).

Thermal and Light-triggered Release of ssDNA

Light-triggered release of antisense DNA oligonucleotides (ssDNA) was investigated using three types of fluorescently tagged ssDNAs (**Error! Reference source not found.**): i) n 18-base sequence that was chemically unmodified (short ssDNA), ii) an 18-base ssDNA with sequence identical to the first except chemically modified with phosphorothioate (phosphorothioate-modified short ssDNA), and iii) a 50-base ssDNA that was chemically unmodified (long ssDNA). Oligonucleotides with phosphorothioate linkages were chosen because this chemical modification minimizes enzymatic degradation by nucleases and increases antisense oligonucleotide activity.[223] These chemically modified oligonucleotides have been extensively used both *in vitro* and *in vivo*.[223-225] Because the phosphorothioate-

modified short DNA sequence is used to downregulate GFP *in vitro,* we needed to ensure that it could be released from the vector in a manner similar to the non-modified DNA. The short and long ssDNA were designed to investigate the correlation between sequence length and releasing profile.

Short ssDNA	5'-GAGCTGCACGCTGCCGTC-3'
Phosphorothioate-modified short ssDNA	5'-*A*G*C*T*G*C*A*C*G*C*T*G*C*C*G*T*C-3'
Long ssDNA	5'-CGGCAATCAGGTTGACCGTACATC ATAGCAGGCTAGGTTGGTCGCAGTC-3'
siRNA antisense strand	5'-AUAGACGUUGUGGCUGUUGUA-3'
siRNA sense strand	5'-UACAACAGCCACAACGUCUAU-3'

Table 6-1. ssDNA and siRNA sequences used.*Phosphorothioate modification

For the thermally-induced release of the three fluorescently-tagged ssDNAs from the NS-PLL delivery vector, the solution is slowly heated in a temperature-controlled water bath (**Error! Reference source not found.**). Light-induced release was measured with respect to the ambient temperature of the solution, which increases upon laser irradiation due to photothermal heating by the irradiated nanoshells.

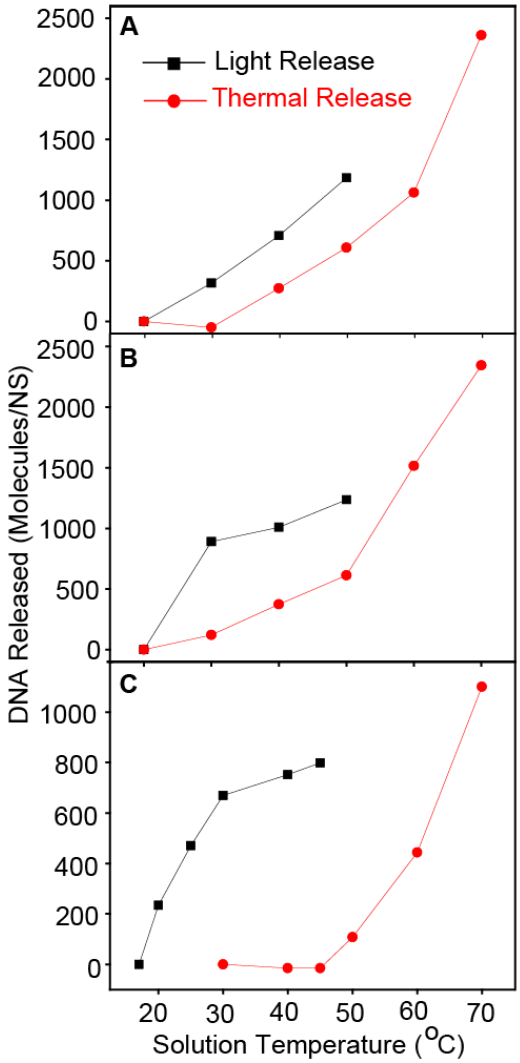

Figure 6-2. Thermal and laser-triggered release of ssDNA from Au nanoshell-PLL vector. Thermal release (red circles) and light release (black squares) of (A) short ssDNA (18 bases), (B) Phosphorothioate-modified short ssDNA (18 bases), and (C) long ssDNA (50 bases).

For all three ssDNAs studied, the laser irradiation resulted in ssDNA release at lower solution temperatures compared to thermal release (**Error! Reference source not found.**). The release of some of the ssDNAs was detected immediately upon laser irradiation (**Error! Reference source not found.**, black squares). In contrast, for the thermal treatment (red

dots), the ssDNA was released gradually as the solution temperature was increased. For light-induced treatment, a significant number of ssDNA molecules are released below 37 ^{o}C. Achieving ssDNA release at or near 37^{o}C (physiological temperature) is particularly important for avoiding hyperthermic cell death. [226-227]

The difference between thermal and light-induced release profiles does not necessarily reflect a difference in release mechanism. For both thermally-induced and light-induced release, the solution temperature is recorded. For light-induced release, the localized heating around each nanoshell results in a nonuniform thermal profile and the macroscopic solution temperature does not reflect the temperature at the illuminated nanoshell surface. Localized heating in the direct, nanoscale vicinity around the nanoshell could release the ssDNA prior to increasing the ambient solution temperature. Additional nonthermal mechanisms may be involved, such as photon-induced transfer of 'hot' electrons, generated by laser excitation, to the polylysine peptide. This would reduce the electrostatic interaction between the polylysine and ssDNA and enable release with little or no temperature increase of the local environment.[217]

We compare the total number of DNA molecules attached to a PLL-functionalized nanoshell, termed "loading capacity", to the number of ssDNA molecules released from a nanoshell during the thermal and light release processes (**Error! Reference source not ound.**). The loading capacity was determined by a previously reported method (See methods, supporting information).[115, 217] The phosphorothioate-modified short ssDNA has a much higher loading capacity (8182 DNA molecule/nanoshell) compared to the short ssDNA (3050 DNA molecules/nanoshell), even though the DNA base composition and sequence length are identical (**Error! Reference source not found.**). This could be a result of the

hosphorothioate modification, which replaces a nonbridging oxygen in the phosphate backbone with a sulfur atom. These additional sulfur atoms may potentially bind to the Au surface of the nanoshells, increasing the loading capacity of this molecule. Despite its greater loading capacity, the number of molecules released per nanoshell is strikingly similar for both the phosphorothioate-modified short ssDNA (thermal release: 2345 DNA/nanoshell; light release: 1236 DNA/nanoshell) and the chemically unmodified short ssDNA (thermal release: 2357 DNA/nanoshell; light release: 1182 DNA/nanoshell). This also suggests that some of the phosphorothioate-modified ssDNA strands are covalently attached to the Au surface through the sulfur group in the phosphorothioate modification, preventing its release under these conditions. Only the electrostatically associated oligonucleotides are released for the light-induced and the thermally-induced treatments in these experiments.

Since the interaction between the ssDNA and PLL is predominantly electrostatic, the length of the DNA sequence should affect the profile of the release. Shorter oligonucleotide sequences should interact less strongly with PLL and thus be released at lower temperatures. To validate this hypothesis, we compared the release profiles of short (18 bases) and long (50 bases) ssDNA (**Error! Reference source not found.**). For the thermal process, the short sDNA begins to release between 30-40°C (**Error! Reference source not found.**A), while the long ssDNA begins to release between 40-50°C (**Error! Reference source not found.**C). For the light-induced process, both the short and the long ssDNAs are released at a lower solution temperature relative to the thermal treatments. The number of long ssDNA molecules released per NS (~800) is significantly lower than the number of short ssDNA molecules released per NS (~1180) although the loading capacities of the two sequences are similar (3200 molecules/NS) (**Error! Reference source not found.**). This is expected due to

he increase in electrostatic interactions between the long ssDNA and PLL. These measurements were performed at the same ambient temperature with the same laser exposure time. Therefore, by varying the length of the polylysine and ssDNA, it should be possible to control the number of ssDNA molecules released into the system while keeping all other conditions constant.

	Loading Capacity (DNA/nanoshell)	Light Release (DNA/nanoshell)	Thermal Release (DNA/nanoshell)
Short ssDNA	3050	1182	2357
Phosphorothioate-modified short ssDNA	8182	1236	2345
Long ssDNA	3189	799	1097

Table 6-2. Quantification of ssDNA loading capacity, light release and thermal release.

Cellular Uptake of Nanoshell-Polylysine Delivery Vectors

For effective delivery of antisense oligonucleotides and siRNA, the NS-PLL delivery vector must be uptaken within the cell and escape the endosome. To facilitate cell uptake, the NS-PLL was incubated with H1299 cells for two hours in serum-containing cell culture medium. After incubation, the cells were either fixed and cellular uptake was investigated using dark-field microscopy (Figure 6-3A) and fluorescence microscopy (**Error! Reference source not found.**B), or the number of nanoshells uptaken per cell was quantified by inductively coupled plasma mass spectrometry (**Error! Reference source not found.**D). Nanoshells of this size both absorb and scatter light making them easily visible in dark-field microscopy as diffraction-limited bright spots (Figure 6-3A). The cell membrane is marked

by the red fluorescence dye, Alexa Fluor 555 WGA (wheat germ agglutinin). **Error! Reference source not found.**C shows the merged dark-field and fluorescence images demonstrating the colocalization of NS-PLL within cells.

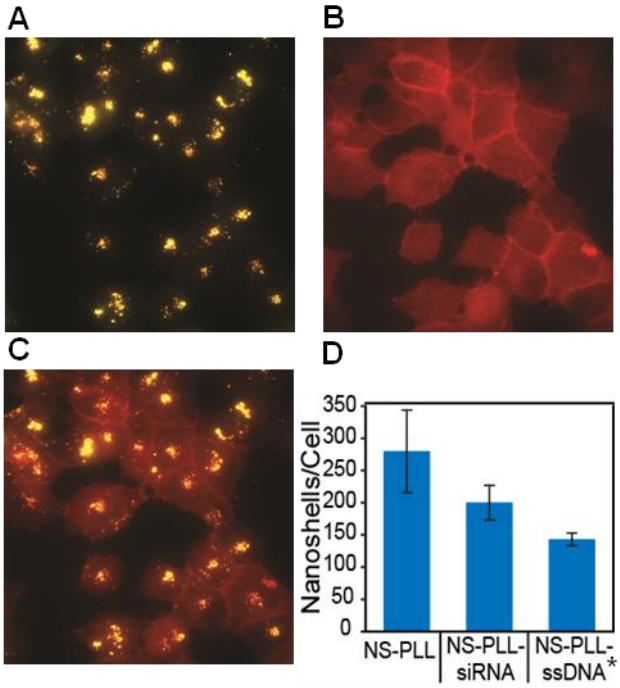

Figure 6-3.Cell uptake of NS-PLL delivery vectors in H1299 cells. (A-C) Dark-field/fluorescence images showing (A) polylysine nanoshells (NS-PLL), (B) cell membrane stained red with Alexa Fluor 555 WGA, and (C) A and B merged together showing polylysine nanoshells uptaken in cells. (D) Quantification of the number of nanoshells per cell determined by Inductively Coupled Plasma Mass Spectrometry (ICP-MS) after a I_2/KI gold etch procedure. Error bars represent standard deviations (n = 5).

Since neither dark-field nor fluorescence microscopy can definitively determine whether nanoshells are endocytosed or remain outside the cell but associate with the cell membrane, ICP-MS was used to confirm and quantify nanoshell cellular uptake. Uptake was quantified in H1299 cells respectively treated with three NS-PLL constructs: 1) polylysine nanoshells (NS-PLL), 2) polylysine nanoshells with phosphorothioate-modified short ssDNA

electrostatically attached (NS-PLL-ssDNA), and 3) polylysine nanoshells with siRNA electrostatically attached (NS-PLL-siRNA). After a 12 hour incubation of these constructs, the media was aspirated off and the cells were washed twice with phosphate buffered saline. To eliminate noninternalized nanoshells, a Iodine/Potassium Iodide (I_2/KI) etchant procedure was performed [222] (See methods, supporting information). The etchant rapidly oxidizes any gold at the exterior of the cell membrane, and is nontoxic at low concentrations. Using this method with ICP-MS, we detected that 277 ± 64 NS-PLL per cell, 198 ± 28 NS-PLL-siRNA per cell, and 141 ± 10 NS-PLL-ssDNA per cell were internalized in H1299 cells, respectively (**Error! Reference source not found.**D). In principle, combining the measurement of the number of internalized nanoparticles with the light-induced release profile can enable us to determine the number of oligonucleotides delivered within the cell.

While repeating experiments to confirm reproducibility, the number of nanoshells uptaken was observed to vary among different samples. We hypothesized that the cellular uptake depended on the surface charge of the polylysine nanoshell delivery vectors. To investigate, we measured the zeta (ζ)-potential for each sample (Table 6-3). A control sample of bare nanoshells has a negative ζ-potential (-23.23 ± 3.9 mV). Attachment of PLL to the NSs results in a net positive ζ-potential (14.27 ± 3.6 mV). After attachment of the negatively charged siRNA or ssDNA, the ζ-potential decreased accordingly. Interestingly, the ssDNA causes a significantly larger decrease (0.28 ± 4.41 mV), indicating that a greater number of ssDNA molecules were attached to the NS-PLL compared to double-stranded siRNA molecules (10.74 ± 2.2 mV). This was expected due to the higher affinity of the phosphorothioate-modified ssDNA to the NS-PLL complex. There is also a significant difference in the conformation between single-stranded DNA and double-stranded siRNA,

which could possibly allow more of the smaller ssDNA sequences to bind to the polylysine compared to the larger double-stranded siRNA.

Sample	Surface Potential (mV)
Nanoshells (NS)	-23.23 ± 3.9
NS-PLL	14.27 ± 3.6
NS-PLL-siRNA	10.74 ± 2.2
NS-PLL-ssDNA*	0.28 ± 4.4

Table 6-3. ζ-potential measurements. *Phosphorothioate-modified short ssDNA. Error represents standard deviations (n=5).

The highest cellular uptake was recorded with the NS-PLL sample with the highest positive ζ-potential, while the lowest cellular uptake was obtained for NS-PLL-ssDNA, with the lowest ζ-potential. This correlation between net positive charge of the particle and uptake highlights the importance of carrier surface chemistry to the uptake mechanism.

Previous studies regarding the uptake of cationic peptides, polymers, and nanoparticles suggest an adsorptive endocytosis pathway.[228-231] First, the positively charged polylysine-functionalized nanoshells adsorb onto the negatively charged cell membrane surface and are then internalized via endocytosis. It was recently shown that adsorption of particles to the cell membrane is the rate-limiting step for this mechanism.[222] Because the NS-PLL sample has the greatest positive charge, this is likely to increase its interactions with the cell surface and reduce the time needed for adsorption. Therefore, a greater number of the NS-PLL particles are adsorbed onto the cell membrane and ultimately internalized.[222]

Downregulation of Green Fluorescence Protein *in vitro*

To study the ability of the NS-PLL delivery vector to release RNAi therapeutic oligonucleotides *in vitro*, fluorescence microscopy was used to visualize the release of fluorescently tagged ssDNA from NS-PLL within the H1299 lung cancer cells. The NS-PLL-ssDNA sample was incubated with H1299 cells in an identical procedure as the cell uptake studies presented earlier. The ssDNA is tagged on the 5' end with Alexa Fluor 488, a green fluorophore. After the two hour incubation, the media is aspirated off and replaced with fresh media. Half of the cells do not undergo a laser treatment (Figure 6-4A) and the other half are irradiated with a laser treatment, 2.5 W/cm^2 for 2 minutes (Figure 6-4B). Finally, the cells are fixed and the cell membrane is stained red by Alexa Fluor 555 WGA. **Error! Reference source not found.**A shows that without laser treatment the green fluorescence is very weak most likely because the Alexa Fluor 488 fluorescence is quenched due to the proximity of the ssDNA to the gold nanoshell surface. In Figure 3B, the laser treatment results in an increased brightness of the green fluorescence because the ssDNA is released from the NS-PLL delivery vector which eliminates the quenching. Additionally, in the laser treatment group, it appears that the green fluorescence is more spread throughout the cell, indicating that the DNA has escaped from the endosome.

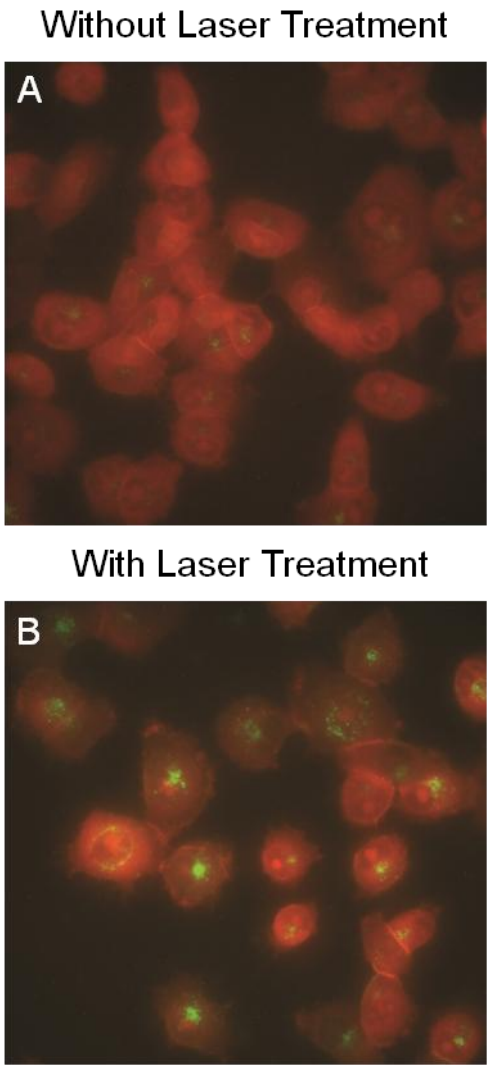

Figure 6-4. Fluorescence images H1299 cells incubated with NS-PLL-ssDNA. The ssDNA is fluorescently tagged with Alexa Fluor 488 (Green). (A) Without laser treatment, the green fluorescence is quenched due to the proximity of the ssDNA to the gold nanoshell surface. (B) With laser treatment, the ssDNA is released, which eliminates the quenching, resulting in brighter green fluorescence spread throughout the cell.

The rupturing of the endosome in response to laser irradiation has been the subject of intense research recently.[232-234] The light-controlled rupturing is dependent on both the laser intensity and time of laser irradiation. For both high continuous wave (CW) laser intensity (~10^5 W/cm^2) and pulsed laser irradiation conditions, the photothermal properties of the

nanoparticle results in the heating of the surrounding environment, thus leading to endosomal membrane disruption.[233]For low CW laser intensity irradiation conditions, like the conditions used within this study (2.5 W/cm^2 for 2 minutes), the increase in temperature is minimal suggesting a non thermal, photochemical mechanism.[69, 217] Krpetić et al, recently showed that lower laser irradiation powers (<20 W/cm2 for 2 minutes) resulted in a minimal temperature increase and significant endosome damage.[232] The authors concluded that by controlling the laser power and exposure time, highly selective localized damage can be inflicted to the endosomal membrane without inducing cell death.[232] This endosomal escape is crucial for the therapeutic oligonucleotides to be effective.

To study the ability of the NS-PLL delivery vector to controllably deliver RNAi therapeutic oligonucleotide *in vitro*, a lung cancer cell line (H1299-dsGFP/dsRFP) that expresses destabilized green fluorescent protein (GFP) and destabilized red fluorescent protein (RFP) was used. Destabilized fluorescent proteins were chosen because they have short half-lives that allow for monitoring of downregulation shortly after administration of the molecular therapeutics.[235-237] The GFP was used as the target reporter for determining downregulation of gene and protein expression by phosphorothioate-modified single-stranded antisense DNA oligonucleotide (AON-GFP) or siRNA specific to GFP mRNA (siRNA-GFP). The RFP served as a reference protein to ensure accurate measurements of GFP despite variations in fluorescence intensity due to variations in cell number. This was achieved by designing the siRNA and antisense oligos to downregulate GFP without affecting the RFP. Thus, for all measurements, the peak fluorescence intensity of GFP was normalized by the peak intensity of RFP (GFP/RFP).[237]

Three separate polylysine nanoshell complexes were prepared: NS-PLL, NS-PLL-siRNA, and NS-PLL-ssDNA. Here, the ssDNA was identical to the phosphorothioate-modified short ssDNA used in the extracellular release studies described earlier. The antisense oligonucleotides and siRNA sequences used in these experiments were chosen from previous studies and have been previously investigated for specificity [27, 236, 238] and, furthermore, were compared to scrambled sequences to ensure specific downregulation of GFP (Figure 6-5).

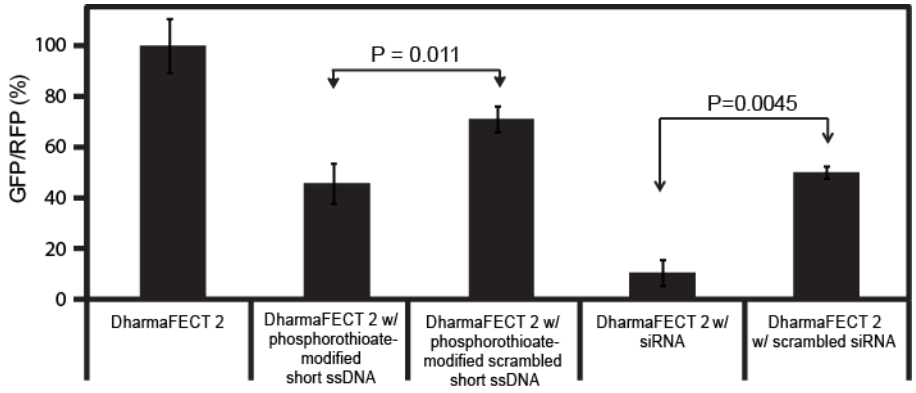

Figure 6-5. GFP/RFP (%) of H1299-GFP/RFP cell line treated with DharmaFECT 2 transfection reagent, DharmaFECT 2 with phosphorothioate-modified short ssDNA DharmaFECT 2 with phosphorothioate-modified scrambled short ssDNA, DharmaFECT 2 with siRNA and DharmaFect 2 with scrambled siRNA.

The downregulation of GFP by antisense oligonucleotides (**Error! Reference source not found.**A) and siRNA (**Error! Reference source not found.**B) delivered via NS-PLL delivery vectors was monitored by measuring the peak fluorescence intensity of both GFP and RFP at specific time points: prior to incubation (0 hours), after incubation and prior to laser treatment (12 hours), and after laser treatment (15, 18, 24, and 36 hours). The laser treatment for the NS-PLL sample, which had neither siRNA nor ssDNA attached, resulted in negligible GFP downregulation (**Error! Reference source not found.**C, NS-PLL). In

figures 3A and 3B, the "with laser" and "without laser" are normalized percentages to the "with laser" and "without laser" of the NS-PLL sample, respectively. During the incubation period (0-12 hours), GFP expression was downregulated by antisense ssDNA to 72 ± 5% (**Error! Reference source not found.**A) and by siRNA to 80 ± 5% (**Error! Reference source not found.**B). This downregulation was likely due to the AON-GFP and siRNA-GFP partially bound to the PLL which came off the delivery vector during cell incubation. At 12 hours, half of the cells were irradiated with the laser for 2 minutes. At 18 hours, six hours after laser treatment, GFP downregulation for the laser-treated samples had reached its minimum (~47% for antisense ssDNA and ~49% for siRNA, **Error! Reference source not found.**C). Therefore, the laser-treated samples resulted in an additional ~23% and ~31% GFP downregulation for antisense ssDNA and siRNA, respectively, when compared to the non-laser treated samples. This difference in downregulation indicates that the laser treatment controllably released the gene therapeutics from the NS-PLL delivery vector. The samples not treated with the laser showed no further downregulation after the incubation period. In fact, GFP expression increased shortly after incubation, indicating that the initial downregulation observed during incubation was limited to the ssDNA or siRNA released during incubation. Because GFP is continuously produced and expressed within the cell, after the ssDNA or siRNA is consumed, the GFP/RFP percentage gradually increases, approaching its pretreatment value after 24 hours following laser irradiation.

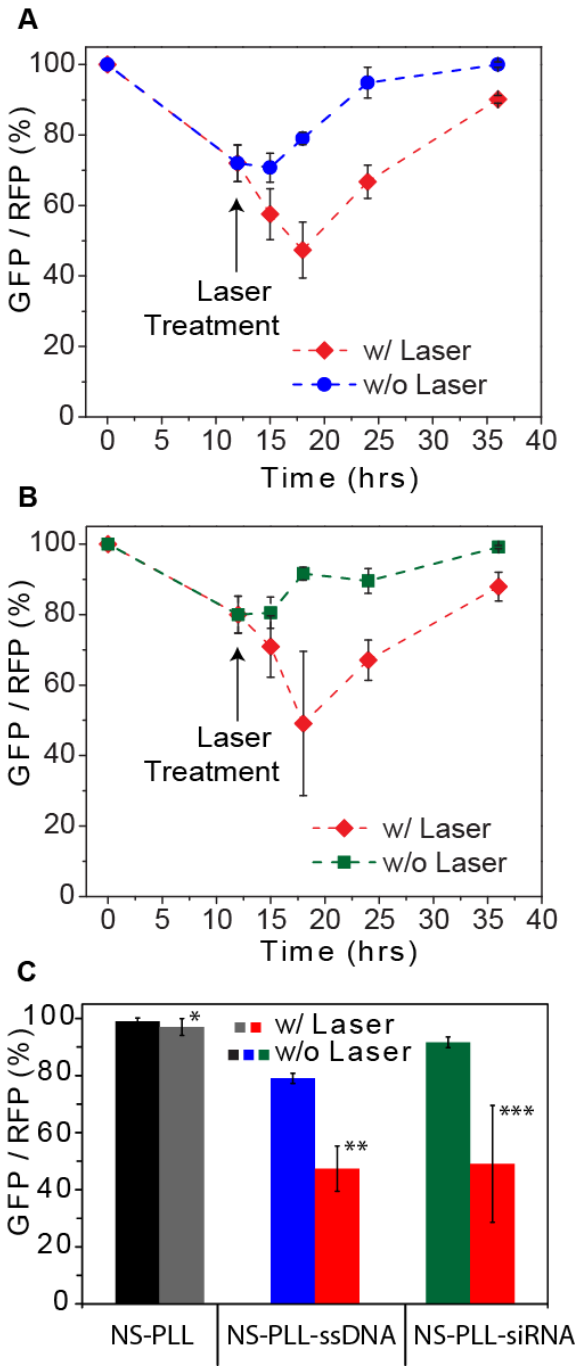

Figure 6-6. Downregulation of green fluorescent protein (GFP) in H1299 GFP/RFP cell line by antisense ssDNA and siRNA using Nanoshell polylysine (NS-PLL) delivery vectors. (A, B) Percent GFP/RFP fluorescence as a function of time with and without laser treatment for NS-PLL delivery vectors carrying with (A) Antisense ssDNA and (B) siRNA. (C) Percent GFP/RFP fluorescence at 18 hours (6 hours after laser treatment). Data displayed as mean ± SEM (n=3). Unpaired t-tests: *P = 0.5934, **P = 0.0176, ***P = 0.1071.

The observed magnitude of the downregulation of GFP is similar for both delivery vectors, despite their difference in ζ-potential. The data in Table 6-3 suggests that fewer siRNA molecules are attached to the NS-PLL delivery vector compared to antisense ssDNA, because the NS-PLL-siRNA sample has a higher positive ζ-potential. However, **Error! Reference source not found.**C shows that both samples had ~50% downregulation of GFP when treated with the laser. This observation correlates well with studies showing that siRNA is more efficient in silencing genes and downregulating their proteins expression relative to phosphorothioate-modified antisense ssDNA.[223, 236] Interestingly, we observed a greater downregulation of GFP for light-triggered release of RNAi oligonucleotides when the cells were trypsinized prior to laser treatment compared to adhered cells (data not shown). Any effect that this trypsin procedure would have on protein expression is negated because the GFP downregulation data shown in Figure 6-6 is normalized to the NS-PLL group that also underwent the trypsin procedure.

From a kinetic point of view, GFP downregulation reaches its maximum at approximately 6 hours after laser treatment. This time frame for observing GFP downregulation is consistent with both experimental and theoretical results that used antisense oligonucleotides and siRNA to downregulate short half-life destabilized proteins.[235-237] Additionally, the light-triggered delivery process is significantly different from traditional passive transfection reagents such as liposomes and dendrimers. With a transfection reagent, the delivery of the RNAi oligonucleotides occurs over multiple hours, if not days, because these RNAi oligonucleotides must slowly escape the endosome, dissociate from the transfection reagent, and finally diffuse to the mRNA in the cytosol. In the case of

light-triggered delivery, the vast majority of the oligonucelotides is released during the short laser irradiation treatment (2 minutes). Therefore, it is likely that the gene silencing and the subsequent protein expression downregulation occurs faster due to the higher initial concentration of released RNAi oligonucleotides in the cytosol of cells. Further studies would be needed to determine if light-induced processes, or combinations of light-controlled processes, could be used to more generally modify cellular processes in this manner.

In estimating the amount of therapeutic RNAi oligonucleotides delivered, we hypothesize that the percentage of the RNAi oligonucleotides released intracellularly is similar to the extracellular release, in which a maximum of ~1200 ssDNA were released per nanoshell. This hypothesis is theorized since the laser radiation takes place within the "water window," where water and tissue are maximally transparent, such that the cellular environment should have a minimal effect on the NS response to laser irradiation. [39] Additionally, the release of the RNAi oligonucleotides is due to either the local heat generated around the nanoshell or the generation of hot electrons on the gold surface, neither of which should be affected by the cellular environment. If this hypothesis is correct, by using the ICP-MS nanoshell uptake result for NS-PLL-ssDNA (~141 nanoshells/cell) and the number of ssDNA released extracellularly below 37°C (~1000 ssDNA/NS), then a maximum of ~141,000 antisense oligonucleotides would be released inside the cell. After converting this number to moles and dividing by the intracellular volume ($4x10^{-12}$ L)[235, 239], we can estimate that ~ 60 nM of antisense oligonucleotides are delivered inside each cell via light-triggered release from the NS-PLL vector. This approximate concentration correlates well to the ~50% GFP downregulation we observed, according to both previously reported experimental results and theoretical models.[235-236, 240] Although this is an approximation, it

points to future capabilities for delivering known amounts of therapeutic molecules using vectors such as our polylysine nanoshell complex at specific time points, to study the kinetics of physical, chemical, and biological processes within live cells. The efficiency of the polylysine nanoshell delivery vector demonstrated here can be improved by increasing the intracellular uptake, optimizing laser irradiation conditions, and the integration of targeting moieties for studies *in vivo*.

Cell Viability Assay

The cell viability of the H1299-GFP/RFP cell line after incubation with the polylysine nanoshell delivery vectors and subsequent laser treatment was investigated by using a XTT assay (Figure 6-7). Incubation of the nanoshell-polylysine delivery vectors with no laser treatment resulted in 82 ± 6% cell survival. After laser irradiation, there was 88 ± 7% cell survival, indicating that the laser treatment is not detrimental to the cells. This may come as a surprise considering Au nanoshells are well known for photothermal cancer therapy, but the laser power and exposure time used in this study (1.27 W/cm^2, 2 min) were significantly less than those used for photothermal induction of cell death (4W/cm^2, 3-6 min).[15, 78, 214, 227]

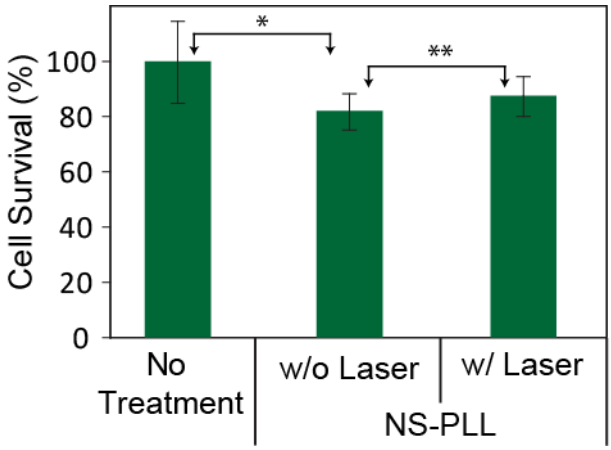

Figure 6-7. Analysis of NS-PLL nanoparticle-associatedcytotoxicity by XTT assay. Percent survival of H1299 cells with no treatment compared to cells incubated with Nanoshell-Polylysine (NS-PLL) delivery vector without laser treatment (w/o Laser) and with laser treatment (w/ Laser), mean ± standard deviation (n=3). Unpaired t-tests: *P = 0.1237, **P = 0.3747.

The NS-PLL sample was chosen for cell viability because this sample had the greatest uptake of nanoshells, and therefore it would have had the greatest possibility to cause photothermal cell death. The small decrease in the percent of cell survival in the non-irradiated sample could possibly result from a variety of factors, including the high ζ-potential of this sample or free polylysine that is not attached to the nanoshell.[241] Additionally, nanoparticle concentration and incubation time have been shown to affect cell viability.[242] Cationic transfection reagents that show low toxicity are often linked with polyethylene glycol (PEG), which reduces toxicity without affecting transfection efficiency, but attachment of PEG to our NS-PLL platform has yet to be investigated.

6.3. Conclusions

In this work, we have quantitatively demonstrated the remotely-controlled, light-triggered release of antisense ssDNA from polylysine nanoshell vectors. The cellular uptake of the NS-PLL complex in H1299 lung cancer cells was investigated by fluorescence microscopy, dark-field microscopy, and ICP-MS. This polylysine nanoshell complex was successfully used as a nonviral delivery vector that could controllably release antisense oligonucleotide ssDNA and siRNA to silence the target reporter GFP gene and downregulate GFP protein expression *in vitro*. One particulary important aspect of this NS-PLL delivery vector is the laser treatment results in escape from the endosome. Neither the polylysine nanoshells nor the laser treatment showed any significant evidence of cytotoxicity, indicating

that this nanoparticle complex may be a useful delivery vector for RNAi molecular therapeutics. This complex could further be used to quantify the number of molecules delivered intracellularly, which could have extensive applications in studying the rates of specific processes within living cells.

6.4. Experimental Methods

Nanoshell synthesis. Au nanoshells were synthesized according to a previously published method.[35] The dimensions of the silica core and the Au shell ($[r_1, r_2]$ = [60, 82] nm) were designed so that the peak plasmon resonance in an aqueous suspension occurred at 800 nm, corresponding to the laser excitation wavelength used in this experiment (Fig. S1, Supporting Information). The concentration of nanoshells in water is determined by the following equation which is derived from beer's law:

$$\frac{\#\,Nanoshells}{mL} = \frac{2.303 x A_{peak}}{\sigma_{ext} x b}$$

where A_{peak}=experimental absorption at the peak plasmon resonance wavelength, σ_{ext} = theoretical extinction cross section at the peak plasmon resonance wavelength taken from Mie theory, b = path length of the cuvette in centimeters.

Polylysine Attachment to Nanoshells. The Cysteine (C)-Tyrosine (Y)-Serine (S)-Lysine$(K)_{50}$ (PLL) peptide was custom synthesized (Biomatik USA, LLC) The peptide was received as a lyophilized powder and resuspended in Milli-Q water to a concentration of 500 μM. Once the concentration of nanoshells is known, this PLL peptide is added to the solution of nanoshells in 100,000 molar excess of PLL. This solution was allowed to incubate for 24 hours on a rocker at room temperature. The excess PLL was removed via two

centrifugation cycles (350 rcf for 15 minutes) and resuspended in Milli-Q water. ζ-potential measurements confirmed PLL attachment (Table 6-3).

ssDNA or siRNA loading. Antisense ssDNA and siRNA were custom synthesized by Integrated DNA Technologies, IDT and Qiagen, respectively. ssDNA and siRNA was resuspended in TE buffer and nuclease-free water, respectively, to a final concentration of ~100 μM. An 50,000 molar excess of ssDNA or siRNA was added to the Au nanoshell/PLL suspension previously prepared and allowed to incubate for 24 hours on a rocker at room temperature. The nanoshell solution was placed in the refrigerator at 4°C and allowed to gently settle down for 48 hours. Afterwards, the supernatant was pipetted off and the pellet was resuspended in Milli-Q water. (Note: For the fluorescein-tagged-ssDNA release experiments, resuspension in TE buffer (IDT, pH=7.5) is necessary to ensure that the pH is constant since the emission properties of fluorescein are pH dependent.)

Loading Capacity of Fluorescently-tagged ssDNA on the NS-PLL vector. Two aliquots of 500 uL of NS-PLL-ssDNA were pipettes into two separate 1.5mL eppindorf tubes. In one tube, 500 uL of TE buffer was added and in the other tube 500 uL of 12mM mercaptoethanol (diluted in TE buffer) was added. Both tubes were covered in aluminum foil and were gently mixed on a rocker plate for 24 hours. Mercaptoethanol displaces the polylysine and ssDNA attached to the nanoshell. After 24 hours, both samples were centrifuged to remove the nanoshells, then the supernatants were measured in a fluorolog (excitation wavelength: 495 nm, Emission wavelengths: 505-540 nm). The difference in fluorolog intensity between samples was used to calculate the difference in DNA concentration by using a standard curve of DNA concentration versus fluorescence intensity.

The DNA concentration was then divided by the nanoshell concentration, which is calculated by UV-VIS absorbance measurement.

Thermal and light-triggered release of ssDNA. Thermal release was performed by slowly heating the NS-PLL-ssDNA sample (~1°C/min) while stirring, ensuring that the sample temperature was homogeneous during the entire course of the measurement. The light release was performed by placing a fiber-coupled 800 nm continuous wave laser above the sample and stirring during laser irradiation. For both thermal and laser treatments, the solution temperature was monitored with a thermocouple. The release of the fluorescently tagged ssDNA was quantified by taking aliquots out of the sample as the solution temperature increased. Each aliquot was centrifuged immediately to separate the nanoshells from the released ssDNA in the supernatant and the fluorescence intensity of the supernatant was measured to determine the number of released ssDNA per nanoshell.

Cell culture. The H1299 and H1299-GFP/RFP lung cancer cell lines were incubated at 5% CO_2, 37°C with RPMI 1640 media with L-glutamine supplemented with 10% heat-inactivated fetal bovine serum and 1% antibiotic solution. 0.25% Trypsin-EDTA was used for cell passaging.

NS-PLL cellular uptake. The H1299-GFP/RFP lung cancer cells were seeded in 4-well chamber slides at 5000 cells/well 24 hours prior to incubation with NS-PLL delivery vectors. The nanoshells were added to the serum containing media in a NS:cell ratio of 5,000:1 and allowed to incubate for 2 hours. Then, the cell culture medium was aspirated off, the cells were washed twice with 1x phosphate buffered saline, the cells were fixed with 4% paraformaldehyde, and stained with Alexa Fluor 555 according to manufacturer instructions. The walls of the chamber slide were removed, and the cells were mounted

using Vectashield mounting medium for fluorescence (Vector Laboratories) and 22x50 mm rectangular cover glass (n=1.5) Dark-field and fluorescence images were taken on a Cytoviva microscope equipped with dual-mode fluorescence module and a x-cite light source. For quantification of nanoshells uptaken in cells, ICP-MS measurements were performed. After a 12 hour incubation, the media was aspirated off, the cells were washed twice with PBS, the I_2/KI etchant procedure was perfomed (see methods, supporting information), live cells were sorted and counted using flow cytometry, digested with aqua regia, and then the gold content was measured with the ICP-MS (see methods, supporting information).

Fluorescence images for light-triggered release. NS-PLL-ssDNA delivery vectors were incubated with cells in an identical manner to NS-PLL uptake. The ssDNA is fluorescently tagged with Alexa Fluor 488 (Integrated DNA technologies, IDT) After two hours, the media was aspirated off, the cells were washed twice with 1x phosphate buffered saline, fresh media was added. The laser treatment group under went a laser treatment (2.5 W/cm^2, 2 minutes). Immediately afterwards, the media was aspirated off, fixed, and stained in an identical procedure as the NS-PLL cellular uptake experiments and imaged with a Cytoviva microscope.

Laser treatment for GFP downregulation. H1299-GFP/RFP cells were plated in a 12-well plate at a density of 95,000 cells/well 12 hours before incubation with NS-PLL, NS-PLL-ssDNA, and NS-PLL-siRNA delivery vectors. These NS-PLL delivery vectors were incubated with cells in an identical manner as the NS-PLL cell uptake experiments. After incubation the cell culture media was aspirated of, the cells were washed with PBS, trypsinized, and resupsended in cell culture media. Half of each cell suspension was

irradiated with an 800 nm CW laser for 2 minutes at 2.5 W/cm^2 and the other half did not undergo laser irradiation. The cells are then plated back onto a fresh 24 well plate. Green Fluorescence Protein (GFP) and Red Fluorescence Protein (RFP) were measured at specific time points using a fluorescence plate reader.

GFP/RFP measurements. Green Fluorescence Protein (GFP) and Red Fluorescence Protein (RFP) were measured using a Fluorescence plate reader (Biotek FLx800). For GFP the excitation filter was 485/20 nm and emission filter was 530/25 nm. For RFP the excitation filter was 530/25 and emission filter was 590/35 nm. GFP and RFP measurements were take prior to incubation (0 hours), after incubation and prior to laser treatment (12 hours), and after laser treatment (15, 18, 24, and 36 hours).

Instrumentation. Extinction spectra were obtained using a Cary 5000 UV/Vis/NIR spectrophotometer. Fluorescence emission of fluorescently tagged ssDNA was obtained using Jobin Yvon Fluoromax 3. Biotek FLx800 was used for microplate fluorescence measurements. Perkin Elmer ELAN9000 Inductively Couples Mass Spectrometer. Flow cytometry was done on a BD FACS Aria II.

Inductively-Coupled Mass Spectrometry Measurements. The I_2:KI etchant was made by mixing Iodine (I2, Aldrich) and potassium iodide (KI, Aldrich) to deionized water with a molar ratio of 1:6. The major role of KI is to increase the solubility of I2 in water. Cells were initially seeded in 6-well plates at a density of 400,000 cells/well 24 hours prior to incubation with nanoshell-*ds*DNA-DAPI complexes. The nanoshells were added to the serum containing media in a NS:Cell ratio of 5,000:1 and allowed to incubate for 12 hours. Then media was aspirated off. The sample was washed with PBS three times, and 1 mL of the I_2/KI etchant (0.17 mM of I_2) was added to the well. After etching at room temperature for 5

min, the solution was removed, the culture plate was washed with 3 times with 2 mL PBS. 500 uL 0.25% Trypsin-EDTA was added. After visual detachment of cells, the trypsin was deactivated by adding 500 uL serum-containing media. This suspension was then analyzed by flow cytometry for viable healthy cells using Propidium Iodide (PI). PI only enters cells apoptotic and necrotic cells which have damaged membranes, binds to the DNA in the nucleus and fluoresces red. PI is excluded from healthy cells. 100,000 cells viable cells (cells that did not fluoresce red) were sorted into a 20-ml scintillation glass vial. Concentrated Aqua regia was added to each glass vial and allowed to sit overnight. (Aqua regia is made of 3:1 of Hydrochloric acid (Sigma Aldrich, 37 wt. % in H_2O, 99.999% trace metals basis):Nitric Acid(Sigma, 70%, ≥99.999% trace metals basis). *WARNING: Aqua regia is dangerous and should be used in a chemical hood because it produces toxic nitrosyl chloride and chlorine gases. Do not cap the aqua regia because it produces gases and will explode if capped.* The next day, the aqua regia was boiled off by using a hot plate inside of a chemical hood. Each vial was then resuspended in 1% Aqua regia and filtered with 0.2 μm filters (PALL Acrodisc 32 mm). Au content was measured via ICP-MS in ppb and then converted to gAu.

Calculation for Number of nanoshells uptaken. Prior to PLL attachment, the silica core radius and Au shell radii were measured from particle size statistics obtained from SEM images of over 100 silica core particles and 100 Au nanoshells. The size of nanoshells (NS) = $[r_1, r_2]$ nm. The Volume of the Au shell per NS was then calculated: Volume of Au shell/NS= $(4/3)\pi(r_2^3-r_1^3)$ cm^3). The grams of Au/NS was then calculated: grams of Au/NS ($\frac{gAu}{NS}$) =Volume of Au shell/NS*(Density of Au ($19.3g/cm^3$)), Flow cytometry gives a specific number of cells (# cells). Inductively Coupled Plasma Mass Spectroscopy (ICP-MS)

was used to quantify grams of Au (gAu). The number of nanoshells per cell was then calculated: $(\#NS/cell) = \frac{gAu}{\frac{gAu}{NS} \bullet \#cells}$

XTT assay. After the laser treatment the cells were allowed to grow for 12 hours, and then the XTT assay (sodium 2,3,-bis(2-methoxy-4-nitro-5-sulfophenyl)-5-[(phenylamino)-carbonyl]-2H-tetrazolium inner salt) was performed according to XTT kit instructions (ATCC).

Chapter 7

Conclusions

The controlled release of biological and nonbiological molecules could have broad applications in the study of cellular processes and in the development of intracellular targeted therapies. Herein, we have shown light-triggered controlled release of DNA, siRNA and DAPI, a fluorescent molecule that intercalates within dsDNA, from plasmon-resonant nanoparticles.

The light-triggered release of the ssDNA, either from dsDNA dehyhybrization attached to the Au nanoparticle surface or desorption from polylysine nanoshells, was investigated by using fluorescently-tagged DNA. Then, the increase in fluorescence intensity, which correlates to release of ssDNA, was monitored as a function of either solution temperature or time. The thermal treatment release, performed by monitoring the DNA release as the solution temperature slowly increases (1°C/min), resulted in definitive release of DNA at elevated temperatures. For laser treated samples, the solution temperature was also monitored with a thermocouple, and it was observed that ssDNA release occurred at lower solution temperatures compared to the thermal treatment. The difference in release behavior between thermal and laser treated samples suggest either a non-equilibrium thermal mechanism or a non-thermal mechanism.

To study the mechanism in more detail, light-triggered dehybridization release of dsDNA was compared between dsDNA attached to Au nanoshells and Au nanorods. For dsDNA attached to Au nanoshells, the light-triggered release is observed to occur at a lower solution temperature compared to the thermal release profile. Surprisingly, the light-triggered release and thermal release profiles for dsDNA attached to Au nanorods were identical. Theoretical calculations were performed to estimate the temperature on the nanoparticle surface for the experimental laser irradiation conditions used. The theoretical temperature increase on the surface of nanoshells and nanorods was calculated to be less than 1 degree Celsius, which suggests that a nonequilibrium thermal mechanism is unlikely. The alternative non-thermal mechanism suggests that charge transfer can occur via the excitation of hot electrons that transfer to the attached dsDNA, which destabilizes the dsDNA by increasing the columbic repulsion. After calculating the near-field enhancements and absorption cross sections for a nanoshell and a nanorod, it was found that nanoshells have a higher absorption cross section and a near-field enhancement which covers a larger volume of the nanoparticle surface. These two qualities of a nanoshell increase the probability of charge transfer to occur on a nanoshell in comparison to a nanorod.

Additionally, we have shown the dsDNA attached to the Au nanoshell surface can be used as a “host” structure to carry a "guest” molecule. In our system, the dsDNA carried DAPI, a small organic fluorescent molecule commonly used in fluorescence microscopy due to its strong association to dsDNA. After dsDNA was attached to nanoshells, an excess of DAPI molecules were added to the sample and the DAPI molecules intercalated into the dsDNA. After the NS-dsDNA-DAPI nanoparticles are endocytosed by the H1299 lung cancer cells, the laser treatment was performed. We hypothesized that if the dsDNA is

dehybridized during the laser irradiation, the intercalated DAPI molecules would dissociate and diffuse to the nucleus and bind to the genomic DNA. To test this hypothesis, using flow cytometry we measured the fluorescence intensity of the nucleus before and after laser irradiation and we observed an increase in fluorescence intensity. This nanoshell-*ds*DNA system could be extended to a multitude of other guest molecules that associate with the host *ds*DNA carrier including small organic fluorophores, steroid hormones, and therapeutic molecules.

Finally, we design a non-viral delivery nanoparticle, which consists of cationic polylysine peptide attached to Au nanoshells. The negatively charged ssDNA and siRNA electrostatically attaches to the positively charged polylysine. Upon laser irradiation at the plasmon resonance wavelength of the nanoshell, the electrostatic attraction is broken. We demonstrate the controllable light-triggered delivery of both ssDNA and siRNA and subsequent GFP protein downregulation within a H1299 lung cancer, GFP-expressing cell line *in vitro*. Light-triggered delivery resulted in ~ 47% and ~49% downregulation of the targeted GFP expression by ssDNA and siRNA, respectively. Cytotoxicity induced by both the polylysine nanoshell delivery vector and the laser irradiation is minimal, as demonstrated by a XTT cell proliferation assay.

Hopefully, this work has laid the groundwork for future applications towards light-triggered controllable release of small molecules, gene therapeutics, proteins, and other biologically relevant molecules. Because this light-triggered release is based upon a host-guest complex attached to a plasmonic particle, additional attachment techniques undoubtedly will be investigated. Light-triggered release has the advantages of delivering molecules with temporal and spatial control, which could minimize drug side effects and

increase efficacy. With additional experiments and optimization, this delivery strategy has the capability to become another tool for clinicians to use towards treating a multitude of genetic diseases.

Appendix A: Supplementary Figures

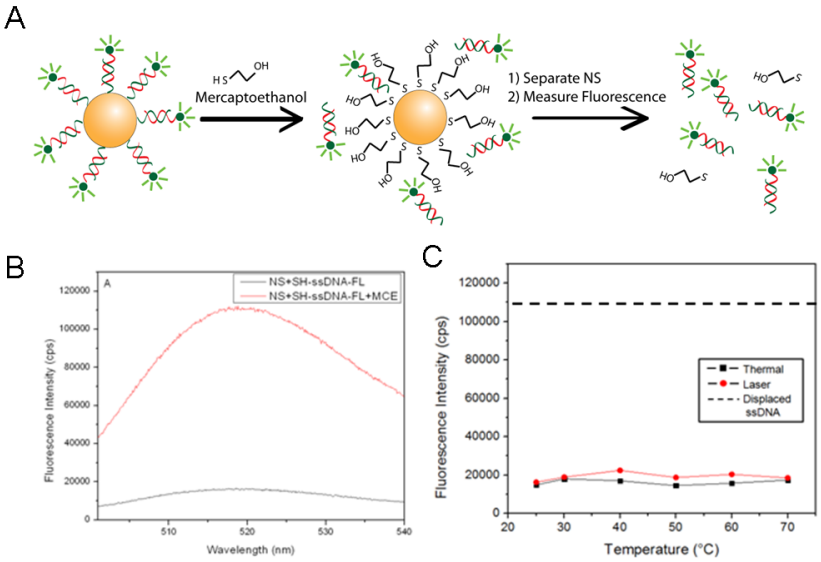

Figure A-1. Effect of thermal and laser treatments on Au-thiol bond stability. (A) Schematic of fluorescein-tagged, thiolated ssDNA attached to a NS. (B) The fluorescence spectrum of the supernatant before (black line) and after (red line) displacement by mercaptoethanol (MCE) of the fluorescein-tagged, thiolated ssDNA.(C) Peak fluorescence intensity (λ = 520nm) of fluorescein in the supernatant as a function of solution temperature for thermal treatment (black squares) and laser treatment (red dots). The dashed line (-----) corresponds to complete release, determined by the peak at 520nm from the red curve in (B).

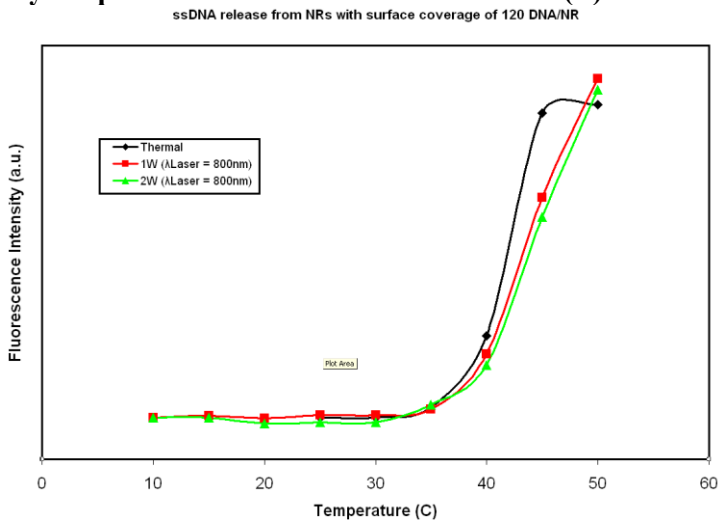

Figure A-2. ssDNA release from dsDNA-NRs with surface coverage of 120 DNA/NR. Fluorescence intensity (a.u.) versus solution temperature (°C).

Appendix B: Protocol for Nanoshell Synthesis

1) Preparing 1% (m/V) Au(III) Chloride Hydrate Salt Solution

1.1) Before nanoshells can be synthesized, the necessary Au(III) Chloride Hydrate solution and 2-3 nm THPC Au colloid needs to be made.

1.2) Prepare a 1% mass/volume (0.02943 M) Au salt solution by adding approximately 5 mL of deionized water to the newly opened 5g bottle of Au(III) Chloride Hydrate ($HAuCl_4$, Sigma Aldrich, 99.999%) and vortex until completely dissolved. Then dilute this 5 mL solution to 500 mL by using a volumetric flask. Store this solution in an amber glass bottle, in a dark cabinet at room temperature, and allow it to age for at least 10 days before use. This solution is good for at least a year, as long as it is stored in the dark at room temperature.

2) Preparing 2-3 nm THPC Au Colloid Solution[243]

2.1) Make a 251.4 mM solution of Tetrakis(hydroxymethyl)phosphonium chloride (THPC) in water by adding 400 μL of THPC (Sigma Aldrich, 80% (w/w) in H_2O) to 33 mL of deionized water.

2.2) Separately, measure 180 mL of deionized water and pour it into a 250 mL flat bottom beaker. Under vigorous stirring add 1.2 mL of 1M NaOH (Acros Organics) followed by 4 mL of the 251.4 mM THPC solution. Allow the solution to stir vigorously for 5 minutes.

2.3) While waiting, measure out 6.75 mL of the 1% (m/v) Au(III) Chloride Hydrate salt solution into a small beaker. After waiting the 5 minutes, under vigorous stirring, in one quick motion, add the 6.75 mL of the 1% (m/v) Au salt solution. The color of the solution

changes instantly from colorless to brown. Store the solution in a capped container at 4°C and allow it to age for at least 14 days. This THPC Au colloid solution produces the best nanoshells when used from 14 days – 8 weeks old.

3) Synthesis of the Silica Cores

3.1) Spherical Silica cores can either be synthesized or purchased commercially. For highly reproducible results, buying commercial cores is recommended, especially if your primary interest is in one particular nanoshell size and resonance; however the size of the silica cores and the polydispersity should always be checked either by Scanning Electron Microscopy (SEM) or by Dynamic Light Scattering (DLS). The standard deviation should be less than 5% and definitely not exceed 10%.

3.2) The following synthesis of silica cores is commonly called the Stöber recipe[244] and reliably produces spherical silica particles with diameters between 70 and 800 nm. If you need particle sizes outside of this range consult the literature for additional silica particle protocols.

3.3) Distill Tetraethylorthosilicate (TEOS Sigma Aldrich 99.99%) if desired. In order to make very monodisperse silica particles it is necessary to distill the TEOS. Distillation will result in silica particles with 5-10% polydispersity.

3.4) The following procedure makes 120 nm diameter silica particles. To make silica particles with different sizes refer to the literature for the correct ratios of ethanol, ammonium hydroxide, and tetraethylorthosilicate. Nanoshells can be synthesized on different sized silica particles. When changing to a different sized core, the centrifuge speeds will vary. See table B-1 for suggested centrifuge speeds.

3.5) Measure out 100 mL of 200 proof ethanol and pour it into a clean 200 mL polypropylene bottle. Add 5.7 mL of ammonium hydroxide (Sigma Aldrich, 28% NH3 in H_2O). Under vigorous stirring, add 1.5 mL of tetraethylorthosilicate (TEOS) (Sigma Aldrich, 99.999%). Allow to react for 8 hours or overnight.

3.6) Measure the size of the silica particles by a Scanning Electron Microscope (SEM), a Tunneling Electron Microscope (TEM), or Dynamic Light Scattering (DLS) instrument. The polydispersity should be less than 5% and not exceed 10%.

3.7) The silica particles are washed by centrifugation. Centrifuge speeds vary with silica particle size (Table B-1). For 120 nm diameter silica particles, centrifuge at 3500 rcf for 30 minutes. After centrifuging, pour off the excess supernatant. Resuspend the silica particles into 40 mL of deionized water with a probe sonicator (Do not allow the solution to become warm). Repeat the centrifugation and resuspension in water again.

3.8) Centrifuge again and resuspend the silica particles in 40 mL of 200 proof ethanol. Repeat the centrifugation and resuspension in ethanol again. Centrifuge once more and resuspend in ethanol to a volume of 40 ml.

Silica Diameter (nm)	Silica nanoparticles	Seed	Nanoshells
80 nm	6000 rcf	3000 rcf	600 rcf
120 nm	3500 rcf	1500 rcf	350 rcf
180 nm	1500 rcf	800 rcf	200 rcf
270 nm	1000 rcf	500 rcf	70 rcf

Table B-1. Suggested Centrifuge Speeds for silica particles, seed particles, and nanoshells dependent upon silica particle diameter.

4) Functionalizing the Silica Cores with 3-Aminopropyltriethoxysilane

4.1) Once the silica core particles are complete they have to be coated with aminopropyltriethoxysilane (APTES) (Sigma Aldrich, 99.99%).

4.2) Pour the 40 mL of silica particle/ethanol suspension into a 50-mL clean polypropylene bottle. Under vigorous stirring, add the APTES and wait 10 minutes, then decrease the stirring speed and stir for 8 h or overnight.

4.3) After stirring overnight, pour the solution into a clean glass beaker and place on a hot plate. Using low heat, bring the solution to a boil. Boil for 1 hour. Total evaporation of the ethanol solvent during boiling is prevented by the continuous addition of ethanol.

4.4) Clean the APTES functionalized cores with 3 steps of centrifugation and resuspension in 200 proof ethanol. The final resuspension in ethanol should be to a volume of 10 mL. These APTES functionalized silica cores can be used for 3 or more years as long as the solution is capped tightly and sealed with parafilm, which ensures the silica cores will not dry out.

5) Making the "Seed" Particles: Attachment of THPC Au Colloid to APTES Functionalized Silica Particles

5.1) Before a Au shell can be grown around the silica cores, the 2-3 nm THPC Au colloid needs to be attached to the outside of the APTES-functionalized silica particles.

5.2) Prepare 5 mL of 1M NaCl solution in deionized water. Measure out 40 mL of aged THPC Au colloid solution into a 50 mL centrifuge tube. Sonicate the APTES functionalized cores with either a probe sonicator or a bath sonicator for 1-2 minutes.

5.3) Using two micropipettes, add 1 mL of the 1M NaCl solution to the THPC Au colloid solution, followed immediately by 400 uL of the APTES-functionalized silica

particles. Quickly cap the centrifuge tube, vortex, and place in a bath sonicator at medium power for 2 minutes. Take out and let the solution sit at room temperature for a minimum of 8 hours to a maximum of 48 hours.

5.4) To remove the excess THPC Au colloid, centrifuge at 1500 rcf for 15 minutes (Centrifuge speeds will vary with particle size, Table B-1). The supernatant will still be a dark brown color, but the darker soft pellet should be visible at the bottom of the centrifuge tube. Carefully pipette off the supernatant and resuspend the seed particles in deionized water by vortexing and bath sonication at medium power.

5.5) Repeat centrifugation and resuspension until the supernatant is colorless. Two centrifugation and resuspension cycles typically works fine. Three centrifugation and resuspension cycles is the maximum. The final resuspension should give a UV-Vis extinction (absorbance) measurement of 1.0 with a cuvette path length of 1 cm (Figure B-1). This solution can either be used immediately for nanoshell synthesis or can be stored, for later use, at 4°C for 2-3 months.

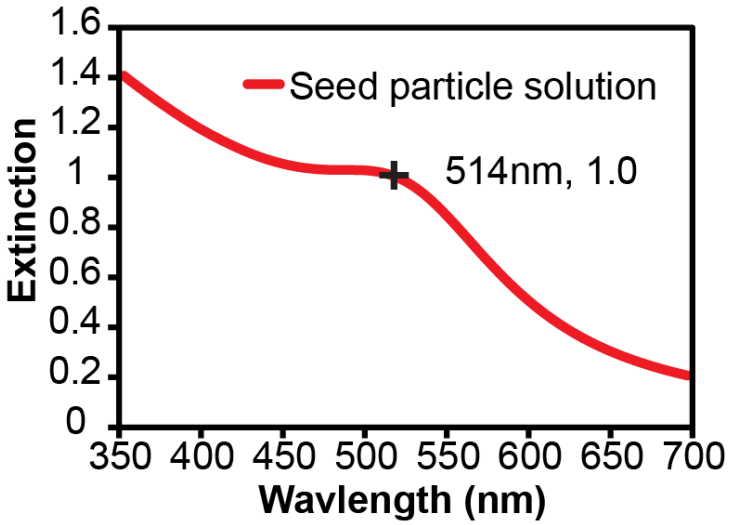

Figure B-1. UV-Vis extinction spectrum of seed solution.

6) Preparing Au Salt/Potassium Carbonate Electroless Plating Solution

6.1) The Au shell is grown around the silica core by an electroless plating method that requires an aged Au solution, therefore make this solution at least 48 hours before nanoshell synthesis is performed.

6.2) Measure out 200 mL of deionized water and put it into an amber bottle. Add 50 mg of potassium carbonate and then add 3 mL of aged Au salt solution (1% $HAuCl_4$). Cap the container and shake rigorously for 30 s to mix the solution. Store the solution in a dark cabinet at room temperature. Use the solution after 48 hours and before 7 days old. The final concentrations of potassium carbonate and Au(III) Chloride Hydrate are 1.8 mM and 435 μM (0.01478% (m/v)), respectively.

7) Au Shell Growth via Electroless Plating

7.1) The growth of the Au shell proceeds by mixing different volumes of the seed particle solution to the Au salt/potassium carbonate electroless plating solution and then adding a fixed volume of reductant. For this protocol, formaldehyde is used as the reductant (Sigma Aldrich, 36.5-38% in H_2O); however, other reductants such as Carbon Monoxide and Sodium borohydride can be used.

7.2) Sonicate the solution of seed particles for 1 – 2 minutes in the bath sonicator and get 10 plastic cuvettes (4 ml capacity) and number them 1-10. Add 3 mL of the electroless plating solution to each plastic cuvette.

7.3) Add 40 μL of the seed particle solution to cuvette number 1. Increase the volume of seed solution added to each cuvette by 10μL increments up to the tenth cuvette, which should have 130 uL seed in it. Add 15 uL formaldehyde solution (Sigma Aldrich, 36.5-38% in H_2O) to each cuvette. Cap the cuvette, shake vigorously for 3 minutes, and allow

to stand for 2 minutes. The solution will change from colorless to a color which is dependent upon the size of silica core and the thickness of the Au shell.

7.4) Using a UV-VIS-NIR Spectrophotometer, take an extinction measurement of each cuvette to determine the plasmon resonance peak of each nanoshell sample. Adding more seed particles will result in thinner shells that redshift the plasmon resonance and adding less seed will result in thicker shells that blue shift the plasmon resonance (Figure B-4). See troubleshooting in the discussion section if none of the cuvettes resulted in the desired plasmon resonance wavelength.

7.5) Scale up your nanoshell batch by repeating the above procedure with a larger volume of plating solution, seed solution, and formaldehyde in the selected ratio that resulted in the desired plasmon resonance. Stir for 10 minutes. Centrifuge the nanoshells at the required speed (Table B-1) for 20 minutes. Pipette off the supernatant from the nanoshell pellet and resuspend the pellet in deionized water by vortexing and bath sonication at medium power. Repeat centrifugation 1-2 more times.

7.6) Always check to see if the Au shell is complete by either SEM or TEM. A UV-Vis-NIR spectrum might look good, but the shell can still have cracks in it, which is undesirable for most nanoshell applications.

8) Representative Results

An UV-Vis-NIR extinction spectrum and a scanning electron microscope (SEM) image of a [60, 74] nm nanoshell is shown in figure B-2 and B-3, respectively. It is very important to look at the nanoshells with a SEM to make sure the synthesized nanoshells are free of cracks, holes, defects, or aggregates. For a well-synthesized batch of nanoshells on 120 nm diameter silica cores the extinction spectrum should look similar to figure B-2. The

peak largest peak at ~800 nm is the dipole resonance and the shoulder at ~600 nm is the quadruple resonance. Also, the peak: trough ratio should be a 3 or greater (peak: trough ≥ 3). For example, the spectrum in figure B-2, the peak intensity at ~800 nm is 2 and the trough ~500nm is ~0.45 making the ratio ~4

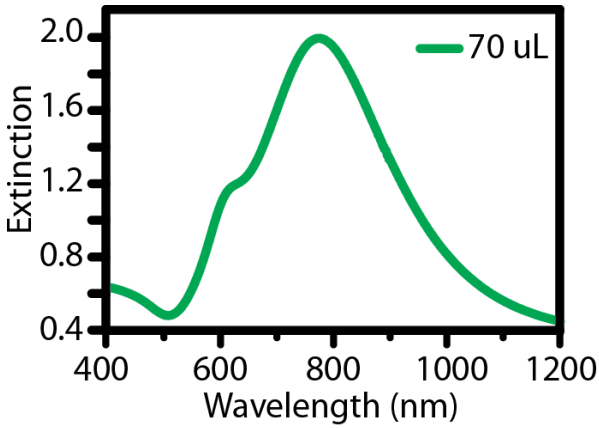

Figure B-2. Silica core/Au shell nanoshell, [r_1, r_2] = [60, 74] nm. The peak (2 at ~800nm) to trough (.45 at ~500nm) ratio should be a minimum of~ 3 for complete shells.

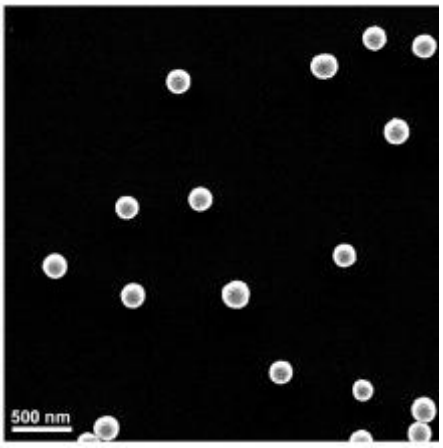

Figure B-3. Scanning electron microscope image of a [r_1, r_2] = [60, 74] nm Au nanoshells.

Figure B-4 shows how the extinction spectra change as the volume of seed particles is varied. Adding the least amount of seed results in the thickest shell and the quadrupole peak is larger (Figure B-4A). As the volume of seed is increased, the Au shell thickness decreases, the quadruple becomes smaller, and the dipole peak redshifts to longer wavelengths (Figure B-4B-C). If an excess of seed is added, the Au shell is incomplete, the quadrupole is not visible, and the dipole peak blueshifts (Figure B-4D). Additionally, if the nanoshell extinction spectrum has a peak: trough ratio less than 3, then this is strong indication that the Au shell is incomplete.

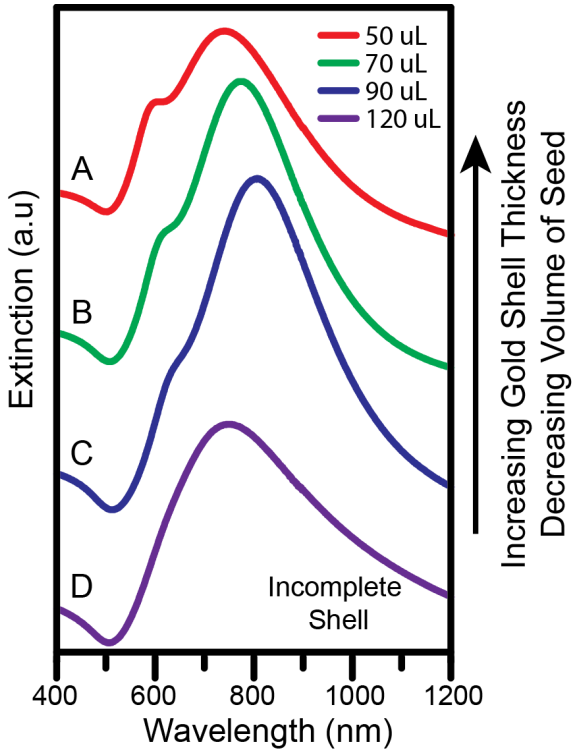

Figure B-4. Extinction spectra of Au nanoshells fabricated on 120nm diameter silica particles. Decreasing the volume of seed particle solution results in a thicker Au shell and a blueshift of the the plasmon resonance. (A) Complete nanoshells with thick Au shell. (B-C) The Au shell becomes thinner as the volume of seed added is increased and the plasmon resonance redshifts. The quadrupole (~600 nm) becomes smaller for thinner shells. (D) Incomplete Au shell. The quadruple (~600 nm) is not visible for incomplete shells. Figure adapted from Ref. [245]

The peak: trough ratio and plasmon resonance extinction line shape (dipole quadrupole, and sometimes octopole peak intensities) will vary when changing the size of the silica core and the thickness of the Au shell. For example nanoshells synthesized on a 80 nm diameter silica core with a 10 nm thick Au shell, do not have a quadrupole shoulder. Therefore, theoretical calculations (Mie theory, COMSOL Multiphysics, etc) should be performed to predict the line shape and peak: trough ratio of the nanoshell extinction spectrum.

Name of the reagent	Company	Catalogue number	Comments
Au(III) Chloride Hydrate	Sigma Aldrich	254169	99.999%
Tetrakis(hydroxymethyl)phosphonium Chloride Solution	Sigma Aldrich	404861	(80% in H_2O)
1M Sodium Hydroxide	Acros Organics	124260010	
Tetraethyl Orthosilicate	Sigma Aldrich	333859	99.999%
Ammonium Hydroxide	Sigma Aldrich	338818	28% NH3 in H20, ≥99.99% trace metals basis
200 Proof Ethyl Alcohol	Sigma Aldrich	459844	
(3-Aminopropyl)triethoxysilane	Sigma Aldrich	A3648	
Sodium Chloride	Sigma Aldrich	S7653	
Potassium carbonate	Sigma Aldrich	P5833	
Formaldehyde solution	Sigma Aldrich	F8775	36.5-38% in H_2O

Table B-2. Reagents needed for synthesis of silica-Au nanoshells.

References

1. Levin, C. S.; Kundu, J.; Barhoumi, A.; Halas, N. J., Nanoshell-based substrates for surface enhanced spectroscopic detection of biomolecules. *Analyst* **2009,** *134*, 1745-1750.

2. Kundu, J.; Levin, C. S.; Halas, N. J., Real-time monitoring of lipid transfer between vesicles and hybrid bilayers on Au nanoshells using surface enhanced Raman scattering (SERS). *Nanoscale* **2009,** *1*, 114-117.

3. Willets, K. A.; Van Duyne, R. P., Localized surface plasmon resonance spectroscopy and sensing. In *Annual Review of Physical Chemistry*, Annual Reviews: Palo Alto, 2007; Vol. 58, pp 267-297.

4. Stiles, P. L.; Dieringer, J. A.; Shah, N. C.; Van Duyne, R. R., Surface-Enhanced Raman Spectroscopy. In *Annual Review of Analytical Chemistry*, Annual Reviews: Palo Alto, 2008; Vol. 1, pp 601-626.

5. Liu, N.; Mesch, M.; Weiss, T.; Hentschel, M.; Giessen, H., Infrared Perfect Absorber and Its Application As Plasmonic Sensor. *Nano Letters* **2010,** *10*, 2342-2348.

6. Svedendahl, M.; Chen, S.; Dmitriev, A.; Käll, M., Refractometric Sensing Using Propagating versus Localized Surface Plasmons: A Direct Comparison. *Nano Letters* **2009,** *9*, 4428-4433.

7. Huang, X. H.; El-Sayed, I. H.; Qian, W.; El-Sayed, M. A., Cancer cell imaging and photothermal therapy in the near-infrared region by using gold nanorods. *Journal of the American Chemical Society* **2006,** *128*, 2115-2120.

8. Loo, C.; Lin, A.; Hirsch, L.; Lee, M. H.; Barton, J.; Halas, N. J.; West, J.; Drezek, R., Nanoshell-enabled photonics-based imaging and therapy of cancer. *Technol. Cancer Res. Treat.* **2004,** *3*, 33-40.

9. Agrawal, A.; Huang, S.; Lin, A. W. H.; Lee, M.-H.; Barton, J. K.; Drezek, R. A.; Pfefer, T. J., Quantitative evaluation of optical coherence tomography signal enhancement with gold nanoshells. *Journal of Biomedical Optics* **2006,** *11*, 041121.

10. Bardhan, R.; Chen, W. X.; Bartels, M.; Perez-Torres, C.; Botero, M. F.; McAninch, R. W.; Contreras, A.; Schiff, R.; Pautler, R. G.; Halas, N. J*., et al.*, Tracking of Multimodal Therapeutic Nanocomplexes Targeting Breast Cancer in Vivo. *Nano Lett.* **2010,** *10*, 4920-4928.

11. Bardhan, R.; Chen, W. X.; Perez-Torres, C.; Bartels, M.; Huschka, R. M.; Zhao, L. L.; Morosan, E.; Pautler, R. G.; Joshi, A.; Halas, N. J., Nanoshells with Targeted Simultaneous Enhancement of Magnetic and Optical Imaging and Photothermal Therapeutic Response. *Adv. Funct. Mater.* **2009,** *19*, 3901-3909.

12. Tam, F.; Goodrich, G. P.; Johnson, B. R.; Halas, N. J., Plasmonic enhancement of molecular fluorescence. *Nano Letters* **2007,** *7*, 496-501.

13. Chen, W.; Bardhan, R.; Bartels, M.; Perez-Torres, C.; Pautler, R. G.; Halas, N. J.; Joshi, A., A Molecularly Targeted Theranostic Probe for Ovarian Cancer. *Molecular Cancer Therapeutics* **2010,** *9*, 1028-1038.

14. Lal, S.; Clare, S. E.; Halas, N. J., Nanoshell-Enabled Photothermal Cancer Therapy: Impending Clinical Impact. *Accounts of Chemical Research* **2008,** *41*, 1842-1851.

15. O'Neal, D. P.; Hirsch, L. R.; Halas, N. J.; Payne, J. D.; West, J. L., Photo-thermal tumor ablation in mice using near infrared-absorbing nanoparticles. *Cancer Letters* **2004,** *209*, 171-176.

16. Jain, P. K.; Huang, X.; El-Sayed, I. H.; El-Sayed, M. A., Noble Metals on the Nanoscale: Optical and Photothermal Properties and Some Applications in Imaging, Sensing, Biology, and Medicine. *Accounts of Chemical Research* **2008,** *41*, 1578-1586.

17. Hardin, B. E.; Yum, J.-H.; Hoke, E. T.; Jun, Y. C.; Péchy, P.; Torres, T. s.; Brongersma, M. L.; Nazeeruddin, M. K.; Grätzel, M.; McGehee, M. D., High Excitation Transfer Efficiency from Energy Relay Dyes in Dye-Sensitized Solar Cells. *Nano Letters* **2010,** *10*, 3077-3083.

18. Cao, L.; Fan, P.; Vasudev, A. P.; White, J. S.; Yu, Z.; Cai, W.; Schuller, J. A.; Fan, S.; Brongersma, M. L., Semiconductor Nanowire Optical Antenna Solar Absorbers. *Nano Letters* **2010,** *10*, 439-445.

19. Ferry, V. E.; Sweatlock, L. A.; Pacifici, D.; Atwater, H. A., Plasmonic Nanostructure Design for Efficient Light Coupling into Solar Cells. *Nano Letters* **2008,** *8*, 4391-4397.

20. Liao, H.; Nehl, C. L.; Hafner, J. H., Biomedical applications of plasmon resonant metal nanoparticles. *Nanomedicine* **2006,** *1*, 201-208.

21. American Cancer Society. *Cancer Facts & Figures 2008*; Atlanta:American Cancer Society; **2008**.

22. Elbashir, S. M.; Harborth, J.; Lendeckel, W.; Yalcin, A.; Weber, K.; Tuschl, T., Duplexes of 21-nucleotide RNAs mediate RNA interference in cultured mammalian cells. *Nature* **2001,** *411*, 494-498.

23. Devi, G. R., siRNA-based approaches in cancer therapy. *Cancer Gene Therapy* **2006,** *13*, 819-829.

24. de Fougerolles, A.; Vornlocher, H.-P.; Maraganore, J.; Lieberman, J., Interfering with disease: a progress report on siRNA-based therapeutics. *Nat Rev Drug Discov* **2007,** *6*, 443-453.

25. Patil, S. D.; Rhodes, D. G.; Burgess, D. J., DNA-based therapeutics and DNA delivery systems: A comprehensive review. *AAPS Journal* **2005,** *7*, E61-E77.

26. Pouton, C. W.; Seymour, L. W., Key issues in non-viral gene delivery. *Advanced Drug Delivery Reviews* **2001,** *46*, 187-203.

27. Rosi, N. L.; Giljohann, D. A.; Thaxton, C. S.; Lytton-Jean, A. K. R.; Han, M. S.; Mirkin, C. A., Oligonucleotide-modified gold nanoparticles for intracellular gene regulation. *Science* **2006,** *312*, 1027-1030.

28. Stephens, A. C.; Rivers, R. P. A., Antisense oligonucleotide therapy in cancer. *Current Opinion in Molecular Therapeutics* **2003,** *5*, 118-122.

29. Check, E., Gene therapy: A tragic setback. *Nature* **2002,** *420*, 116-118.

30. Aagaard, L.; Rossi, J. J., RNAi therapeutics: Principles, prospects and challenges. *Adv Drug Del Rev* **2007,** *59*, 75-86.

31. Braun, G. B.; Pallaoro, A.; Wu, G. H.; Missirlis, D.; Zasadzinski, J. A.; Tirrell, M.; Reich, N. O., Laser-Activated Gene Silencing via Gold Nanoshell-siRNA Conjugates. *ACS Nano* **2009,** *3*, 2007-2015.

32. Davis, M. E.; Zuckerman, J. E.; Choi, C. H. J.; Seligson, D.; Tolcher, A.; Alabi, C. A.; Yen, Y.; Heidel, J. D.; Ribas, A., Evidence of RNAi in humans from systemically administered siRNA via targeted nanoparticles. *Nature* **2010,** *464*, 1067-1070.

33. Karmali, P. P.; Chaudhuri, A., Cationic Liposomes as non-viral carriers of gene medicines: Resolved issues, open questions, and future promises. *Med Res Rev* **2007,** *27*, 696-722.

34. Kim, D. H.; Rossi, J. J., Strategies for silencing human disease using RNA interference. *Nat Rev Genet* **2007,** *8*, 173-184.

35. Oldenburg, S. J.; Averitt, R. D.; Westcott, S. L.; Halas, N. J., Nanoengineering of optical resonances. *Chem. Phys. Lett.* **1998,** *288*, 243-247.

36. Tam, F.; Moran, C.; Halas, N., Geometrical Parameters Controlling Sensitivity of Nanoshell Plasmon Resonances to Changes in Dielectric Environment. *The Journal of Physical Chemistry B* **2004,** *108*, 17290-17294.

37. Bardhan, R.; Grady, N. K.; Ali, T.; Halas, N. J., Metallic Nanoshells with Semiconductor Cores: Optical Characteristics Modified by Core Medium Properties. *ACS Nano* **2010,** *4*, 6169-6179.

38. Wang, H.; Tam, F.; Grady, N. K.; Halas, N. J., Cu Nanoshells: Effects of Interband Transitions on the Nanoparticle Plasmon Resonance. *The Journal of Physical Chemistry B* **2005,** *109*, 18218-18222.

39. Weissleder, R., A clearer vision for in vivo imaging. *Nature Biotechnology* **2001,** *19*, 316-317.

40. Brinson, B. E.; Lassiter, J. B.; Levin, C. S.; Bardhan, R.; Mirin, N.; Halas, N. J., Nanoshells made easy: Improving Au layer growth on nanoparticle surfaces. *Langmuir* **2008,** *24*, 14166-14177.

41. Oldenburg, S. J.; Averitt, R. D.; Westcott, S. L.; Halas, N. J., Nanoengineering of optical resonances. *Chem. Phys. Lett.* **1998,** *288*, 243-247.

42. Duff, D. G.; Baiker, A.; Edwards, P. P., A New Hydrosol of Gold Clusters. 1. Formation and Particle Size Variation. *Langmuir* **1993,** *9*, 2301-2309.

43. Prodan, E.; Radloff, C.; Halas, N. J.; Nordlander, P., A hybridization model for the plasmon response of complex nanostructures. *Science* **2003,** *302*, 419-422.

44. Sau, T. K.; Murphy, C. J., Seeded high yield synthesis of short Au nanorods in aqueous solution. *Langmuir* **2004,** *20*, 6414-6420.

45. Zuloaga, J.; Prodan, E.; Nordlander, P., Quantum Plasmonics: Optical Properties and Tunability of Metallic Nanorods. *ACS Nano* **2010,** *4*, 5269-5276.

46. Orendorff, C. J.; Murphy, C. J., Quantitation of Metal Content in the Silver-Assisted Growth of Gold Nanorods. *J. Phys. Chem. B* **2006,** *110*, 3990-3994.

47. Barlogie, B.; Raber, M. N.; Schumann, J.; Johnson, T. S.; Drewinko, B.; Swartzendruber, D. E.; Gohde, W.; Andreeff, M.; Freireich, E. J., Flow-cytometry in Clinical Cancer-research. *Cancer Research* **1983,** *43*, 3982-3997.

48. Giepmans, B. N. G.; Adams, S. R.; Ellisman, M. H.; Tsien, R. Y., Review - The fluorescent toolbox for assessing protein location and function. *Science* **2006,** *312*, 217-224.

49. Uherek, C.; Wels, W., DNA-carrier proteins for targeted gene delivery. *Advanced Drug Delivery Reviews* **2000,** *44*, 153-166.

50. Crooke, S. T., Molecular mechanisms of action of antisense drugs. *Biochimica Et Biophysica Acta-Gene Structure and Expression* **1999,** *1489*, 31-44.

51. Whitehead, K. A.; Langer, R.; Anderson, D. G., Knocking down barriers: advances in siRNA delivery. *Nature Reviews Drug Discovery* **2009,** *8*, 129-138.

52. Stull, R. A.; Szoka, F. C., Antigene, Ribozyme, and Aptamer Nucleic-acid Drugs - Progress and Prospects. *Pharmaceutical Research* **1995,** *12*, 465-483.

53. Stephenson, M. L.; Zamecnik, P. C., Inhibition of Rous-sarcoma Viral-RNA Translation by a Specific Oligodeoxyribonucleotide. *Proceedings of the National Academy of Sciences of the United States of America* **1978,** *75*, 285-288.

54. Gewirtz, A. M., Oligonucleotide therapeutics: A step forward. *Journal of Clinical Oncology* **2000,** *18*, 1809-1811.

55. Israel, Z. H.; Domb, A. J., Polymers in gene therapy: Antisense delivery systems. *Polymers for Advanced Technologies* **1998,** *9*, 799-805.

56. Langer, R.; Tirrell, D. A., Designing materials for biology and medicine. *Nature* **2004,** *428*, 487-492.

57. Ghosh, P.; Han, G.; De, M.; Kim, C. K.; Rotello, V. M., Gold nanoparticles in delivery applications. *Adv Drug Del Rev* **2008,** *60*, 1307-1315.

58. Carter, P. J.; Samulski, R. J., Adeno-associated viral vectors as gene delivery vehicles (review). *International Journal of Molecular Medicine* **2000,** *6*, 17-27.

59. Han, G.; Martin, C. T.; Rotello, V. M., Stability of gold nanoparticle-bound DNA toward biological, physical, and chemical agents. *Chemical Biology & Drug Design* **2006,** *67*, 78-82.

60. Salem, A. K.; Searson, P. C.; Leong, K. W., Multifunctional nanorods for gene delivery. *Nature Materials* **2003,** *2*, 668-671.

61. Hong, R.; Han, G.; Fernandez, J. M.; Kim, B. J.; Forbes, N. S.; Rotello, V. M., Glutathione-mediated delivery and release using monolayer protected nanoparticle carriers. *Journal of the American Chemical Society* **2006,** *128*, 1078-1079.

62. Polizzi, M. A.; Stasko, N. A.; Schoenfisch, M. H., Water-soluble nitric oxide-releasing gold nanoparticles. *Langmuir* **2007,** *23*, 4938-4943.

63. Han, G.; You, C.-C.; Kim, B.-j.; Turingan, R. S.; Forbes, N. S.; Martin, C. T.; Rotello, V. M., Light-Regulated Release of DNA and Its Delivery to Nuclei by Means of Photolabile Gold Nanoparticles. *Angewandte Chemie* **2006,** *118*, 3237-3241.

64. Lee, S. E.; Liu, G. L.; Kim, F.; Lee, L. P., Remote Optical Switch for Localized and Selective Control of Gene Interference. *Nano Lett.* **2009,** *9*, 562-570.

65. Hu, M.; Chen, J.; Li, Z.-Y.; Au, L.; Hartland, G. V.; Li, X.; Marquez, M.; Xia, Y., Gold nanostructures: engineering their plasmonic properties for biomedical applications. *Chemical Society Reviews* **2006,** *35*, 1084-1094.

66. Link, S.; Ei-Sayed, M. A., Optical properties and ultrafast dynamics of metallic nanocrystals. *Annual Review of Physical Chemistry* **2003,** *54*, 331-366.

67. Govorov, A. O.; Zhang, W.; Skeini, T.; Richardson, H.; Lee, J.; Kotov, N. A., Gold nanoparticle ensembles as heaters and actuators: melting and collective plasmon resonances. *Nanoscale Research Letters* **2006,** *1*, 84-90.

68. Richardson, H. H.; Carlson, M. T.; Tandler, P. J.; Hernandez, P.; Govorov, A. O., Experimental and Theoretical Studies of Light-to-Heat Conversion and Collective Heating Effects in Metal Nanoparticle Solutions. *Nano Letters* **2009,** *9*, 1139-1146.

69. Govorov, A. O.; Richardson, H. H., Generating heat with metal nanoparticles. *Nano Today* **2007,** *2*, 30-38.

70. Hu, M.; Hartland, G. V., Heat dissipation for Au particles in aqueous solution: Relaxation time versus size. *Journal of Physical Chemistry B* **2002,** *106*, 7029-7033.

71. Fu, A. H.; Micheel, C. M.; Cha, J.; Chang, H.; Yang, H.; Alivisatos, A. P., Discrete nanostructures of quantum dots/Au with DNA. *Journal of the American Chemical Society* **2004,** *126*, 10832-10833.

72. Yavas, O.; Leiderer, P.; Park, H. K.; Grigoropoulos, C. P.; Poon, C. C.; Leung, W. P.; Do, N.; Tam, A. C., Optical Reflectance and Scattering Studies of Nucleation and Growth of Bubbles at a Liquid-Solid Interface Induced by Pulsed Laser-Heating. *Physical Review Letters* **1993,** *70*, 1830-1833.

73. Link, S.; Burda, C.; Nikoobakht, B.; El-Sayed, M. A., How long does it take to melt a gold nanorod? A femtosecond pump-probe absorption spectroscopic study. *Chemical Physics Letters* **1999,** *315*, 12-18.

74. Aguirre, C. M.; Moran, C. E.; Young, J. F.; Halas, N. J., Laser-induced reshaping of metallodielectric nanoshells under femtosecond and nanosecond plasmon resonant illumination. *Journal of Physical Chemistry B* **2004,** *108*, 7040-7045.

75. Huttmann, G.; Birngruber, R., On the possibility of high-precision photothermal microeffects and the measurement of fast thermal denaturation of proteins. *Ieee Journal of Selected Topics in Quantum Electronics* **1999,** *5*, 954-962.

76. Hirsch, L. R.; Stafford, R. J.; Bankson, J. A.; Sershen, S. R.; Rivera, B.; Price, R. E.; Hazle, J. D.; Halas, N. J.; West, J. L., Nanoshell-mediated near-infrared thermal therapy of tumors under magnetic resonance guidance. *Proceedings of the National Academy of Sciences of the United States of America* **2003,** *100*, 13549-13554.

77. Jain, P. K.; Huang, X.; El-Sayed, I. H.; El-Sayad, M. A., Review of some interesting surface plasmon resonance-enhanced properties of noble metal nanoparticles and their applications to biosystems. *Plasmonics* **2007,** *2*, 107-118.

78. Gobin, A. M.; Lee, M. H.; Halas, N. J.; James, W. D.; Drezek, R. A.; West, J. L., Near-infrared resonant nanoshells for combined optical imaging and photothermal cancer therapy. *Nano Lett.* **2007,** *7*, 1929-1934.

79. Pissuwan, D.; Valenzuela, S. M.; Cortie, M. B., Therapeutic possibilities of plasmonically heated gold nanoparticles. *Trends in Biotechnology* **2006,** *24*, 62-67.

80. Knight, M. W.; Sobhani, H.; Nordlander, P.; Halas, N. J., Photodetection with active optical antennas. *Science* **2011,** *332*, 702-4.

81. Jin, R. C.; Cao, Y. W.; Mirkin, C. A.; Kelly, K. L.; Schatz, G. C.; Zheng, J. G., Photoinduced conversion of silver nanospheres to nanoprisms. *Science* **2001,** *294*, 1901-1903.

82. Redmond, P. L.; Brus, L. E., "Hot electron" photo-charging and electrochemical discharge kinetics of silver nanocrystals. *J Phys Chem C* **2007,** *111*, 14849-14854.

83. Lindstrom, C. D.; Zhu, X. Y., Photoinduced electron transfer at molecule-metal interfaces. *Chem. Rev.* **2006,** *106*, 4281-4300.

84. Wang, H.; Brandl, D. W.; Nordlander, P.; Halas, N. J., Plasmonic nanostructures: Artificial molecules. *Accounts of Chemical Research* **2007,** *40*, 53-62.

85. Nikoobakht, B.; El-Sayed, M. A., Preparation and growth mechanism of gold nanorods (NRs) using seed-mediated growth method. *Chemistry of Materials* **2003,** *15*, 1957-1962.

86. Schwartzberg, A. M.; Olson, T. Y.; Talley, C. E.; Zhang, J. Z., Synthesis, characterization, and tunable optical properties of hollow gold nanospheres. *Journal of Physical Chemistry B* **2006,** *110*, 19935-19944.

87. Breslauer, K. J.; Frank, R.; Blocker, H.; Marky, L. A., Predicting DNA Duplex Stability from the Base Sequence. *Proceedings of the National Academy of Sciences of the United States of America* **1986,** *83*, 3746-3750.

88. Crothers, D. M.; Zimm, B. H., Theory of Melting Transition of Synthetic Polynucleotides - Evaluation of Stacking Free Energy. *Journal of Molecular Biology* **1964,** *9*, 1-&.

89. Devoe, H., Stability of Helical Polynucleotides - Base Contributions. *Journal of Molecular Biology* **1962,** *4*, 500-&.

90. SantaLucia, J., A unified view of polymer, dumbbell, and oligonucleotide DNA nearest-neighbor thermodynamics. *Proceedings of the National Academy of Sciences of the United States of America* **1998,** *95*, 1460-1465.

91. SantaLucia, J.; Allawi, H. T.; Seneviratne, A., Improved nearest-neighbor parameters for predicting DNA duplex stability. *Biochemistry* **1996,** *35*, 3555-3562.

92. Delcourt, S. G.; Blake, R. D., Stacking Energies in DNA. *Journal of Biological Chemistry* **1991,** *266*, 15160-15169.

93. Doktycz, M. J.; Goldstein, R. F.; Paner, T. M.; Gallo, F. J.; Benight, A. S., Studies of DNA Dumbbells 1. Melting Curves of 17 DNA Dumbells with Different Duplex STEM Sequences Linked by T4 Endloops - Evaluation of the Nearest-Neighbor Stacking Interactions in DNA. *Biopolymers* **1992,** *32*, 849-864.

94. Freier, S. M.; Kierzek, R.; Jaeger, J. A.; Sugimoto, N.; Caruthers, M. H.; Neilson, T.; Turner, D. H., Improved Free-Energy Parameters for Predictions of RNA Duplex Stability. *Proceedings of the National Academy of Sciences of the United States of America* **1986,** *83*, 9373-9377.

95. Gotoh, O.; Tagashira, Y., Stabilities of Nearest-neighbor Doublets in Double-helical DNA Determined by Fitting Calculated Melting Profiles to Observed Profiles. . *Biopolymers* **1981,** *20*, 1033-1042.

96. Quartin, R. S.; Wetmur, J. G., Effect of Ionic-strength on the Hybridization of Oligodeoxynucleotides with Reduced Charge due to Methylphosphonate linkanges to Unmodified Oligonucleotides Containing the Complementary Sequence. *Biochemistry* **1989,** *28*, 1040-1047.

97. Sugimoto, N.; Nakano, S.; Yoneyama, M.; Honda, K., Improved thermodynamic parameters and helix initiation factor to predict stability of DNA duplexes. *Nucleic Acids Research* **1996,** *24*, 4501-4505.

98. Wartell, R. M.; Benight, A. S., Thermal-denaturation of DNA-molecules - A Comparison of Theory and Experiment. *Physics Reports-Review Section of Physics Letters* **1985,** *126*, 67-107.

99. Owczarzy, R.; You, Y.; Moreira, B. G.; Manthey, J. A.; Huang, L. Y.; Behlke, M. A.; Walder, J. A., Effects of sodium ions on DNA duplex oligomers: Improved predictions of melting temperatures. *Biochemistry* **2004,** *43*, 3537-3554.

100. Seferos, D. S.; Prigodich, A. E.; Giljohann, D. A.; Patel, P. C.; Mirkin, C. A., Polyvalent DNA Nanoparticle Conjugates Stabilize Nucleic Acids. *Nano Letters* **2009,** *9*, 308-311.

101. Wu, G. H.; Milkhailovsky, A.; Khant, H. A.; Fu, C.; Chiu, W.; Zasadzinski, J. A., Remotely triggered liposome release by near-infrared light absorption via hollow gold nanoshells. *J. Am. Chem. Soc.* **2008,** *130*, 8175-8177.

102. Giljohann, D. A.; Seferos, D. S.; Prigodich, A. E.; Patel, P. C.; Mirkin, C. A., Gene Regulation with Polyvalent siRNA-Nanoparticle Conjugates. *Journal of the American Chemical Society* **2009,** *131*, 2072-2073.

103. Ghosh, P. S.; Kim, C.-K.; Han, G.; Forbes, N. S.; Rotello, V. M., Efficient Gene Delivery Vectors by Tuning the Surface Charge Density of Amino Acid-Functionalized Gold Nanoparticles. *Acs Nano* **2008,** *2*, 2213-2218.

104. Takahashi, H.; Niidome, Y.; Yamada, S., Controlled release of plasmid DNA from gold nanorods induced by pulsed near-infrared light. *Chem. Commun.* **2005**, 2247-2249.

105. Chen, C. C.; Lin, Y. P.; Wang, C. W.; Tzeng, H. C.; Wu, C. H.; Chen, Y. C.; Chen, C. P.; Chen, L. C.; Wu, Y. C., DNA-gold nanorod conjugates for remote control of localized gene expression by near infrared irradiation. *JACS* **2006,** *128*, 3709-3715.

106. Wijaya, A.; Schaffer, S. B.; Pallares, I. G.; Hamad-Schifferli, K., Selective Release of Multiple DNA Oligonucleotides from Gold Nanorods. *Acs Nano* **2009,** *3*, 80-86.

107. Braun, G. B.; Pallaoro, A.; Wu, G.; Missirlis, D.; Zasadzinski, J. A.; Tirrell, M.; Reich, N. O., Laser-Activated Gene Silencing via Gold Nanoshell-siRNA Conjugates. *Acs Nano* **2009,** *3*, 2007-2015.

108. Lu, W.; Zhang, G.; Zhang, R.; Flores, L. G.; Huang, Q.; Gelovani, J. G.; Li, C., Tumor Site–Specific Silencing of NF-κB p65 by Targeted Hollow Gold Nanosphere–Mediated Photothermal Transfection. *Cancer Research* **2010,** *70*, 3177-3188.

109. Rhim, W.-K.; Kim, J.-S.; Nam, J.-M., Lipid-Gold-Nanoparticle Hybrid-Based Gene Delivery. *Small* **2008,** *4*, 1651-1655.

110. Noh, S. M.; Kim, W.-K.; Kim, S. J.; Kim, J. M.; Baek, K.-H.; Oh, Y.-K., Enhanced cellular delivery and transfection efficiency of plasmid DNA using positively charged biocompatible colloidal gold nanoparticles. *Biochimica Et Biophysica Acta-General Subjects* **2007,** *1770*, 747-752.

111. Huang, X.; Qian, W.; El-Sayed, I. H.; El-Sayed, M. A., The potential use of the enhanced nonlinear properties of gold nanospheres in photothermal cancer therapy. *Lasers in Surgery and Medicine* **2007,** *39*, 747-753.

112. Prodan, E.; Nordlander, P., Electronic structure and polarizability of metallic nanoshells. *Chemical Physics Letters* **2002,** *352*, 140-146.

113. Oldenburg, S. J.; Jackson, J. B.; Westcott, S. L.; Halas, N. J., Infrared extinction properties of gold nanoshells. *Applied Physics Letters* **1999,** *75*, 2897-2899.

114. Oldenburg, S. J.; Westcott, S. L.; Averitt, R. D.; Halas, N. J., Surface enhanced Raman scattering in the near infrared using metal nanoshell substrates. *Journal of Chemical Physics* **1999,** *111*, 4729-4735.

115. Demers, L. M.; Mirkin, C. A.; Mucic, R. C.; Reynolds, R. A.; Letsinger, R. L.; Elghanian, R.; Viswanadham, G., A fluorescence-based method for determining the surface coverage and hybridization efficiency of thiol-capped oligonucleotides bound to gold thin films and nanoparticles. *Anal. Chem.* **2000,** *72*, 5535-5541.

116. Brewood, G. P.; Rangineni, Y.; Fish, D. J.; Bhandiwad, A. S.; Evans, D. R.; Solanki, R.; Benight, A. S., Electrical detection of the temperature induced melting transition of a DNA hairpin covalently attached to gold interdigitated microelectrodes. *Nucleic Acids Research* **2008,** *36*, e98.

117. Sun, Y.; Harris, N. C.; Kiang, C. H., Melting transition of directly linked gold nanoparticle DNA assembly. *Physica A-Statistical Mechanics and Its Applications* **2005,** *350*, 89-94.

118. Meunier-Prest, R.; Raveau, S.; Finot, E.; Legay, G.; Cherkaoui-Malki, M.; Latruffe, N., Direct measurement of the melting temperature of supported DNA by electrochemical method. *Nucleic Acids Research* **2003,** *31*, e150.

119. Cederquist, K. B.; Keating, C. D., Curvature Effects in DNA:Au Nanoparticle Conjugates. *Acs Nano* **2009,** *3*, 256-260.

120. Hill, H. D.; Millstone, J. E.; Banholzer, M. J.; Mirkin, C. A., The Role Radius of Curvature Plays in Thiolated Oligonucleotide Loading on Gold Nanoparticles. *Acs Nano* **2009,** *3*, 418-424.

121. Thierry, B., Drug Nanocarriers and Functional Nanoparticles: Applications in Cancer Therapy. *Curr Drug Deliv* **2009,** *6*, 391-403.

122. Yamashita, S.; Fukushima, H.; Akiyama, Y.; Niidome, Y.; Mori, T.; Katayama, Y.; Niidome, T., Controlled-release system of single-stranded DNA triggered by the photothermal effect of gold nanorods and its in vivo application. *Bioorganic & Medicinal Chemistry* **2011,** *19*, 2130-2135.

123. Sun, Y. G.; Mayers, B.; Xia, Y. N., Metal nanostructures with hollow interiors. *Advanced Materials* **2003,** *15*, 641-646.

124. Chen, J.; Saeki, F.; Wiley, B. J.; Cang, H.; Cobb, M. J.; Li, Z. Y.; Au, L.; Zhang, H.; Kimmey, M. B.; Li, X. D.*, et al.*, Gold nanocages: Bioconjugation and their potential use as optical imaging contrast agents. *Nano Letters* **2005,** *5*, 473-477.

125. Liang, H. P.; Wan, L. J.; Bai, C. L.; Jiang, L., Gold hollow nanospheres: Tunable surface plasmon resonance controlled by interior-cavity sizes. *Journal of Physical Chemistry B* **2005,** *109*, 7795-7800.

126. Skrabalak, S. E.; Chen, J. Y.; Sun, Y. G.; Lu, X. M.; Au, L.; Cobley, C. M.; Xia, Y. N., Gold Nanocages: Synthesis, Properties, and Applications. *Accounts of Chemical Research* **2008,** *41*, 1587-1595.

127. Jana, N. R.; Gearheart, L.; Murphy, C. J., Wet chemical synthesis of high aspect ratio cylindrical gold nanorods. *Journal of Physical Chemistry B* **2001,** *105*, 4065-4067.

128. Norman, T. J.; Grant, C. D.; Magana, D.; Zhang, J. Z.; Liu, J.; Cao, D. L.; Bridges, F.; Van Buuren, A., Near infrared optical absorption of gold nanoparticle aggregates. *Journal of Physical Chemistry B* **2002,** *106*, 7005-7012.

129. Brinson, B. E.; Lassiter, J. B.; Levin, C. S.; Bardhan, R.; Mirin, N.; Halas, N. J., Nanoshells Made Easy: Improving Au Layer Growth on Nanoparticle Surfaces. *Langmuir* **2008,** *24*, 14166-14171.

130. Melancon, M. P.; Lu, W.; Yang, Z.; Zhang, R.; Cheng, Z.; Elliot, A. M.; Stafford, J.; Olson, T.; Zhang, J. Z.; Li, C., In vitro and in vivo targeting of hollow gold nanoshells directed at epidermal growth factor receptor for photothermal ablation therapy. *Molecular Cancer Therapeutics* **2008,** *7*, 1730-1739.

131. El-Sayed, I. H.; Huang, X. H.; El-Sayed, M. A., Surface plasmon resonance scattering and absorption of anti-EGFR antibody conjugated gold nanoparticles in cancer diagnostics: Applications in oral cancer. *Nano Letters* **2005,** *5*, 829-834.

132. Loo, C.; Hirsch, L.; Lee, M. H.; Chang, E.; West, J.; Halas, N. J.; Drezek, R., Gold nanoshell bioconjugates for molecular imaging in living cells. *Opt. Lett.* **2005,** *30*, 1012-1014.

133. Anger, P.; Bharadwaj, P.; Novotny, L., Enhancement and quenching of single-molecule fluorescence. *Physical Review Letters* **2006,** *96*.

134. Kuhn, S.; Hakanson, U.; Rogobete, L.; Sandoghdar, V., Enhancement of single-molecule fluorescence using a gold nanoparticle as an optical nanoantenna. *Physical Review Letters* **2006,** *97*.

135. Stranik, O.; Nooney, R.; McDonagh, C.; MacCraith, B. D., Optimization of nanoparticle size for plasmonic enhancement of fluorescence. *Plasmonics* **2007,** *2*, 15-22.

136. Cade, N. I.; Ritman-Meer, T.; Kwakwa, K. A.; Richards, D., The plasmonic engineering of metal nanoparticles for enhanced fluorescence and Raman scattering. *Nanotechnology* **2009,** *20*.

137. Sharrna, P.; Brown, S.; Walter, G.; Santra, S.; Moudgil, B., Nanoparticles for bioimaging. *Advances in Colloid and Interface Science* **2006,** *123*, 471-485.

138. Hahn, M. A.; Singh, A. K.; Sharma, P.; Brown, S. C.; Moudgil, B. M., Nanoparticles as contrast agents for in-vivo bioimaging: current status and future perspectives. *Analytical and Bioanalytical Chemistry* **2011,** *399*, 3-27.

139. Pan, Y.; Neuss, S.; Leifert, A.; Fischler, M.; Wen, F.; Simon, U.; Schmid, G.; Brandau, W.; Jahnen-Dechent, W., Size-dependent cytotoxicity of gold nanoparticles. *Small* **2007,** *3*, 1941-1949.

140. Pan, Y.; Leifert, A.; Ruau, D.; Neuss, S.; Bornemann, J.; Schmid, G.; Brandau, W.; Simon, U.; Jahnen-Dechent, W., Gold Nanoparticles of Diameter 1.4 nm Trigger Necrosis by Oxidative Stress and Mitochondrial Damage. *Small* **2009,** *5*, 2067-2076.

141. Poon, L.; Zandberg, W.; Hsiao, D.; Erno, Z.; Sen, D.; Gates, B. D.; Branda, N. R., Photothermal Release of Single-Stranded DNA from the Surface of Gold Nanoparticles Through Controlled Denaturating and Au-S Bond Breaking. *ACS Nano* **2010,** *4*, 6395-6403.

142. Jones, M. R.; Millstone, J. E.; Giljohann, D. A.; Seferos, D. S.; Young, K. L.; Mirkin, C. A., Plasmonically Controlled Nucleic Acid Dehybridization with Gold Nanoprisms. *Chemphyschem* **2009,** *10*, 1461-1465.

143. Barhoumi, A.; Huschka, R.; Bardhan, R.; Knight, M. W.; Halas, N. J., Light-induced release of DNA from plasmon-resonant nanoparticles: Towards light-controlled gene therapy. *Chem. Phys. Lett.* **2009,** *482*, 171-179.

144. Wijaya, A.; Hamad-Schifferli, K., Ligand customization and DNA functionalization of gold nanorods via round-trip phase transfer ligand exchange. *Langmuir* **2008,** *24*, 9966-9969.

145. Johnson, P. B.; Christy, R. W., Optical-Constants of Noble-Metals. *Phys. Rev. B* **1972,** *6*, 4370-4379.

146. Cole, J. R.; Mirin, N. A.; Knight, M. W.; Goodrich, G. P.; Halas, N. J., Photothermal Efficiencies of Nanoshells and Nanorods for Clinical Therapeutic Applications. *J Phys Chem C* **2009,** *113*, 12090-12094.

147. Yamashita, S.; Fukushima, H.; Akiyama, Y.; Niidome, Y.; Mori, T.; Niidome, T., Controlled-release system of single-stranded DNA triggered by the photothermal effect of gold nanorods and its in vivo application. *Bioorganic and Medicinal Chemistry* **2011,** *19*, 2130-2135.

148. Maillard, M.; Huang, P. R.; Brus, L., Silver nanodisk growth by surface plasmon enhanced photoreduction of adsorbed Ag+. *Nano Lett.* **2003,** *3*, 1611-1615.

149. Brus, L., Noble Metal Nanocrystals: Plasmon Electron Transfer Photochemistry and Single-Molecule Raman Spectroscopy. *Acc. Chem. Res.* **2008,** *41*, 1742-1749.

150. Wu, X. M.; Thrall, E. S.; Liu, H. T.; Steigerwald, M.; Brus, L., Plasmon Induced Photovoltage and Charge Separation in Citrate-Stabilized Gold Nanoparticles. *Journal of Physical Chemistry C* **2010,** *114*, 12896-12899.

151. Baffou, G.; Quidant, R.; de Abajo, F. J. G., Nanoscale Control of Optical Heating in Complex Plasmonic Systems. *ACS Nano* **2010,** *4*, 709-716.

152. Baffou, G.; Quidant, R.; Girard, C., Heat generation in plasmonic nanostructures: Influence of morphology. *Appl. Phys. Lett.* **2009,** *94*.

153. Nitzan, A.; Brus, L. E., Can Photochemistry be Enhanced on Rough Surfaces. *J. Chem. Phys.* **1981,** *74*, 5321-5322.

154. Nitzan, A.; Brus, L. E., Theoretical-Model for Enhanced Photochemistry on Rough Surfaces. *J. Chem. Phys.* **1981,** *75*, 2205-2214.

155. Langer, R., Drug delivery and targeting. *Nature* **1998,** *392*, 5-10.

156. Panyam, J.; Labhasetwar, V., Biodegradable nanoparticles for drug and gene delivery to cells and tissue. *Adv. Drug Delivery Rev.* **2003,** *55*, 329-347.

157. Niidome, T.; Huang, L., Gene therapy progress and prospects: Nonviral vectors. *Gene Ther.* **2002,** *9*, 1647-1652.

158. Shea, L. D.; Smiley, E.; Bonadio, J.; Mooney, D. J., DNA delivery from polymer matrices for tissue engineering. *Nat. Biotechnol.* **1999,** *17*, 551-554.

159. Richardson, T. P.; Peters, M. C.; Ennett, A. B.; Mooney, D. J., Polymeric system for dual growth factor delivery. *Nature Biotechnology* **2001,** *19*, 1029-1034.

160. Kim, C. K.; Ghosh, P.; Pagliuca, C.; Zhu, Z. J.; Menichetti, S.; Rotello, V. M., Entrapment of Hydrophobic Drugs in Nanoparticle Monolayers with Efficient Release into Cancer Cells. *J. Am. Chem. Soc.* **2009,** *131*, 1360-1361.

161. LaVan, D. A.; McGuire, T.; Langer, R., Small-scale systems for in vivo drug delivery. *Nat. Biotechnol.* **2003,** *21*, 1184-1191.

162. Kim, S. Y.; Shin, I. L. G.; Lee, Y. M.; Cho, C. S.; Sung, Y. K., Methoxy poly(ethylene glycol) and epsilon-caprolactone amphiphilic block copolymeric micelle containing indomethacin. II. Micelle formation and drug release behaviours. *J. Controlled Release* **1998,** *51*, 13-22.

163. Chilkoti, A.; Dreher, M. R.; Meyer, D. E.; Raucher, D., Targeted drug delivery by thermally responsive polymers. *Adv. Drug Delivery Rev.* **2002,** *54*, 613-630.

164. Boussif, O.; Lezoualch, F.; Zanta, M. A.; Mergny, M. D.; Scherman, D.; Demeneix, B.; Behr, J. P., A Versatile Vector for Gene and Oligonucleotide Transfer into Cells in Culture and In-Vivo-Polythylenimine. *Proc. Natl. Acad. Sci. U S A* **1995,** *92*, 7297-7301.

165. Shalek, A. K.; Robinson, J. T.; Karp, E. S.; Lee, J. S.; Ahn, D. R.; Yoon, M. H.; Sutton, A.; Jorgolli, M.; Gertner, R. S.; Gujral, T. S.*, et al.*, Vertical silicon nanowires as a universal platform for delivering biomolecules into living cells. *Proc. Natl. Acad. Sci. U. S. A.* **2010,** *107*, 1870-1875.

166. Chen, C. C.; Lin, Y. P.; Wang, C. W.; Tzeng, H. C.; Wu, C. H.; Chen, Y. C.; Chen, C. P.; Chen, L. C.; Wu, Y. C., DNA-gold nanorod conjugates for remote control of localized gene expression by near infrared irradiation. *J. Am. Chem. Soc.* **2006,** *128*, 3709-3715.

167. Takahashi, H.; Niidome, Y.; Yamada, S., Controlled release of plasmid DNA from gold nanorods induced by pulsed near-infrared light. *Chem. Commun.* **2005**, 2247-2249.

168. Lee, S. E.; Liu, G. L.; Kim, F.; Lee, L. P., Remote Optical Switch for Localized and Selective Control of Gene Interference. *Nano Lett.* **2009,** *9*, 562-570.

169. Han, G.; You, C. C.; Kim, B. J.; Turingan, R. S.; Forbes, N. S.; Martin, C. T.; Rotello, V. M., Light-regulated release of DNA and its delivery to nuclei by means of photolabile gold nanoparticles. *Angew. Chem. Int. Ed.* **2006,** *45*, 3165-3169.

170. Barhoumi, A.; Huschka, R.; Bardhan, R.; Knight, M. W.; Halas, N. J., Light-induced release of DNA from plasmon-resonant nanoparticles: Towards light-controlled gene therapy. *Chem. Phys. Lett.* **2009,** *482*, 171-179.

171. Prodan, E.; Nordlander, P.; Halas, N. J., Electronic structure and optical properties of gold nanoshells. *Nano Lett.* **2003,** *3*, 1411-1415.

172. Wang, H.; Brandl, D. W.; Nordlander, P.; Halas, N. J., Plasmonic nanostructures: Artificial molecules. *Acc. Chem. Res.* **2007,** *40*, 53-62.

173. El-Sayed, I. H.; Huang, X.; El-Sayed, M. A., Selective laser photo-thermal therapy of epithelial carcinoma using anti-EGFR antibody conjugated gold nanoparticles. *Cancer Lett. (Amsterdam, Netherlands)* **2006,** *239*, 129-135.

174. Hirsch, L. R.; Stafford, R. J.; Bankson, J. A.; Sershen, S. R.; Rivera, B.; Price, R. E.; Hazle, J. D.; Halas, N. J.; West, J. L., Nanoshell-mediated near-infrared thermal therapy of tumors under magnetic resonance guidance. *Proc. Natl. Acad. Sci. USA* **2003,** *100*, 13549-13554.

175. Richardson, H. H.; Carlson, M. T.; Tandler, P. J.; Hernandez, P.; Govorov, A. O., Experimental and Theoretical Studies of Light-to-Heat Conversion and Collective Heating Effects in Metal Nanoparticle Solutions. *Nano Lett.* **2009,** *9*, 1139-1146.

176. Hirsch, L. R.; Jackson, J. B.; Lee, A.; Halas, N. J.; West, J. L., A whole blood immunoassay using gold nanoshells. *Anal.Chem.* **2003,** *75*, 2377-2381.

177. Sershen, S. R.; Westcott, S. L.; Halas, N. J.; West, J. L., Temperature-sensitive polymer-nanoshell composites for photothermally modulated drug delivery *J. Biomed. Mater. Res.* **2000,** *51*, 293-298.

178. Hirsch, L. R.; Gobin, A. M.; Lowery, A. R.; Tam, F.; Drezek, R. A.; Halas, N. J.; West, J. L., Metal nanoshells. *Ann. Biomed. Eng.* **2006,** *34*, 15-22.

179. Loo, C.; Lowery, A.; Halas, N. J.; J, W.; Drezek, R., Immunotargeted nanoshells for integrated cancer imaging and therapy. *Nano Lett.* **2005,** *5*, 709-711.

180. O'Neal, D. P.; Hirsch, L. R.; Halas, N. J.; Payne, J. D.; West, J. L., Photo-thermal tumor ablation in mice using near infrared-absorbing nanoparticles. *Cancer Lett. (Amsterdam, Netherlands)* **2004,** *209*, 171-176.

181. Oldenburg, S. J.; Jackson, J. B.; Westcott, S. L.; Halas, N. J., Infrared extinction properties of gold nanoshells. *Appl. Phys. Lett.* **1999,** *75*, 2897-2899.

182. Weissleder, R., A clearer vision for in vivo imaging. *Nature Biotechnology* **2001,** *19*, 316-317.

183. Stephens, A. C.; Rivers, R. P. A., Antisense oligonucleotide therapy in cancer. *Curr. Opin. Mol. Ther.* **2003,** *5*, 118-122.

184. Neto, B. A. D.; Lapis, A. A. M., Recent Developments in the Chemistry of Deoxyribonucleic Acid (DNA) Intercalators: Principles, Design, Synthesis, Applications and Trends. *Molecules* **2009,** *14*, 1725-1746.

185. Ihmels, H.; Otto, D., Intercalation of organic dye molecules into double-stranded DNA general principles and recent developments. *Top. Curr. Chem.* **2005,** *258*, 161-204.

186. Barcellona, M. L.; Gratton, E., The fluorescence properties of a DNA probe. 4'-6-Diamidino-2-phenylindole (DAPI). *Eur Biophys J.* **1990,** *17*, 315-323.

187. Manzini, G.; Xodo, L.; Barcellona, M. L.; Quadrifoglio, F., Interaction of 4′-6-diamidino-2-phenylindole 2HCl with synthetic and natural deoxy- and ribonucleic acids *J. Biosci.* **1985,** *8*, 699-711.

188. Kapuściński, J.; Szer, W., Interactions of 4', 6-diamidine-2-phenylindole with synthetic polynucleotides. *Nucl. Acids Res.* **1979,** *6*, 3519-3534.

189. Kubista, M.; Aakerman, B.; Norden, B., Characterization of interaction between DNA and 4',6-diamidino-2-phenylindole by optical spectroscopy. *Biochemistry* **1986,** *26*, 4545-4553.

190. Lin, M. S.; Comings, D. E.; Alfi, O. S., Optical studies of the interaction of 4′-6-diamidino-2-phenylindole with DNA and metaphase chromosomes. *Chromosoma* **1977,** *60*, 15-25.

191. Oldenburg, S. J.; Averitt, R. D.; Westcott, S. L.; Halas, N. J., Nanoengineering of optical resonances *Chem. Phys. Lett.* **1998,** *288*, 243-247.

192. Oldenburg, S. J.; Jackson, J. B.; Westcott, S. L.; Halas, N. J., Infrared extinction properties of gold nanoshells. *Appl. Phys. Lett.* **1999,** *75*, 2897-2899

193. Jung, K. S.; Kim, M. S.; Lee, G. J.; Cho, T. S.; Kim, E. K.; Yi, S. Y., Conformation of Single Stranded Poly(dA) and Its Interaction with 4', 6-Diamidino-2-phenylindole. *Bull. Korean Chem. Soc.* **1997,** *18*, 510-514.

194. Breusegem, S. Y.; Clegg, R. M.; Loontiens, F. G., Base-sequence Specificity of Hoechst 33258 and DAPI Binding to Five (A/T)4 DNA Sites with Kinetic Evidence for more than One High-affinity Hoechst 33258-AATT Complex. *J. Mol. Biol.* **2002,** *315*, 1049-1061.

195. Ochsenkuhn, M. A.; Jess, P. R. T.; Stoquert, H.; Dholakia, K.; Campbell, C. J., Nanoshells for Surface-Enhanced Raman Spectroscopy in Eukaryotic Cells: Cellular Response and Sensor Development. *Acs Nano* **2009,** *3*, 3613-3621.

196. Chithrani, B. D.; Ghazani, A. A.; Chan, W. C. W., Determining the size and shape dependence of gold nanoparticle uptake into mammalian cells. *Nano Lett.* **2006,** *6*, 662-668.

197. Giljohann, D. A.; Seferos, D. S.; Patel, P. C.; Millstone, J. E.; Rosi, N. L.; Mirkin, C. A., Oligonucleotide loading determines cellular uptake of DNA-modified gold nanoparticles. *Nano Lett.* **2007,** *7*, 3818-3821.

198. Lydon, M. J.; Keeler, K. D.; Thomas, D. B., Vital DNA Staining and Cell Sorting by Flow Micro-Fluorometry. *J. Cell. Physiol.* **1980,** *102*, 175-181.

199. Taylor, I. W., A Rapid Single Step Staining Technique for DNA Analysis by Flow Microfluorimetry. *J. Histochem. Cytochem.* **1980,** *28*, 1021-1024.

200. Dengler, W. A.; Schulte, J.; Berger, D. P.; Mertelsmann, R.; Fiebig, H. H., Development of a Propidium Iodide Fluorescence Assay for Proliferation and Cytotoxicity Assays. *Anti-Cancer Drugs* **1995,** *6*, 522-532.

201. Hendry, L. B.; Mahesh, V. B.; Bransome, E. D.; Ewing, D. E., Small molecule intercalation with double stranded DNA: Implications for normal gene regulation and for predicting the biological efficacy and genotoxicity of drugs and other chemicals. *Mutat. Res.* **2007,** *623*, 53-71.

202. Wheate, N. J.; Brodie, C. R.; Collins, J. G.; Kemp, S.; Aldrich-Wright, J. R., DNA intercalators in cancer therapy: Organic and inorganic drugs and their spectroscopic tools of analysis. *Mini-Rev. Med. Chem.* **2007,** *7*, 627-648.

203. Soutschek, J.; Akinc, A.; Bramlage, B.; Charisse, K.; Constien, R.; Donoghue, M.; Elbashir, S.; Geick, A.; Hadwiger, P.; Harborth, J.*, et al.*, Therapeutic silencing of an endogenous gene by systemic administration of modified siRNAs. *Nature* **2004,** *432*, 173-178.

204. Zimmermann, T. S.; Lee, A. C. H.; Akinc, A.; Bramlage, B.; Bumcrot, D.; Fedoruk, M. N.; Harborth, J.; Heyes, J. A.; Jeffs, L. B.; John, M.*, et al.*, RNAi-mediated gene silencing in non-human primates. *Nature* **2006,** *441*, 111-114.

205. John, M.; Constien, R.; Akinc, A.; Goldberg, M.; Moon, Y.-A.; Spranger, M.; Hadwiger, P.; Soutschek, J.; Vornlocher, H.-P.; Manoharan, M.*, et al.*, Effective RNAi-mediated gene silencing without interruption of the endogenous microRNA pathway. *Nature* **2007,** *449*, 745-U12.

206. Luo, D.; Saltzman, W. M., Synthetic DNA delivery systems. *Nat. Biotechnol.* **2000,** *18*, 33-37.

207. Mintzer, M. A.; Simanek, E. E., Nonviral Vectors for Gene Delivery. *Chem. Rev.* **2009,** *109*, 259-302.

208. Elsabahy, M.; Nazarali, A.; Foldvari, M., Non-Viral Nucleic Acid Delivery: Key Challenges and Future Directions. *Curr Drug Deliv* **2011,** *8*, 235-244.

209. Taratula, O.; Garbuzenko, O. B.; Kirkpatrick, P.; Pandya, I.; Savla, R.; Pozharov, V. P.; He, H. X.; Minko, T., Surface-engineered targeted PPI dendrimer for efficient intracellular and intratumoral siRNA delivery. *J Control Release* **2009,** *140*, 284-293.

210. Morille, M.; Passirani, C.; Vonarbourg, A.; Clavreul, A.; Benoit, J.-P., Progress in developing cationic vectors for non-viral systemic gene therapy against cancer. *Biomaterials* **2008,** *29*, 3477-3496.

211. Jin, S.; Ye, K. M., Nanoparticle-mediated drug delivery and gene therapy. *Biotechnol. Progr.* **2007,** *23*, 32-41.

212. Duncan, B.; Kim, C.; Rotello, V. M., Gold nanoparticle platforms as drug and biomacromolecule delivery systems. *J Control Release* **2010,** *148*, 122-127.

213. Ganta, S.; Devalapally, H.; Shahiwala, A.; Amiji, M., A review of stimuli-responsive nanocarriers for drug and gene delivery. *J Control Release* **2008,** *126*, 187-204.

214. Stern, J. M.; Stanfield, J.; Kabbani, W.; Hsieh, J.-T.; Cadeddu, J. A., Selective prostate cancer thermal ablation with laser activated gold nanoshells. *J Urol* **2008,** *179*, 748-753.

215. Bardhan, R.; Chen, W. X.; Perez-Torres, C.; Bartels, M.; Huschka, R. M.; Zhao, L. L.; Morosan, E.; Pautler, R. G.; Joshi, A.; Halas, N. J., Nanoshells with Targeted Simultaneous Enhancement of Magnetic and Optical Imaging and Photothermal Therapeutic Response. *Adv Funct Mater* **2009,** *19*, 3901-3909.

216. Murphy, C. J.; Gole, A. M.; Stone, J. W.; Sisco, P. N.; Alkilany, A. M.; Goldsmith, E. C.; Baxter, S. C., Gold Nanoparticles in Biology: Beyond Toxicity to Cellular Imaging. *Acc. Chem. Res.* **2008,** *41*, 1721-1730.

217. Huschka, R.; Zuloaga, J.; Knight, M. W.; Brown, L. V.; Nordlander, P.; Halas, N. J., Light-Induced Release of DNA from Gold Nanoparticles: Nanoshells and Nanorods. *J. Am. Chem. Soc.* **2011,** *133*, 12247-12255.

218. Huschka, R.; Neumann, O.; Barhoumi, A.; Halas, N. J., Visualizing Light-Triggered Release of Molecules Inside Living Cells. *Nano Lett.* **2010,** *10*, 4117-4122.

219. Choi, Y. H.; Liu, F.; Kim, J. S.; Choi, Y. K.; Park, J. S.; Kim, S. W., Polyethylene glycol-grafted poly-L-lysine as polymeric gene carrier. *J Control Release* **1998,** *54*, 39-48.

220. Ghosh, P. S.; Kim, C. K.; Han, G.; Forbes, N. S.; Rotello, V. M., Efficient Gene Delivery Vectors by Tuning the Surface Charge Density of Amino Acid-Functionalized Gold Nanoparticles. *ACS Nano* **2008,** *2*, 2213-2218.

221. Han, S.; Mahato, R. I.; Sung, Y. K.; Kim, S. W., Development of biomaterials for gene therapy. *Mol Ther* **2000,** *2*, 302-317.

222. Cho, E. C.; Xie, J.; Wurm, P. A.; Xia, Y., Understanding the Role of Surface Charges in Cellular Adsorption versus Internalization by Selectively Removing Gold Nanoparticles on the Cell Surface with a I2/KI Etchant. *Nano Lett.* **2009,** *9*, 1080-1084.

223. Grunweller, A.; Wyszko, E.; Bieber, B.; Jahnel, R.; Erdmann, V. A.; Kurreck, J., Comparison of different antisense strategies in mammalian cells using locked nucleic acids, 2 '-O-methyl RNA, phosphorothioates and small interfering RNA. *Nucleic Acids Res.* **2003,** *31*, 3185-3193.

224. Agrawal, S.; Temsamani, J.; Tang, J. Y., Pharmokinetics, Biodistribution, and Stability of Oligodeoxynucleotide Phosphorothioates in Mice *Proc Natl Acad Sci U S A* **1991,** *88*, 7595-7599.

225. Neurath, M. F.; Pettersson, S.; Zum Büschenfelde, K. H. M.; Strober, W., Local administration of antisense phosphorothioate oligonucleotides to the p65 subunit of NF-kappa B abrogates established experimental colitis in mice. *Nature Medicine* **1996,** *2*, 998-1004.

226. Huang, X. H.; Jain, P. K.; El-Sayed, I. H.; El-Sayed, M. A., Determination of the minimum temperature required for selective photothermal destruction of cancer cells with the use of immunotargeted gold nanoparticles. *Photochem. Photobiol.* **2006,** *82*, 412-417.

227. Hirsch, L. R.; Stafford, R. J.; Bankson, J. A.; Sershen, S. R.; Rivera, B.; Price, R. E.; Hazle, J. D.; Halas, N. J.; West, J. L., Nanoshell-mediated near-infrared thermal therapy of tumors under magnetic resonance guidance. *Proc Natl Acad Sci U S A* **2003,** *100*, 13549-13554.

228. Zauner, W.; Ogris, M.; Wagner, E., Polylysine-based transfection systems utilizing receptor-mediated delivery. *Adv Drug Del Rev* **1998,** *30*, 97-113.

229. Shen, W. C.; Ryser, H. J. P., Conjugation of Poly-L-Lysine to Albumin and Horseradish-Peroxidase - Novel Method of Enhancing Cellular Uptake of Proteins. *Proc Natl Acad Sci U S A* **1978,** *75*, 1872-1876.

230. Ryser, H. J. P.; Drummond, I.; Shen, W. C., The Cellular Uptake of Horseradish-Peroxidase and its Poly(lysine) Conjugate by Cultured Fibroblasts is Qualitatively similar Despite a 900-Fold Difference in Rate. *J. Cell. Physiol.* **1982,** *113*, 167-178.

231. Leonetti, J.-P.; Degols, G.; Lebleu, B., Biological Activity of Oligonucleotide-Poly(L-lysine) Conjugates: Mechanism of Cell Uptake. *Bioconjugate Chem.* **1990,** *1*, 149-153.

232. Krpetić, Z. e.; Nativo, P.; Sée, V.; Prior, I. A.; Brust, M.; Volk, M., Inflicting Controlled Nonthermal Damage to Subcellular Structures by Laser-Activated Gold Nanoparticles. *Nano Lett.* **2010,** *10*, 4549-4554.

233. Carregal-Romero, S.; Ochs, M.; Rivera-Gil, P.; Ganas, C.; Pavlov, A. M.; Sukhorukov, G. B.; Parak, W. J., NIR-light triggered delivery of macromolecules into the cytosol. *J Control Release* **2012,** *159*, 120-127.

234. Lukianova-Hleb, E. Y.; Belyanin, A.; Kashinath, S.; Wu, X.; Lapotko, D. O., Plasmonic nanobubble-enhanced endosomal escape processes for selective and guided intracellular delivery of chemotherapy to drug-resistant cancer cells. *Biomaterials* **2012,** *33*, 1821-1826.

235. Bartlett, D. W.; Davis, M. E., Insights into the kinetics of siRNA-mediated gene silencing from live-cell and live-animal bioluminescent imaging. *Nucleic Acids Res.* **2006,** *34*, 322-333.

236. Bertrand, J. R.; Pottier, M.; Vekris, A.; Opolon, P.; Maksimenko, A.; Malvy, C., Comparison of antisense oligonucleotides and siRNAs in cell culture and in vivo. *Biochem. Biophys. Res. Commun.* **2002,** *296*, 1000-1004.

237. Eguchi, A.; Meade, B. R.; Chang, Y. C.; Fredrickson, C. T.; Willert, K.; Puri, N.; Dowdy, S. F., Efficient siRNA delivery into primary cells by a peptide transduction domain-dsRNA binding domain fusion protein. *Nat. Biotechnol.* **2009,** *27*, 567-571.

238. Kim, S. H.; Mok, H.; Jeong, J. H.; Kim, S. W.; Park, T. G., Comparative evaluation of target-specific GFP gene silencing efficiencies for antisense ODN, synthetic

siRNA, and siRNA plasmid complexed with PEI-PEG-FOL conjugate. *Bioconjugate Chem.* **2006,** *17*, 241-244.

239. Chiu, D. T.; Zare, R. N., Assaying for peptides in individual Aplysia neurons with mass spectrometry. *Proc Natl Acad Sci U S A* **1998,** *95*, 3338-3340.

240. Bartlett, D. W.; Davis, M. E., Effect of siRNA nuclease stability on the in vitro and in vivo kinetics of siRNA-mediated gene silencing. *Biotechnol. Bioeng.* **2007,** *97*, 909-921.

241. Lv, H. T.; Zhang, S. B.; Wang, B.; Cui, S. H.; Yan, J., Toxicity of cationic lipids and cationic polymers in gene delivery. *J Control Release* **2006,** *114*, 100-109.

242. Fischer, D.; Li, Y. X.; Ahlemeyer, B.; Krieglstein, J.; Kissel, T., In vitro cytotoxicity testing of polycations: influence of polymer structure on cell viability and hemolysis. *Biomaterials* **2003,** *24*, 1121-1131.

243. Duff, D. G.; Baiker, A.; Edwards, P. P., A new hydrosol of gold clusters. 1. Formation and particle size variation. *Langmuir* **1993,** *9*, 2301-2309.

244. Stober, W.; Fink, A.; Bohn, E., Controlled Growth of Monodisperse Silica Spheres in Micron Size Range. *Journal of Colloid and Interface Science* **1968,** *26*, 62-69.

245. Tam, F. Optimization of the nanoshell geometry for plasmon enhanced fluorescence. Ph.D. Dissertation, Rice University, Houston, **2007.** Rice University Electronic Theses and Dissertations